Devolatilization of Coal of Northeastern India in Argon, Air, and Oxygen-Enriched Air under Fluidized Bed Conditions

Thesis

submitted in partial fulfillment of the

requirements for the degree of

DOCTOR OF PHILOSOPHY

by

Ramesh Chandra Borah

Department of Chemical Engineering

Indian Institute of Technology Guwahati

Guwahati - 781039, India

Devolatilization of Coal of Northeastern India in Argon, Air, and Oxygen-Enriched Air under Fluidized Bed Conditions

Ramesh Chandra Borah

Devolatilization of Coal of Northeastern India in Argon, Air, and Oxygen-Enriched Air under Fluidized Bed Conditions

Thesis

submitted in partial fulfillment of the

requirements for the degree of

DOCTOR OF PHILOSOPHY

by

Ramesh Chandra Borah

Department of Chemical Engineering

Indian Institute of Technology Guwahati

Guwahati - 781039, India

February 2010

Dedication

To My parents and family

CERTIFICATE

It is certified that the work contained in the thesis entitled **"Devolatilization of Coal of Northeastern India in Argon, Air, and Oxygen-Enriched Air under Fluidized Bed Conditions"**, by *Ramesh Chandra Borah* has been carried out under our guidance and supervision. The work documented in this thesis has not been submitted to any other University or Institute for the award of any other degree or diploma.

(Dr. Pallab Ghosh)
Associate Professor
Department of Chemical Engineering
Indian Institute of Technology Guwahati
Guwahati - 781039 (India)

(Dr. Paruchuri Gangadhar Rao)
Director
North East Institute of Science & Technology Jorhat
Jorhat - 785006 (India)

ACKNOWLEDGMENT

At first, I would like to express my profound gratitude to **Dr. Pallab Ghosh, Associate Professor, Indian Institute of Technology, Guwahati** for his supervision, and guidance throughout this interesting and industrially important work. Although I have carried out all the experimental work at North East Institute of Science and Technology (NEIST) Jorhat the data were analyzed in consultation with Dr. Pallab Ghosh. I would like to thank Dr**. Pallab Ghosh** for his invaluable support, undaunted encouragement, interesting discussions and crucial contribution, which made him a backbone of this research. I am also indebted to Dr. Ghosh for instilling in me a craving for perfection in performing experiments as well as in documentation. It has really been a remarkable experience working with him.

I would like to express my gratitude to my supervisor, **Dr. Paruchuri Gangadhar Rao, Director, North East Institute of Science and Technology, Jorhat** for providing me inspiring and valuable guidance, flexibility and openness in dealing with the specific and general needs of this research work. His supervision, useful suggestions and invaluable contribution enabled me to complete my work successfully. I have also benefited by the useful advice given by him from time to time.

I would like to express gratitude to the **Director**, **North East Institute of Science and Technology, Jorhat** for giving me permission and provide all facilities such as the assembly of experimental setup, personal computer, microbalance, and gas cylinders etc.to undertake this work.

I would like to thank my doctoral committee members, **Prof. Aloke K.Ghosal and Dr. Prabir K. Saha** (Department of Chemical Engineering) **Prof. Manabendra Roy** (Department of Chemistry), for their valuable suggestions and constructive criticism during project evaluations, which helped me to make necessary improvements towards various stages of my research work.

I express my thanks to **Mr. Jayanta Jyoti Bora**, of General Engineering Workshop, of NEIST Jorhat for his help in the fabrication of the experimental set-up.

Last but not the least, I would like to express my deepest sense of gratitude to my wife ‘Lakhimi’ and my children ‘Leena’ and ‘Keshab’. Their constant inspiration kept me focused and motivated. Their unconditional love, affection, care, sacrifice and encouragement have been my greatest strength so far. I appreciate the courage, understanding and dedicated support shown by all of them despite many testing times at their end.

NEIST Jorhat *Ramesh Chandra Borah*

ABSTRACT

Devolatilization is the first step in most coal conversion processes such as combustion, gasification and liquefaction. It has a significant influence on the subsequent stages of processing. Oxygen-enriched air can increase the combustion efficiency, boiler efficiency, and sulfur absorption efficiency of atmospheric fluidized bed combustion (AFBC) boilers, and other combustion systems which use coal.

Devolatilization of five coals having volatile matter in the range of 31 to 41% has been studied in argon, air and oxygen-enriched air under fluidized bed conditions at 1123 K and atmospheric pressure. The experiments with oxygen-enriched air were performed using air containing 30% oxygen. The diameter of the coal particles varied between 4 and 9.5 mm. The variation of devolatilization time (t_v) with particle diameter (d_v) was expressed by the correlation, $t_v = Ad_v^n$, where A and n are the parameters of the correlation. The variation of mass of coal particle with time was described by an exponential correlation, $V = V_0 + (V_\infty - V_0)\left[1 - \exp\left(-ct^m\right)\right]$, where c and m are the correlation parameters.

The superficial gas velocity was found to have a significant effect on the rate of devolatilization. The devolatilization rate increased with the increase in the oxygen concentration in the fluidizing gas. Therefore, the parameters of the correlations were further correlated with the superficial gas velocity and oxygen concentration. The correlations developed in this study fitted the mass versus time profiles of the coal particles during devolatilization in a satisfactory manner. The same correlations were found to be appropriate for predicting devolatilization of a batch of coal particles. The correlations developed in this study will be useful for the design of fluidized bed combustors.

RESEARCH PUBLICATIONS

1. R.C. Borah, P. Ghosh, P.G. Rao, Devolatilization of coals of north-eastern India under fluidized bed conditions in oxygen-enriched air, Fuel Processing Technology, 89 (2008) 1470–1478.
2. R.C. Borah, P.G. Rao, P. Ghosh, Devolatilization of coals of northeastern India in inert atmosphere and in air under fluidized bed conditions, Fuel Processing Technology 91(2010) 9–16.
3. Ramesh C. Borah, Pallab Ghosh, Paruchuri G. Rao, Devolatilization of Coal in Fluidized Bed, submitted to International Journal of Energy research (under revision, September 2010).
4. R.C. Borah, P.G. Rao, Pallab Ghosh, *Devolatilization of Coal in Argon, Air, and Oxygen-Enriched Air*, VDM Publishing House Ltd., Beau Basin, Mauritius (2010).

CONTENTS

LIST OF FIGURES

LIST OF TABLES

CHAPTER 1

INTRODUCTION TO COAL CONVERSION PROCESSES

1.1 Introduction

Coal has been an important energy resource for more than hundred years, and it will continue to be an important energy resource in the 21st century as well. Coal has fueled the industrial revolution in the previous two centuries. With the advent of the automobile, airplanes, and the extensive use of electricity, oil became the dominant fuel during the twentieth century. The growth of oil as the "most widely used fossil fuel" was supported by the steadily-dropping prices from 1920 to 1973. During the "oil shocks" of 1973 and 1979, the price of oil increased from 5 to 45 US$/barrel, and there was a spontaneous shift away from oil. Coal, natural gas, and nuclear resources became the major sources of electricity generation. In fact, coal has been the fastest-growing fossil fuel in terms of use from 2003 to 2008. Conservation measures have been adopted, which have resulted in the increase of the energy efficiency.

India's primary energy resource is not oil, but coal. Coal has been a mainstay of Indian energy. The main source of coal is the domestic collieries. India's rapidly-developing economy warrants a sharp increase in energy demand. Coal accounted for 53% of India's energy consumption in 2007, and the demand is set to grow over the coming decades. Use of coal for the generation of electricity is projected to grow 2% every year. Its share in electricity generation will approximately double by the year 2030. This will increase not only the domestic production but also the imports of coal. Over the next two decades, coal import is projected to be tripled as compared to the amount imported at present. Because coal is cheap and abundant domestically, it may

seem like the perfect solution to India's energy requirements. However, coal is the most-polluting fossil fuel. There are several adverse health, environmental and economic consequences associated with the use of coal. In fact, Indian coal is one of the dirtiest coals in the world. Its high ash content and the lack of infrastructure to clean it early in the process create a huge environmental risk for India. Coal is the most polluting fuel in terms of the greenhouse gases, and it already accounts for 65% of the CO_2 emissions in India. In addition to harmful carbon dioxide gas emissions, "black carbon" (fine char particles) is produced during the burning of coal. Black carbon is often neglected as a pollutant. However, it is responsible for one-fifth of the global warming. It stays in the atmosphere for only a few weeks, but creates more local warming problems than the emissions from most other fuels.

Although the reserve of coal in India is large as compared to oil and natural gas, the utilization of coal has been restricted because the traditional methods of coal conversion (e.g., combustion) result in some complications in the conversion efficiency and adverse impacts on the environment. In a conventional coal-fired power plant, combustion in the boiler and furnace converts the chemical energy in coal to heat, which is used to generate high temperature, and produce high-pressure steam to drive the steam turbine. These traditional methods of coal conversion have higher CO_2 emissions (per unit of useful energy produced) than oil or gas conversion technologies. Currently, there is intensive research going on the capture, sequestration and storage of CO_2. Although many Indian coals have low ash content, yet some of them contain high amounts of sulfur (e.g., the coals of northeastern India). High- temperature conversion of coal results in the emission of nitrogen and sulfur in the coal as NO_x and SO_2. These gases are responsible for acid rain and smog.

The conventional methods of utilization of coal practiced in India have low efficiency and high pollution characteristics as compared to oil and natural gas. A few clean coal technologies, such as Integrated Gasification Combined Cycle (IGCC), and Fluidized Bed Combustion (FBC) have been identified as viable technologies to circumvent these problems. A fundamental understanding of the physical and chemical processes involved in these advanced coal conversion technologies is necessary to achieve a higher efficiency and less adverse impact on the environment.

1.2 Coal reserves in India

India is the 3rd largest coal-producing country, and has the fourth largest reserve of coal in the world (viz. approximately 197 billion tons). Coal deposits in India occur mostly in thick seams and at shallow depths. The reserve for non-coking coal is about 167.45 billion tons (i.e., 85% of the total reserve) while the coking-coal reserve is 29.55 billion tons. Indian coals usually have high ash content (15–45%), and they are of low calorific value. With the present rate of extraction of ~0.8 million tons per day, the reserves are likely to last over the next 100 years. In India, the energy derived from coal is nearly twice that derived from oil. The world statistics show that the energy derived from coal is about 30% lower than that derived from oil.

At present, India has 48 coal washeries having a total capacity of 102 million tons per annum. Of these washeries, 19 are owned by Coal India Limited (CIL). The use of beneficiated coal has gained acceptance in the steel and power plants located at a distance from the pithead. CIL is the largest company in the world in terms of coal production. It contributes to ~85% of coal production in India. Figure 1.1 depicts the various branches of Coal India Limited throughout India.

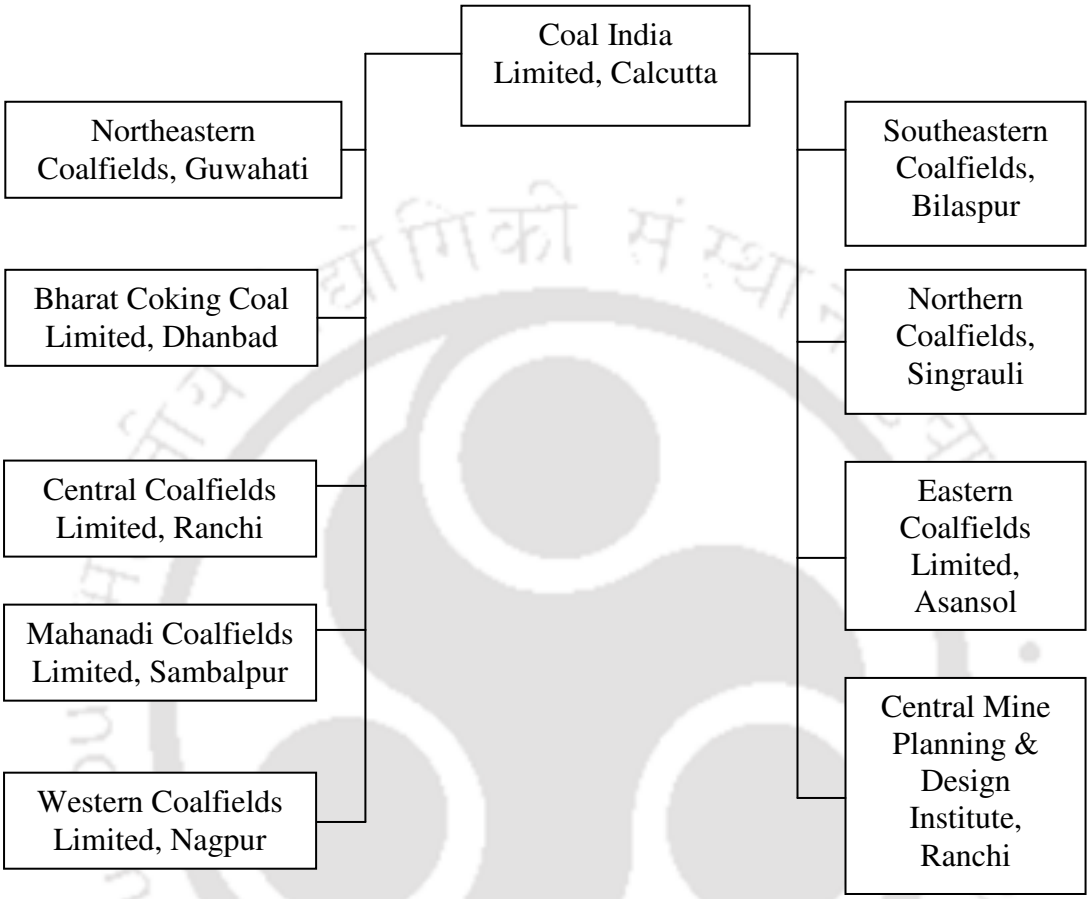

Figure 1.1 Coal India Limited and its subsidiaries.

1.2.1 Coals of northeastern India

The northeastern region of India is comprised of eight states viz. Arunachal Pradesh, Assam, Meghalaya, Mizoram, Manipur, Nagaland, Tripura and Sikkim. Northeastern Coalfield (NEC) (a unit of Coal India Limited) is engaged in carrying out coal mining operations in this region. Coal is produced by both open cast and underground mining methods from the coal-bearing strata, which have been tectonically folded with the coal seams dipping from 30–60 degrees. The coal reserves to a depth of 600 meters aggregate to about 945 million tons. The coal available in this region is tertiary coal, which is unique in character by virtue of its low ash content, and thus of high value.

The coal-bearing tertiary sediments of the northeastern India range from Paleocene to Oligocene geological epochs. These epochs belong to the "tertiary" geological period which ranges from 1.8 to 65 million years ago. The tertiary period of geological age has been divided into several divisions. The Paleocene epoch spans the period 55–65 million years ago. On the other hand, the Oligocene epoch refers to the period between 22 and 39 million years ago. The coal deposits of Meghalaya, and the Mikir and North Cachar hills of Assam generally contain thin seams of Eocene age (38 to 54 million years ago). They were formed under stable shelf condition in peripheral platform areas. The coal deposits of Oligocene epoch occur in a narrow, linear belt of over-thrusts known as the "belt of Schuppen", which extends from Nagaland to Arunachal Pradesh through Assam. They were deposited in near-shore, deltaic wet forest swamps, and in marshy environments close to a geosynclinals trough. The coal seams have attained considerable thickness in the Makum and Namchik–Namphuk coalfields.

A comparison of the coals belonging to the Eocene and Oligocene epochs indicates that these coals are similar in a broad sense. These coals are rich in vitrinite [in which more than 70% (v) mineral matter is free] with moderate amounts of liptinite [> 8% (v) free mineral matter] and inertinite [> 5% (v) free mineral matter]. Vitrinite is a type of *maceral*[*] that has a shiny appearance resembling glass. It is derived from the cell-wall materials or woody tissues of the plants from which the coal was formed. Chemically, it is composed of polymers, cellulose and lignin [1]. Liptinite macerals are considered to be produced from decayed leaf matter, spores, pollen and algal matter. Resins and plant waxes can also be a part of the liptinite macerals. Inertinite is composed of oxidized organic material or fossilized charcoal. It is found as tiny flakes within the sedimentary rocks. The presence of inertinite is significant in the geological record because it signifies that wildfires occurred at the time when the host sediment was deposited. It is also an indication of oxidation due to the atmospheric exposure or fungal decomposition during deposition.

The coals of northeastern India are high in volatile matter [38–57% on dry mineral-matter-free (dmf) basis], sulfur (1–10% dmf basis) and hydrogen (4–9% dmf basis) contents. The carbon content of these coals ranges from 68 to 85% (dmf basis). These coals have caking properties in restricted zones.

The vitrinite reflectance of the Oligocene coals (R_r = 0.53–0.74%) is slightly higher than that of the Eocene coals (R_r = 0.37–0.67%), where R_r is the mean random reflectance. As per the ASTM Standard [2], the Eocene coals are classified as "sub-bituminous C to high-volatile bituminous C", and the Oligocene coals are classified as "sub-bituminous A to high-volatile bituminous B". Microscopic examination of these

[*] "Macerals" are organic components of coal which are analogous to the minerals of rock.

coals shows a number of features which indicate that the coals of northeastern India may have generated hydrocarbons*.

Most of the Eocene and Oligocene coals are suitable for combustion and conversion (e.g., liquefaction) processes. The coals with caking properties are used in blends (e.g., 5–10%) for the production of metallurgical coke provided their sulfur content is below 3% and their ash content is below 10% [3]. The reasons for certain abnormalities in the chemical properties of the Oligocene coals of upper Assam and Arunachal Pradesh have been attributed to the marine environment and unusual conditions of deposition. It has been reported in the literature [4] that marine conditions were responsible for the perhydrous nature of the coals, which increases with the intensity of the marine environment. The graphs of carbon versus oxygen are useful for the identification of the seam and/or the field. It has also been suggested [4] that oxygen was replaced by organic sulfur thereby lowering the oxygen content of these coals. This aided the development of their agglutinating properties.

The coals of northeastern India generally have high sulfur content. In a particular seam, total pyritic and organic sulfur content increases from the floor to the roof of the seam. Upper seams generally contain more sulfur than the seams lying below [5]. Use of these coals has been restricted to a rather low level because of the high sulfur content. Moreover, more than 80% of the sulfur present in these coals is organic in nature. Therefore, it is not possible to remove this sulfur by applying any mechanical means. Free burning of these coals causes environmental pollution leading to acid rains in the nearby areas.

* Coal under certain depositional condition can generate and release hydrocarbons up to liquid petroleum.

1.2.2 Uses of coals of northeastern India

The northeastern region coals are soft and friable. Hence it is very difficult to extract them as lump coals during mining. These coals are used in various sectors, e.g., power, cement, paper, brick burning, cokaries, tea gardens and other local industries.

Use in the power sector

The best way to utilize the coals of northeastern India is by fluidized bed combustion in power plants located centrally in the mining area.

Use in the cement sector

The relatively high heating values of the northeastern coals and the low ash fusion temperature result in improvement in the clinker formation by 7–12% per day. Also, the consumption of gypsum is reduced because of the presence of sulfur in the coal.

Use in the steel sector

Strongly-caking coals of the Makum coalfield of Assam are used as a blend for making coke. About 10% of the Assam coals are used in the coal blend charged to the coke ovens.

1.3 Background of the present research

Northeast Institute of Science and Technology (NEIST) Jorhat had completed its first bench-scale study (150 kg/hr steam production capacity) of burning northeastern coals in a fluidized bed reactor in the year 1978 [6]. The northeastern region has a good deposit of limestone. Limestone is used to absorb sulfur dioxide generated during the burning of high-sulfur coal. Calcined lime (CaO) reacts with

sulfur dioxide to give calcium sulfite, which converts to calcium sulfate in presence of oxygen. Limestone is also used as a bed material for fluidized bed. Coal and limestone are mixed at certain ratios and fed to the fluidized bed combustor to maintain the bed height as well as the SO_2 emission in the flue gas. Various parametric studies have been performed till 1986 in a pilot plant (2000 kg/hr steam or 10000 kg/hr hot water capacity), which was designed and fabricated by Bharat Heavy Electricals Limited (BHEL), Tiruchirappalli (India). The work was extended up to 1990 with the objectives such as: (i) optimization of the calcium/sulfur molar ratio, (ii) finding the optimum sulfur retention temperature, (iii) role of excess air, and (iv) monitoring the flue gas. This research was funded by the Northeastern Council (Shillong, Meghalaya, India) [7].

While the above-mentioned work generated a significant amount of knowledge and brought a reasonable conclusion towards commercialization, yet it has been felt that more accurate data on the characteristics of coal devolatilization are necessary for optimization of the bed height and feed size. This information would increase the combustion and absorption efficiency of the fluidized bed combustor.

1.4 Importance of the present work

Devolatilization is a general term signifying the removal of volatile matters from the coal matrix. Pyrolysis-like conditions are encountered by the coal particles prior to ignition even under oxidizing conditions [8]. The yield of volatile matter in pyrolysis provides deep insight into the proportion of coal volatilized in the devolatilization stage. Devolatilization of coal is also extremely important because the combustion of volatile matter accounts for nearly 50% of the specific energy for fluidized bed combustion of a high-volatile coal [9]. To ensure high boiler efficiency,

it is important that all the volatile matter evolved during devolatilization should burn inside the bed.

The rate of devolatilization of coal in a fluidized bed combustor depends on many parameters, such as particle size, gaseous atmosphere, fluidization velocity, bed temperature, coal type and the amount of volatile matter. During the heating process of the coal particles in fluidized bed, the average heating rate of the individual coal particles depends on their size. The differences in temperature history of the center of the coal particles are mostly influenced by the particle size and the type of coal [10]. The small particles are likely to release volatile matter quickly, but the large particles can release volatile matter above the bed because they are heated at a slower rate than the smaller particles [11]. This causes variations in the composition in the gas. For a particular design of the bed, this variation can retard the conversion of the gaseous components and shift the conversion to the downstream region of the furnace, which can influence burn-up and cause undesirable emissions. In some cases, additional air has to be introduced in the freeboard to reduce the emission levels [7]. Hence, it is important to ascertain the amount of volatile matter released by a single coal particle over time after its injection into the bed. For practical purposes, it would be better to investigate a batch of coal particles, but it has been reported in the literature [12] that the coal particles fuse together during pyrolysis and form a single large particle.

The gaseous atmosphere has a great influence on the devolatilization process. Heat transferred from the fluidized bed to the coal particle is utilized in the drying of the coal particle and the endothermic reactions leading to the formation of the volatiles. The presence of oxygen causes reaction with the volatile matter at the surface of the particles, which results in an increase in the surface temperature. In addition, exothermic reactions in the combustion of char cause increase in the

temperature of the particle and thereby increase heat transfer from the particle to the surrounding medium. Increase in particle temperature increases the rate of drying and devolatilization of coal. Hence it is important to study devolatilization of coal of different particle size relevant to fluidized bed under enriched-oxygen conditions.

Combustion studies on pulverized coal with enriched air have revealed that there is an increase in the flux of oxygen molecules from the bulk towards the particles. As a result, the temperature of the surface of the particles becomes higher. This increases the pyrolysis rate, Stefan flow and oxidation in the boundary layer [13]. But there is a difference between higher oxygen concentration and higher excess-air condition: the latter leads to a higher fluidization velocity. At the higher fluidization velocities, the rate of release of volatile matter is slightly higher because of the better convective heat transfer to the particle [14]. Because nitrogen does not participate in combustion, the volume of nitrogen is quite high at the higher fluidization velocities, and the sensible heat is lost, which is carried away by the excess nitrogen.

Amongst the fluidized bed technologies, Atmospheric Fluidized Bed Combustion (AFBC) is simple and economical because it can use particles of large size, offers flexibility in the type of the fuel used, and reduces erosion and corrosion. Although the other types of fluidized bed (viz. pressurized and circulating fluidized beds) are more efficient in combustion as well as sulfur capture (because of the lower particle size used in these beds, higher recirculation rate and the presence of higher amount of air), yet the costs of production are comparatively higher than AFBC. By the application of oxygen-enriched air in AFBC, the deficiency in combustion and thermal efficiency in comparison with Pressurized Fluidized Bed Combustion (PFBC) and Circulating Fluidized Bed Combustion (CFBC) can be significantly removed, and can be made at par with the PFBC. In oxygen-enriched environment, devolatilization

and combustion of coal particles are likely to occur faster than that with air. Also, there occurs increase in combustion of coal char and volatile matter because of the presence of extra oxygen in the combustion system, which increases the combustion efficiency. Thermal efficiency of the system also increases due to the reduction of the total volume of the flue gas leaving the combustion chamber. Oxygen-enriched combustion method is an effective method to produce a flue gas rich in carbon dioxide [15,16] which can be separated easily and sequestered [17]. It is known that the use of oxygen-enriched air and recycle of char help a gasifier to increase the heating value of the product gas and the cold gas efficiency. The ratio of conversion of carbon to CO_2 and CO increases with the increase of oxygen concentration in the combustion chamber. Air enriched with oxygen can reduce the emission of carbon monoxide in the flue gas of a fluidized bed combustor. The amount of unburned carbon in the flue gas reduces considerably in presence of extra oxygen. However, the cost for oxygen enrichment is higher, owing to the cost involved in the liquefaction of air.

There are several reports in the literature [11,18–20] on devolatilization time of coal particles in presence of air. However, these works have not reported the variation of mass of a single particle with time. There are differences among the results reported in the literature for devolatilization time, which can be attributed to the different experimental conditions employed, and the definitions used to measure the time [21]. To simplify the experimental procedure, a thermogravimetric analyzer (TGA) may be used to measure devolatilization time. However, the rate of heating in a fluidized bed is much greater than that in a TGA, and the devolatilization kinetics varies considerably with such large variation in the heating rate. As a result, it is not reliable to use the results obtained in a TGA to predict the devolatilization in a fluidized bed.

From the foregoing discussion, it is evident that the increase in oxygen concentration in the fluidizing gas increases the exothermic reactions as well as the devolatilization rate. Hence the characteristics of devolatilization differ in inert atmosphere, air, and in air enriched with oxygen. Only devolatilization time has been studied in most of the works reported in the literature. Little emphasis has been given to find out the evolution of volatile matter with respect to time. The other important drawback of the works reported in the literature is that the velocity employed during the studies was much lower than that employed in a commercial AFBC. The mechanism of devolatilization at the higher velocities is therefore rather unknown. The existing methods involving flame extinction time and monitoring of gas evolution perform satisfactorily only at the lower velocities. Therefore, it is necessary to analyze the existing experimental procedure and develop a new set-up to study the characteristics of devolatilization of coal.

1.5 Objectives of the present work

The present research work has been undertaken with the following objectives.

- To study the devolatilization characteristics of coal samples from various collieries of northeastern India (which contain volatile matter in the range of 31% to 41%) in inert, air and oxygen-enriched air (such that the gas contains 30% oxygen) under fluidized bed conditions
- To study the effect of particle size in these three atmospheres
- To develop correlations for devolatilization time, effect of particle size, oxygen concentration, volatile matter content and superficial gas velocity
- To study the mechanism of pyrolysis in different gaseous atmospheres during devolatilization

References

1. W.G. Dow, Kerogen studies and geological interpretations, Journal of Geochemical Exploration 7 (1977) 79–99.
2. American Society for Testing and Materials, Standard Classifications of Coals by Rank [D0388(2005)], West Conshohocken (Pennsylvania), 2005; DOI: 10.1520/D0388-05.
3. H.K. Mishra, R.K. Ghosh, Geology, petrology and utilization potential of some tertiary coals of the northeastern region of India, International Journal of Coal Geology 30 (1996) 65–100.
4. D. Chandra, S. Ghose, S.G. Chaudhuri, Abnormalities in the chemical properties of tertiary coals of upper Assam and Arunachal Pradesh, Fuel 63 (1984) 1318–1323.
5. D. Chandra, S.G. Chaudhuri, S. Ghose, Distribution of sulphur in coal seams with special reference to the tertiary coals of northeastern India, Fuel 59 (1980) 357–359.
6. R. Haque, M.L. Dutta, R.K. Chakrabarty**,** Fluidized bed combustion of high sulfur coals, Journal of the Institute of Energy 52 (1979)173–177.
7. R.C. Borah, B. Mazumder, M.M. Bora, Atmospheric fluidized bed combustion of high sulfur high volatile N.E. region coals of India, Research and Industry 40 (1995) 315–321.
8. P.K. Agarwal, R.D. La Nauze, Transfer processes local to the coal particle: a review of drying, devolatilization and mass transfer in fluidized bed combustion, Chemical Engineering Research and Design 67 (1989) 457–480.
9. K.L. Smith, L.D. Smoot, T.H. Fletcher, R.J. Pugmire, The Structure and Reaction Processes of Coal, Plenum, New York, 1994.
10. M. Komatina, V. Manovic, D. Dakic, An experimental study of temperature of burning coal particle in fluidized bed, Energy and Fuels 20 (2006) 114–119.
11. D.P. Ross, C.A. Heidenreich, D.K. Zhang, Devolatilization times of coal particles in a fluidized bed, Fuel 79 (2000) 873–883.
12. C.N. Eatough, L.D. Smoot, Devolatilization of large coal particles at high pressure, Fuel 75 (1996) 1601–1605.
13. C.A. Gurgel Veras, J. Saastamoinen, J.A. Carvalho (Jr.), M. Aho, Overlapping of the devolatilization and char combustion stages in the burning of coal particles, Combustion and Flame 116 (1999) 567–579.

14. F. Winter, M.E. Prah, H. Hofbauer, Temperature in a fuel particle burning in a fluidized bed: the effect of drying, devolatilization, and char combustion, Combustion and Flame 108 (1997) 302–314.
15. Y.Q. Hu, N. Kobayashi, M. Hasatani, The reduction of recycled-NO_x in coal combustion with O_2/recycled flue gas under low recycling ratio, Fuel 80 (2001) 1851–1855.
16. Y.Q. Hu, S. Naito, N. Kobayashi, M. Hasatani, CO_2, NO_x and SO_2 emissions from the combustion of coal with high oxygen concentration gases, Fuel 79 (2000) 1925–1932.
17. Y. Tan, E. Croiset, M.A. Douglas, K.V. Thambimuthu, Combustion characteristics of coal in a mixture of oxygen and recycled flue gas, Fuel 85 (2006) 507–512.
18. J.F. Stubington, T.Y.S. Chui, S. Saisithidej, Experimental factors affecting coal devolatilization time in fluidized bed combustion, Fuel Science and Technology International 10 (1992) 397–419.
19. J.Q. Zhang, H.A. Becker, R.K. Code, Devolatilization and combustion of large coal particles in a fluidized bed, Canadian Journal of Chemical Engineering 68 (1990) 1010–1017.
20. J.F. Stubington, K.W.K. Ng, B. Moss, P.K. Peeler, Comparison of experimental methods for determining coal particle devolatilization times under fluidized bed combustor conditions, Fuel 76 (1997) 233–240.
21. S.N. Oka, Fluidized Bed Combustion, Dekker, New York, 2004.

CHAPTER 2

LITERATURE REVIEW

2.1 Introduction

This chapter presents a review of the literature on the devolatilization of coals relevant to the fluidized bed gasification and combustion processes. Emphasis has been given on the parameters that are important to improve the efficiency of fluidized bed coal combustion for power generation and steam production. Importance has been given to the coals which contain high volatile matter so that the present study can be helpful for the design and control of commercial fluidized bed combustors or pyrolyzers that use the coals of northeastern India. In this review, the mechanism of devolatilization, the nature of transformation which occurs inside the coal particles, and the products of devolatilization will be discussed. The devolatilization models available in the literature will be reviewed focusing on the type of the models employed, chemical kinetics of coal devolatilization, and the devolatilization of large particles. The present status of knowledge on coal devolatilization will be explained, and an in-depth background of the present study will be presented which will help us to explain the scope of the present work.

2.2 The fundamentals of coal devolatilization

2.2.1 The chemical structure of low-rank coals

It is necessary to understand the chemical structure of low-rank coals to explain the structural changes which occur during coal devolatilization. The chemical structure of coal depends upon the process through which it has formed. Coal

originates from peat, which is formed from plant-matter that deposits or grows in swamps. The transformation from peat to coal occurs via the application of heat and pressure. Generally, the peat-deposit is buried under sediments (e.g., sands and clays), and it is the thickness of this overburden which determines the temperature and pressure to which it is exposed. This thermodynamically-favorable transformation process is termed as *coalification*.

Peat is composed of a significant amount of lignin and cellulose which is present in the original plant deposits. In the first stage of coalification, dewatering and decomposition of the hydrophilic functional groups of peat occur because of the increase of pressure and temperature. The cellulose begins to undergo decomposition while the lignins are preserved, and they become concentrated in peat. Formation of humic acid functional group follows to which cations such as Na^{+}, Ca^{+2}, Mg^{+2}, Fe^{+3} and Al^{+3} can bond to form humates. The ensuing gelation stage involves the formation of colloidal humic gels, which precipitate in void spaces resulting in the reduction of the porosity of peat. As coalification progresses, the oxygen-content of the coal is gradually reduced via decomposition of the carboxyl (–COOH), methoxyl ($-OCH_3$) and carbonyl (>C=O) functional groups, as well as ring oxygen. The final stages of coalification involve the condensation of humic acids to larger molecules, and the removal of aliphatic and alicyclic functional groups. This chemical change indicates that the coal gradually becomes more and more aromatic and carbon-rich in nature [1].

A number of hypothetical models of the structure of coals have been developed. A typical structure proposed for a bituminous coal is depicted in Figure 2.1. As can be observed in this figure, the coal is composed primarily of groups of aromatic ring clusters that are cross-linked by aliphatic or etheric bridges. The size of

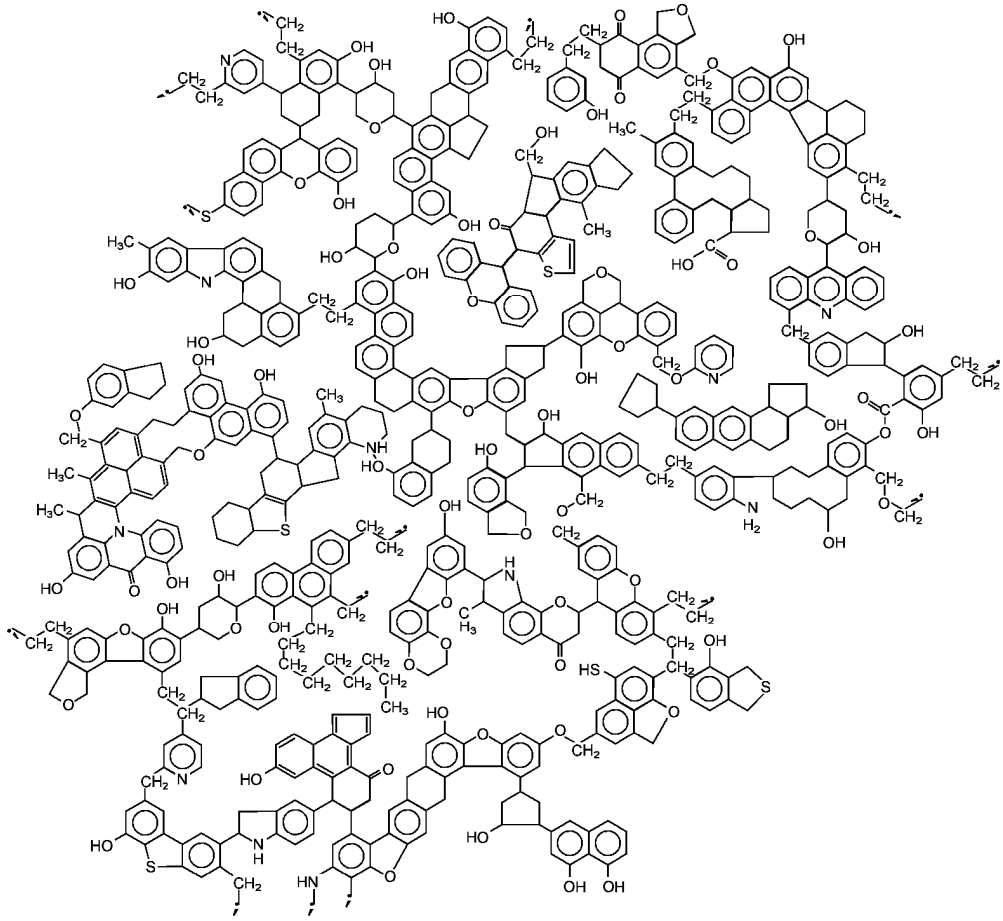

Figure 2.1 Model of bituminous coal structure [2] (reproduced by permission from Elsevier Ltd., © 1984).

the aromatic ring structure varies from one to multiple rings per cluster, and a variety of functional groups (e.g., carbonyl, carboxyl, ether and phenol groups) are attached to the rings. The aromatic rings may be mono-substituted with heteroatoms such as nitrogen, sulfur or carbon. This covalently-bonded chain of aromatic ring clusters is commonly referred to as the "immobile phase". Throughout this continuous chain of aromatic ring-clusters exists small interstices, or holes, in which smaller molecules may be trapped. These molecules are generally aliphatic in nature. However minerals such as quartz (SiO_2) and kaolinitic clays [e.g., $Al_2Si_2O_4(OH)_4$] may also be present. These molecules constitute the so called "mobile phase". Inorganic materials such as Na, K, Ca, Al and Fe are also found within the coal structure. They are typically attached to carboxyl (or similar) groups, or included as chelate complexes [3–5].

2.2.2 General mechanism of coal devolatilization

The physico-chemical transformations which occur during devolatilization have been investigated by a number of workers [3–7]. They have proposed various mechanisms describing the transformations. The mechanism proposed by van Heek and Hodek [5] for devolatilization of coal is shown schematically in Figure 2.2. According to this mechanism, the coal degradation process starts with desorption of moisture and some light gases (mainly methane and nitrogen) at about 393 K. On further heating, distillation of the mobile phase occurs at temperatures above 523 K leading to the formation of tar, particularly the aliphatic tar components. At temperatures greater than 673 K, degradation of the immobile phase starts resulting in the formation of aromatic tar fraction, a number of light gases (e.g., H_2O, CO and CO_2), and low molecular weight hydrocarbons (e.g., CH_4, C_2H_4, C_2H_6, C_3H_6 and C_3H_8). Finally, condensation of vaporized aromatics to char occurs at temperatures above 873 K. This is associated with the decomposition of heterocyclic compounds

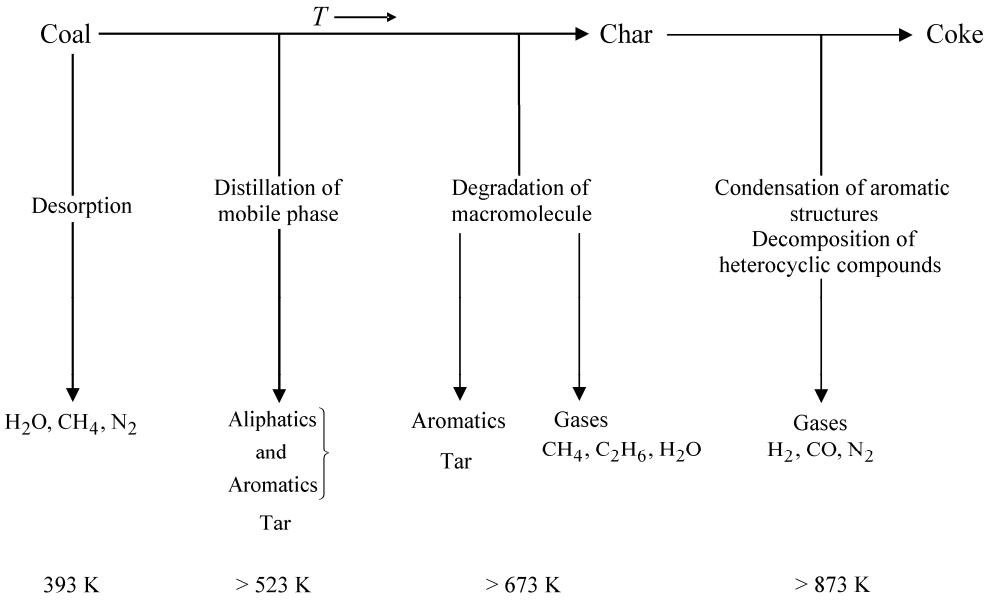

Figure 2.2 The main reactions which occur during coal pyrolysis as per the mechanism of devolatilization proposed by van Heek and Hodek [5] (adapted by permission from Elsevier Ltd., © 1994).

yielding N_2, H_2S and CO. Hydrocracking of the aromatics also occurs which releases H_2 [5].

Solomon et al. [4] proposed the following mechanism which describes the formation of the tar and char fractions.

Stage 1: Depolymerization by the rupture of weaker bridges in the coal macromolecule to release smaller fragments which make up the metaplast

Stage 2: Repolymerization (i.e., cross-linking) of metaplast molecules

Stage 3: Transport of lighter molecules away from the surface of the coal particles by combined vaporization, convection and gas-phase diffusion

Stage 4: Internal transport of molecules to the surface of the coal particles by convection, by diffusion into the pores of non-softening coals, and by liquid-phase diffusion or bubble transport in softening coals. Char is formed from the unreleased or recondensed fragments. Various amounts of loosely-bound guest molecules, usually associated with the extractable material, are also released during devolatilization.

This mechanism is similar to that proposed by van Heek and Hodek [5] except that the metaplast stage described here is called “mobile phase” by van Heek and Hodek [5]. Solomon et al. [3] proposed a structural model for sub-bituminous coal, which is shown in Figure 2.3. Comparing Figures 2.3(a) and 2.3(b), it can be observed that the aliphatic bonds denoted by (2) in Figure 2.3(a) have been ruptured, and the carbon radicals formed in the process picked up hydrogen radicals to form either methyl or ethyl functional groups. The hydrogen radicals have been generated by the dehydrogenation of a hydroaromatic ring such as that shown in the lower right side of the molecule in Figure 2.3(a). These two breakages of aliphatic bonds result in the fragments which are light enough to evolve as tars [3].

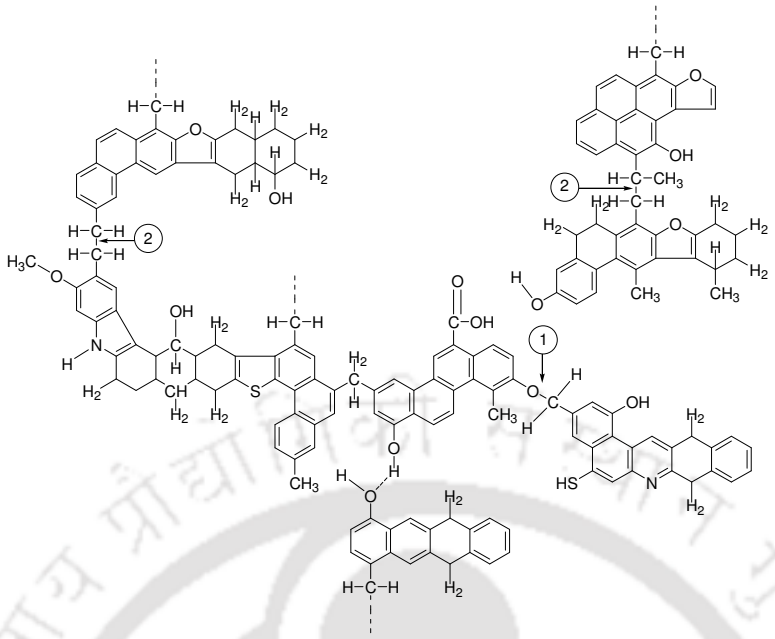

(a)

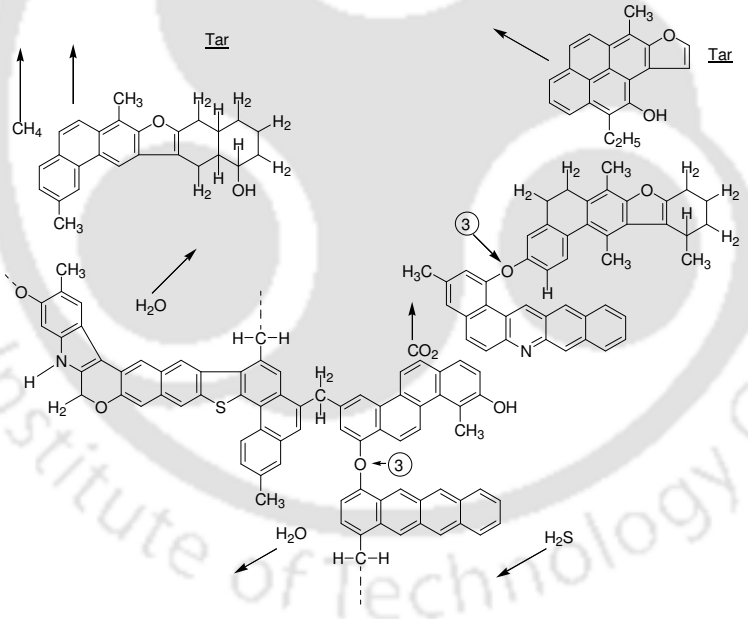

(b)

Figure 2.3 Hypothetical chemical structure of a sub-bituminous coal: (a) parent coal, and (b) during devolatilization [3] (reproduced by permission from Elsevier Ltd., © 1993).

The aliphatic ether bond denoted by (1) in Figure 2.3(a) has been disrupted leading to the formation of a hydroxyl group via a hydrogen radical, which is depicted in Figure 2.3(b). At the position labeled (3) in Figure 2.3(b), condensation of two hydroxyl groups has resulted in the formation of a second aromatic ether bond and the release of H_2O. Other independent transformations have occurred such as the decomposition of the carboxyl group depicted at the center of Figure 2.3(a) to yield CO_2, an aliphatic ether bond has been ruptured releasing a methyl group as CH_4 [on the left side of Figure 2.3(a)], and a mercaptan in the lower right corner of Figure 2.3(a) has detached to form H_2S [3]. These transformations are similar to those described in the mechanism proposed by van Heek and Hodek [5].

The structural changes shown in the Figure 2.3 are the changes that occur during *primary devolatilization*. It is defined as the decomposition of the macromolecular structure of coal. The disintegrated fragments produced from primary devolatilization are small, which can escape from the coal surface [8]. *Secondary devolatilization* is the decomposition of the components evolved during primary devolatilization in the vapor phase.

Pather and Al-Masry [9] have proposed a mechanism of coal devolatilization that involves three stages as described below.

Stage 1: Release of primary volatile matters at the solid–gas interface due to thermal decomposition

Stage 2: Production of secondary volatile matters during the diffusion of gaseous products through the pores within the coal particles

Stage 3: Production of tertiary volatile matters due to the decomposition reactions occurring in the void spaces between the particles

The secondary decomposition described in the stages 2 and 3 by Pather and Al-

Masry [9] is essentially the transformation of tar species which are formed during primary devolatilization through the reactions such as tar cracking, dehydrogenation, aromatization and condensation [10]. The lighter fraction of primary volatile matter is generally stable.

However, at the higher temperatures, the decomposition of benzylic compounds has been reported [10]. Several works have been reported on the secondary decomposition of tar [10–14], which have focussed on the rationalization of the influence of various operating parameters. A mechanism of tar decomposition was proposed by Hesp and Waters [10] based on a bench-scale study of decomposition of tar produced in a carbonizer when passed through a bed of coke in the temperature range of 973–1273 K. This mechanism suggests that tar decomposition takes place in three distinct phases, which are summarized below.

Phase 1: This is the first phase which involves rapid decomposition into gas and carbon. The amount of tar decomposing to gas is directly proportional to the temperature of cracking, and the time required is inversely proportional to temperature. Gas is the main product indicating that the gas-forming reactions are quicker than the reactions which form carbon.

Phase 2: The second phase involves formation of carbon by the secondary decomposition of gas. Hydrogen is also formed, accompanied by slow decomposition of the tar that escapes the cracking reactions in the first step. Since a major part of the total carbon is obtained in this phase, it is called "the phase of carbon formation". It is much longer than the first phase, and its duration is inversely proportional to the temperature of cracking.

Phase 3: The third phase involves slow evolution of gas from tar after the first two phases of decomposition. The amount of gas formed in the third phase is

directly proportional to the amount of tar entering into the third phase, and inversely proportional to the temperature of cracking.

Therefore, it is evident from the literature survey presented in this section that a substantial amount of work has been done to understand the mechanism of devolatilization. The devolatilization process is related to the structure of the parent coal. The structural and mechanistic models form the basis on which the observations regarding the influence of various operating parameters on devolatilization can be analyzed. Experiments can be designed to ascertain the controlling mechanism for fluidized bed combustion and gasification applications.

2.2.3 Effects of operating parameters on coal devolatilization

As the coal devolatilization process is very complex in nature, several parameters have direct and indirect influence over the nature and composition of the products evolved during devolatilization. Of these parameters, the most significant are rank of the coal, particle size, heating rate, gaseous environment, temperature, pressure, superficial gas velocity, oxygen concentration, and the presence of cations which have catalytic effect on coal devolatilization. Moisture content of coal is related to its rank: as the rank of the coal increases, the moisture content decreases. For low-rank coals, the moisture content is high, and the removal of moisture plays an important role in devolatilization. The majority of work done so far is related to the combustion of pulverized coal. However, in recent times, efforts have been made to study devolatilization of large particles related to fluidized bed coal combustion and gasification. The effects of some of these parameters are discussed in detail in the following sections.

2.2.3.1 Temperature of devolatilization

Temperature is an important parameter for any coal devolatilization process [15]. The effects of temperature on the yields of tar, gas and char have been reported by Tyler [16]. It can be seen from his work that the yield of C_1–C_3 hydrocarbons increases linearly with the increase in temperature, while the total volatile yield increases significantly upto ~1000 K, and then becomes invariant with temperature. Several other investigators have confirmed this behavior [10–12,14,17–19]. It is evident from Figures 2.4–2.7 that the yields of the products have different trends as the devolatilization temperature increases. Xu and Tomita [12] have reported that the yield of product is relatively constant up to 873 K, which is also observed in the results reported by Hesp and Waters [10], Tyler [18], and Cliff et al. [19], for several volatile products. The yield of tar increases with temperature up to 873 K, and subsequently decreases by almost 50% beyond this temperature [10,12,19]. Considering the mechanisms of primary and secondary decomposition discussed earlier, this trend suggests that at temperatures lower than 873 K, secondary decomposition reactions are minimal and primary decomposition is dominated by the Stage 1 reactions. Above 873 K, primary decomposition via the Stages 2, 3 and 4 begin to become increasingly more significant, as does the extent of the secondary decomposition reactions.

Xu and Tomita [12] monitored the yields of gases produced when the primary volatiles from a bituminous coal were allowed to pass through a packed bed reactor at various operating temperatures. This enabled the extent of the secondary reactions to be investigated. The yields of the products are summarized in Table 2.1 for a gas-phase residence time of 7 seconds. Table 2.1 confirms that minimal secondary decomposition reactions occur below 873 K. Immediately above 873 K, there is a

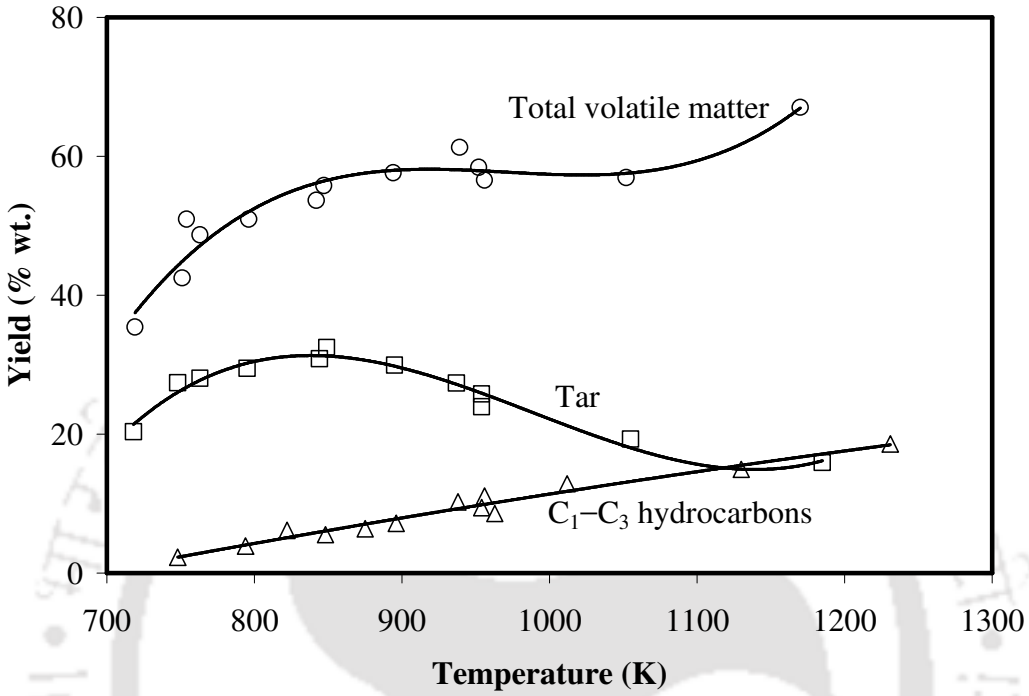

Figure 2.4 Effect of temperature on the yields of tar, total volatile matter and C_1–C_3 hydrocarbons [16] (adapted by permission from Elsevier Ltd., ©1979).

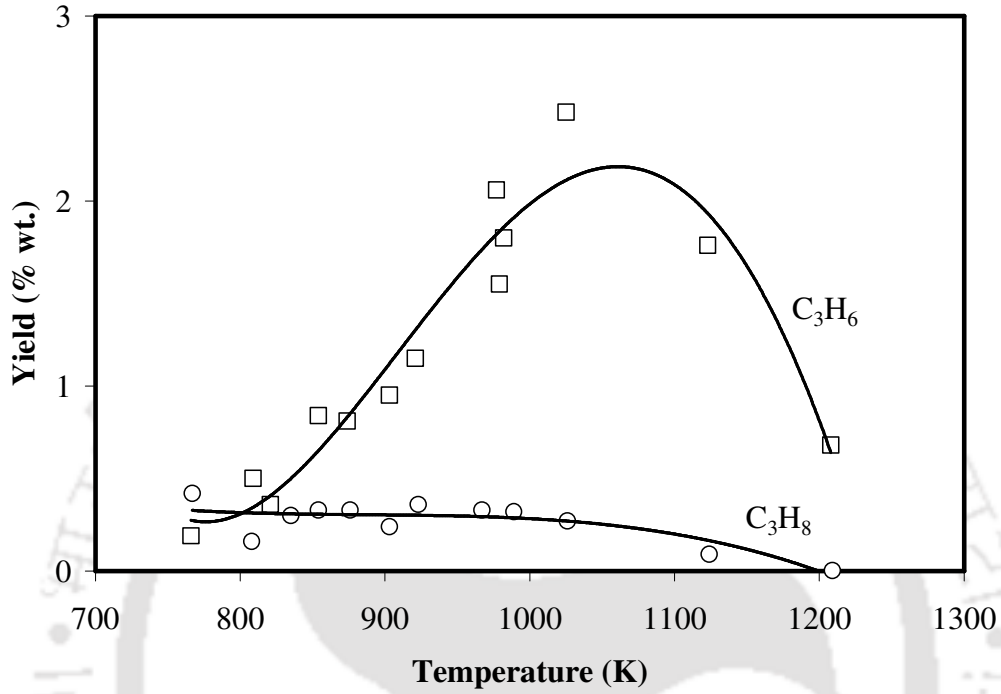

Figure 2.5 Effect of temperature on the yields of C_3H_6 and C_3H_8 [16] (adapted by permission from Elsevier Ltd., ©1979).

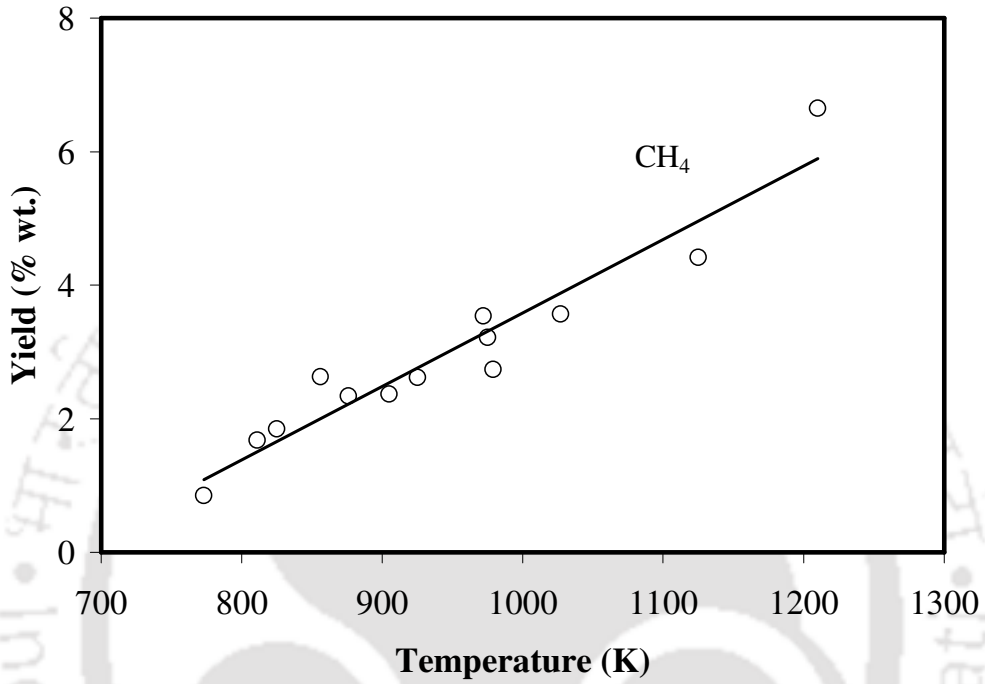

Figure 2.6 Effect of temperature on the yield of CH_4 [16] (adapted by permission from Elsevier Ltd., ©1979).

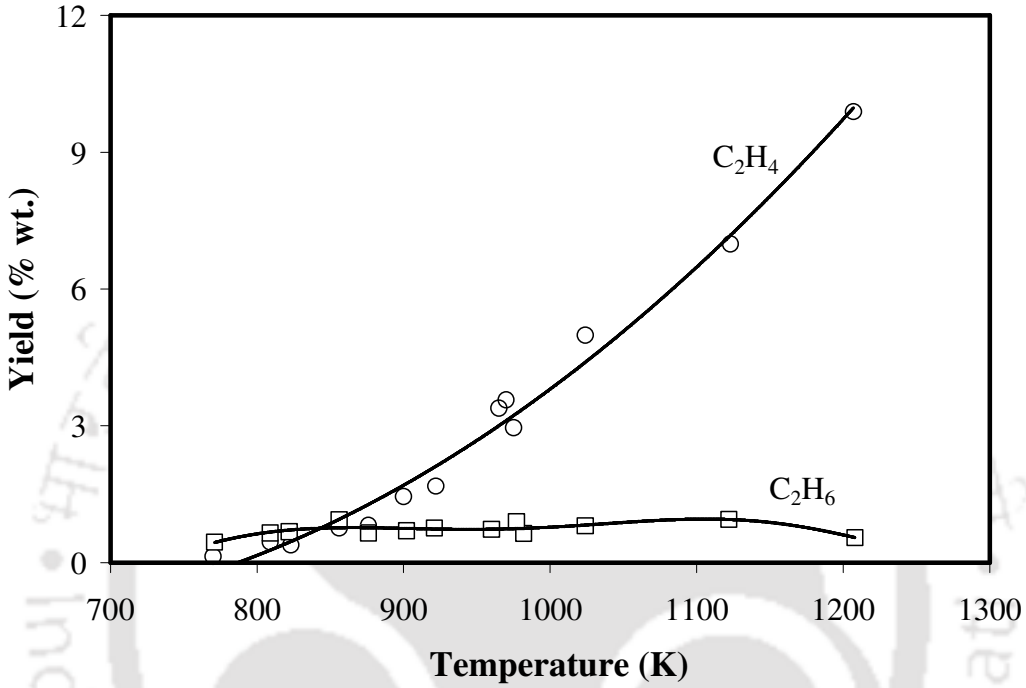

Figure 2.7 Effect of temperature on the yields of C_2H_4 and C_2H_6 [16] (adapted by permission from Elsevier Ltd., ©1979).

Table 2.1 Effect of temperature on the yield of products from a bituminous coal [12]

(adapted by permission from Elsevier Ltd., ©1989)

T (K)	Yield (wt. %)									
	H_2	CO	CO_2	H_2O	CH_4	C_2H_4	C_2H_6	C_3H_6	C_3H_8	C_4
773	0.4	2.1	1.7	4.0	3.5	0.8	0.90	0.60	0.30	0.50
873	0.4	2.0	1.6	4.3	3.6	0.9	1.00	0.80	0.30	0.60
973	0.5	2.5	1.4	4.1	4.6	1.9	1.00	1.30	0.20	0.70
1073	0.6	2.7	1.9	4.1	5.4	3.0	0.50	0.40	0.00	0.20
1173	0.9	3.4	2.0	3.6	5.7	2.0	0.05	0.03	0.00	0.04

T (K)	Yield (wt. %)							
	C_5–C_6	Benzene	Toluene	Xylene	Phenol	Cresol	Xylenol	Coke
773	0.60	0.1	0.3	0.3	0.40	0.6	0.6	1.2
873	0.70	0.2	0.3	0.3	0.40	0.6	0.6	1.4
973	0.40	0.3	0.4	0.4	0.40	0.6	0.4	2.3
1073	0.10	0.8	0.5	0.5	0.30	0.3	0.1	3.1
1173	0.03	1.3	0.2	0.2	0.04	0.1	0.0	4.9

noticeable increase in the yields of H_2, CO, CH_4, C_2H_4, C_3H_6 and benzene. It becomes apparent that the secondary decomposition reactions of Phase 2 occur due to the increase in coke formation. The yields of CO_2 and H_2O remain rather constant while the yields of the majority of the remaining gases tend to decrease steadily with temperature. The results also show that at 1173 K, only H_2, CO, CO_2, H_2O, CH_4, C_2H_4 and benzene are present to a significant level. This agrees with the observations of several other workers [10,18,19]. The decrease in the yield of the heavier products indicates that secondary decomposition has taken place. The products are not limited to hydrogen. They also contain methane and ethylene, and to a lesser extent, benzene. The formation of coke indicates that the Phase 3 decomposition has not been reached because this phase is characterized by the gradual release of H_2 and CO, and only becomes predominant at longer residence times [10]. Calkins et al. [20] examined the thermal cracking of a typical coal tar vapor by measuring the gas yields after passing the tars produced at 873 K through a tar cracker. The thermal cracking reactions were investigated by varying the cracker temperature. It was generally observed that the temperature at which cracking became apparent decreased with increasing carbon chain length. Thermal cracking of 1-butene was observed at 923 K, while for methane, the minimum cracking temperature was ~1273 K. It was interesting to note that the yield of ethylene (a major product of the thermal cracking reactions) increased consistently with temperature.

From the foregoing discussion, it can be concluded that the trends observed in the yield and the distribution of the products of devolatilization with variation of temperature can be rationalized using the mechanisms proposed by Solomon et al. [3], and Hesp and Waters [10] for the primary and secondary decomposition reactions.

2.2.3.2 Effect of pressure

The effect of operating pressure on coal devolatilization is most notably characterized by the decrease in the tar yield, and decrease in the total yield of the volatile matter [17,21]. Ladner [21] noted that the decrease in the yield of tar was accompanied by an increase in the yield of char. Suuberg et al. [17], and Ladner [21] have reported that the total yield of the hydrocarbon gases increased with increasing pressure, which has been supported by Gokhale et al. [22]. Further investigation into the nature of the hydrocarbon gases produced at various pressures suggests that a significant amount of additional gases is produced at the higher pressures, which can be attributed to the increase in methane formation [21,22]. This suggests that the devolatilization mechanism at the high pressures is controlled by the Stages 3 and 4 (primary), and Phase 2 (secondary) decomposition reactions. It should be noted that Phase 2 has been suggested because the increase in the total yield of char indicates that the process is in the phase of char formation.

Increase in the external pressure results in a decrease in the differential pressure existing between the pores and the external particle surface during devolatilization. This suggests that the driving force for the transport of the products out of the particle is reduced, resulting in a longer residence time in the pore structure. This is further enhanced by the decrease in the molecular diffusivity of the product species arising from the increased pressures. Ultimately, the slowdown of the transport processes within the particle extends the contact time of the products with the coal structure, and exposes them to a greater opportunity for the secondary reactions to occur. Thermal cracking reactions of the tar species along with condensation to form char predominate. This leads to the reduced yield of tar, and increased yields of the hydrocarbon gases and char. The primary species formed from the thermal

decomposition of the initial coal structure are not significantly altered by the increase in pressure. However, the effect of pressure is realized during the subsequent transformations.

2.2.3.3 Effect of heating rate

To study the effect of heating rate, one must keep the other parameters constant. Study of devolatilization can be performed in different types of reactor, but factors such as gas phase residence time and particle size must be kept constant so that the product yields are directly comparable. The most common technique that has been used for the study of the effect of heating rate is the wire mesh [17] or micro sample strip reactors [23]. Such reactors typically utilize either wire mesh grid or thin heating elements over which the coal sample is thinly dispersed to enable easy escape of the volatile products. Hence the secondary decomposition is reduced. In these types of reactors, heating rates are in the range of 100–10000 K/s. The amount of sample used in these studies is ~20 mg. Niksa et al. [23] deduced that the effect of heating rate was not uniform and was dependent on the system pressure. It was found that the increase in heating rate increased the total volatile yield *in vacuo*, and the magnitude of increase was in the range of 10–20% when the heating rate was increased from 100−1000 K/s. At higher pressures, the effect of the heating rate is less apparent and can be considered negligible. This suggests that at high pressure, diffusion processes become dominant and limit the rates of the subsequent chemical steps (viz. the Stages 3 and 4 of primary decomposition). Suuberg et al. [17] deduced that the heating rate has a negligible effect on the yields of the products. Ladner [21] reported that increase in heating rate resulted in an increase in oil and tar yields, and a decrease in the yield of char. Similar results have been reported by Peters and Bertling [24]. Their work

was carried out in a fixed bed reactor, and it is possible that the secondary reactions related to the interaction of volatiles with the adjacent char particles occurred in such a reactor. These results highlight the need for careful selection of the experimental arrangement employed.

Loison and Chauvin [25], Jones et al. [26], Eddinger et al. [27], Rau and Robertson [28], Mentser et al. [29], and Anthony et al. [30] have reported increase in volatile yield with increase in the rate of heating. The heating rate employed in these experiments were in the range of 600–50000 K/s. However, this is not feasible for the particle size used in a commercial fluidized bed combustor. Moreover, a single heating rate cannot represent the heating rate for all particles involved in a fluidized bed combustor or gasifier.

Gavalas [31] has compared the results obtained for fixed bed and fluidized bed devolatilization of coals. He found that the yield of tar increased significantly in the fluidized bed rig in comparison to the fixed bed rig. Higher heating rates are expected in a fluidized bed rig suggesting that such heating rates favor tar evolution and limit the secondary reactions. It is likely that the increased heating rate induces a more rapid release of volatiles from the particles, and accordingly there is a greater internal pressure build-up within the pore structure. This pressure build-up causes the products to be expelled from the particles more rapidly and reduces their residence time in the pore structure. This in turn limits secondary tar cracking and condensation reactions, which can explain these results. Stubington and Sasongko [32] have reported the heating rates for 2–20 mm diameter coal particles in industrial fluidized bed combustors at 150 K/s. They calculated the average heating rate from the time of entry of the particle to the bed up to the time of 95% devolatilization (i.e., 95% of the ultimate mass loss).

In an oxidizing atmosphere, there can be a large enhancement of heating rate because of combustion of volatile matter at the surface of the particle, which increases the surface temperature and hence the heating rate. Increase in heating rate induces a more rapid release of volatile matter. A rapid release of volatile matter limits the secondary reactions, thereby increasing the yield of volatiles beyond the proximate volatile content of the coal. It has been reported in the literature [33] that the rapid increase in temperature at the high heating rates decreases the residence time of volatile material. It reduces the influence of cracking and more tarry liquid is produced. However, the yield of the light hydrocarbon gases remains nearly constant. It has also been reported in the literature [33] that the increase in tar yield with increasing heating rate is greater for the low-volatile coals than for the high-volatile coals.

Ross et al. [34] measured the time required for the center of the particle to reach the bed temperature in a fluidized bed in nitrogen and air. The average heating rate was calculated. Figure 2.8 shows the variation of the average heating rate (in air at 1123 K) in fluidized bed with particle diameter. It can be observed from this figure that the average heating rate decreased with the increase in the particle diameter. The reason for this variation is that the coal is not a good conductor of heat and there exists a temperature gradient from the surface of the particle to its center. As the particle diameter increases, the distance between the surface and the center increases. Hence the heat has to travel a longer distance for large particles. Therefore, the heating rate decreases with particle diameter. With the increase in heating rate, more rapid release of volatile matter from the coal particles takes place. As a consequence, an internal pressure builds up within the pore structure.

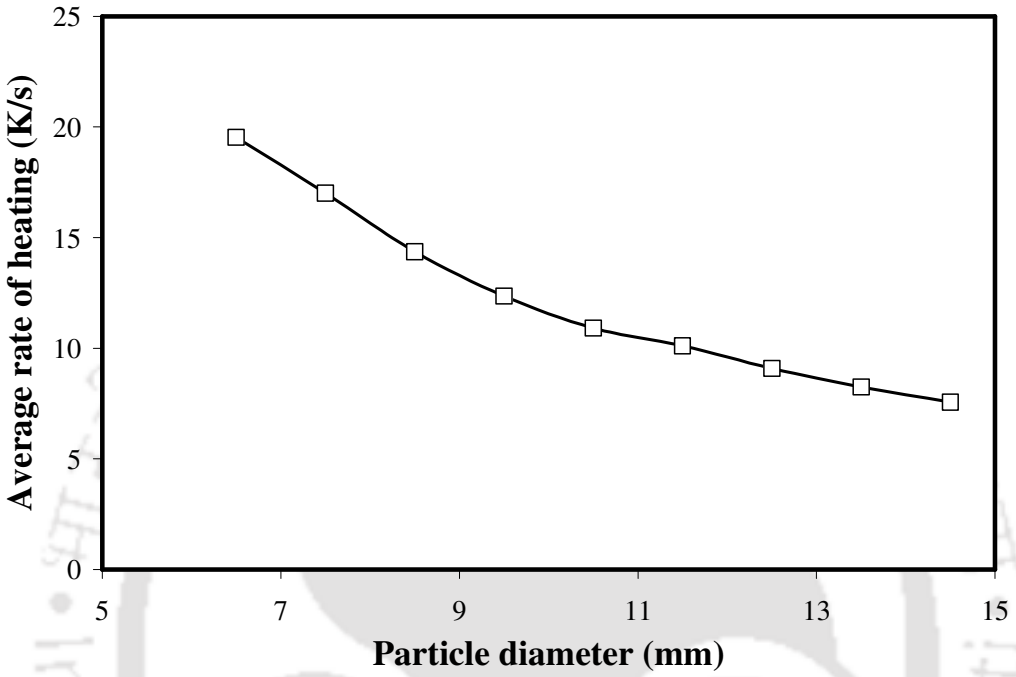

Fig. 2.8 Variation of average heating rate with particle diameter [34] (adapted by permission from Elsevier Ltd., ©2000).

This pressure causes rapid expulsion of the products from the particles, and reduces their residence time in the pores. There may be fissures on the surface of the particles and hence, they may fragment into smaller size.

2.2.3.4 Effect of particle size

It is difficult to characterize the influence of particle size on devolatilization of coal. For the large particles, a number of factors overlap with the devolatilization process. According to Smoot and Smith [35], larger particles do not heat rapidly or uniformly, so that a single temperature cannot be used to characterize the entire particle. The internal char-surface provides a site where secondary reactions occur. The pyrolysis products generated near the center of a particle must migrate outside to escape. During this migration, they may crack, condense, or polymerize, with some carbon deposition taking place. The amount of deposition increases with the increase in the size of the particle, and hence the yield of volatile matter decreases.

It is difficult to isolate the primary and secondary decomposition reactions for the devolatilization of large particles, because there is a tendency for secondary reactions to occur within the pore structure. Morris [36] investigated the effect of particle size on the total yield of volatile matter for particle size in the range of 0.038–2.36 mm. These findings support the fact that the volatile yield decreases with increasing particle size, which is in accordance with the findings of Gokhale et al. [22]. The study of Morris [36] was performed under mild rates of heating (i.e., 0.16–0.5 K/s up to 1173 K). The trend in the total yield of various gaseous species was monitored as a function of particle size for a sub-bituminous coal. The results indicate that there was a slight increase in the tar yield with increasing particle size while the

yields of H_2O, CO, CH_4, H_2 and CO_2 decreased. This can account for the observed decrease in the total yield of volatile matter. Morris [37] has studied devolatilization under similar reaction conditions for high rank coals, but at a higher final temperature. They obtained slightly different results. At temperatures of 1273 K, 1373 K and 1473 K, the methane-yield was found to increase as well as the hydrogen yield. However, the yields of CO and CO_2 were found to decrease with particle size at 1373 K and 1473K, but increased with particle size at 1273 K. This seems to suggest that the effect of particle size is dependent upon the temperature and the coal type, and a transition in the dominating mechanism may occur at ~1273 K for these coals.

Griffin et al. [38] have highlighted the effect of particle size on the tar yield. They used particles having diameter in the range of 0.063–0.075 mm, and 0.106–0.125 mm. At the heating rate of 10 K/s, the tar yield decreased by ~0.5% (by wt.) with the increase in particle size (starting from 0.063–0.075 mm to 0.106–0.125 mm). Higher heating rates (viz., 1000 K/s and 2000 K/s) resulted in a corresponding decrease in the tar yield of 3–4 % and 5–6% (by wt.), respectively. The large particles induce competition between intraparticle transport and secondary reactions within the pore structure [38]. Griffin et al. [38] proposed that the heating rate may modify the effect of particle size via any of the following reasons.

(i) Larger heating rates may increase the driving force for internal mass transfer by intraparticle concentration gradients.

(ii) Changes in heating rate may change the coal morphology and hence the accessibility, surface area, and the chemistry of the reactive interfaces, as well as the characteristic length scales for physical transport. Softening and volatile-generation may temporarily transform the relatively porous coal into a molten material consisting of bubbles,

mineral matter, and unsoftened macerals dispersed in liquid continuum, which, before resolidification, may swell into a cenosphere or other shape, which is drastically different from that of the original coal. The resultant effect can be a major decrease in the distance which the tar must travel to escape the substrate internals.

(iii) The tar yield can vary significantly when the generation and depletion of tar involve significantly different activation energies.

It can be summarized from the above discussion that the devolatilization of large coal particles is a complicated process because no single parameter such as temperature, heating rate or pressure can explain the trends observed in the evolution of volatile matter. Hence, further investigation into the devolatilization process will require careful selection of parameters.

2.2.3.5 Effect of gas velocity

There is no report in the literature on the devolatilization time of coal in a fluidized bed in an inert atmosphere and in air at a high fluidizing velocity. However, there are reports on devolatilization time at low velocities [34, 39–43]. Table 2.2 shows some of the results reported at different fluidization velocities. Several correlations are plotted in Figure 2.9 for the same range of particle size. Comparing these results with Table 2.2, it is observed that the devolatilization time decreases with the increase in velocity. In some works, however, increase in devolatilization rate with increasing superficial velocity has been reported [44]. This has been attributed to the greater convective heat transfer due to the turbulence created by the higher superficial velocity. Similar trends can be observed in air also, which are shown in Figure 2.10.

Table 2.2 Comparison of devolatilization time at different superficial velocities in nitrogen and in air

Measurement technique	Superficial velocity (m/s)	Atmosphere	Correlation, $t_v = Ad^n$		Temperature (K)
			A (s mm^{-n})	n	
Temperature response [34]	0.138	Nitrogen	8.96	0.99	1123
Volatile evolution [40]	0.330		4.15	1.03	1145
Volatile evolution [39]	0.217		9.77	1.08	1123
			4.61	1.48	
			5.18	1.23	
Temperature response [34]	0.138	Air	4.43	1.16	
Flame extinction time [34]	0.138		1.65	1.52	
Flame extinction time [41]	0.100		1.84	1.50	
Flame extinction time [42]	0.312		1.35	1.61	
CO_2 profile [43]	N/A		1.48	1.72	

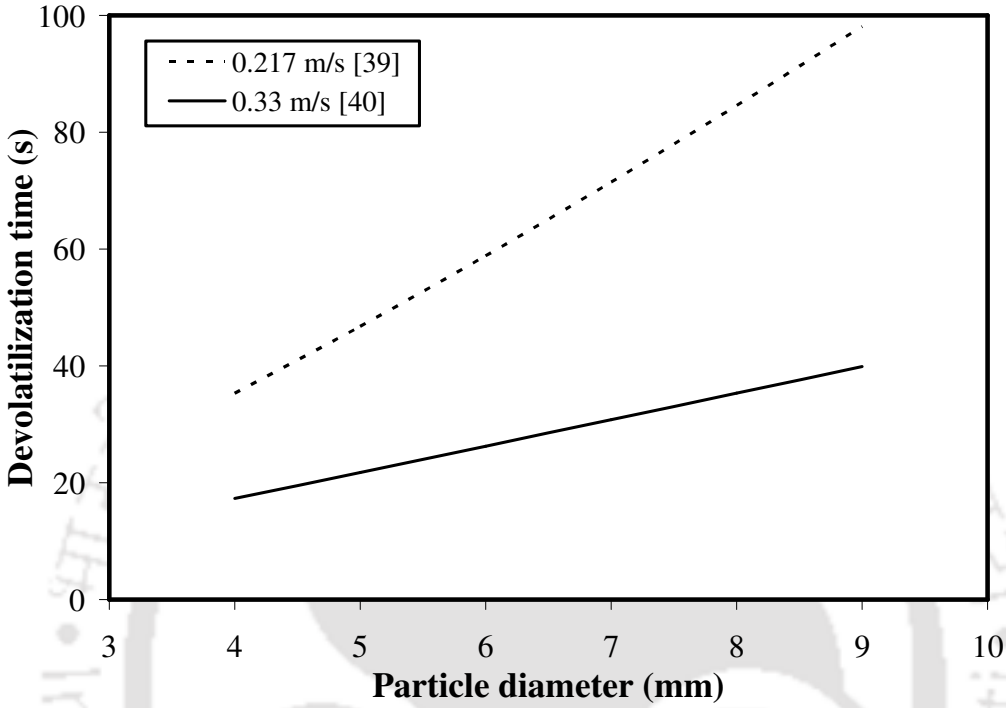

Figure 2.9 Comparison of devolatilization time at different fluidization velocities in nitrogen atmosphere.

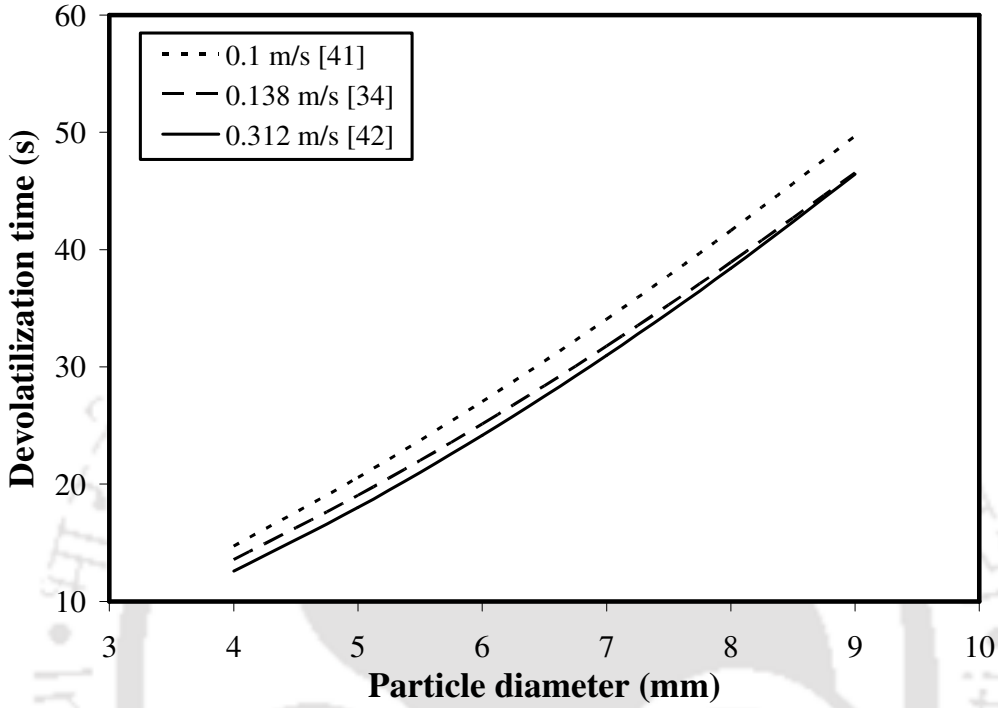

Figure 2.10 Comparison of devolatilization time at different fluidization velocities in air.

in Figures 2.11 and 2.12. The parameter *A* decreases with the increase in superficial velocity. However, the parameter *n* increases with the increase in superficial velocity, and then decreases beyond a certain velocity.

2.2.3.6 Oxygen content

Stubington et al. [45] have studied devolatilization of single coal particles having diameter in the range of 1–5 mm in a thermogravimetric apparatus. The particle was inserted into an already-hot furnace, and the flow rate of gas (viz. nitrogen and air) was maintained at 0–100 cm^3 per minute. They observed a decrease in devolatilization time with increase in temperature and oxygen concentration. This provides further evidence that the presence of oxygen in the gaseous medium helps to reduce the devolatilization time. Because the combustion of volatile matter contributes 50% (or higher) of the total energy evolved during the combustion of a high-volatile coal, it is beneficial if the entire volatile matter evolved from the coal particles burns inside the fluidized bed. However for large particles, the devolatilization time is longer. Therefore, a major fraction of the volatile matter burns in the freeboard section. The energy evolved in the freeboard is transferred by convection. Therefore, the high heat transfer coefficient of fluidized bed (which is a major advantage) cannot be utilized appropriately. If the particle size and oxygen concentration can be optimized, then it may be possible to get higher heat output (i.e., higher boiler efficiency). There is hardly any report in the literature on devolatilization time in oxygen-enriched air. There are some reports at lower oxygen concentrations [46,47], which are presented in Table 2.3 and Figure 2.13. It can be inferred from these results that the devolatilization time decreases with the increase in oxygen concentration.

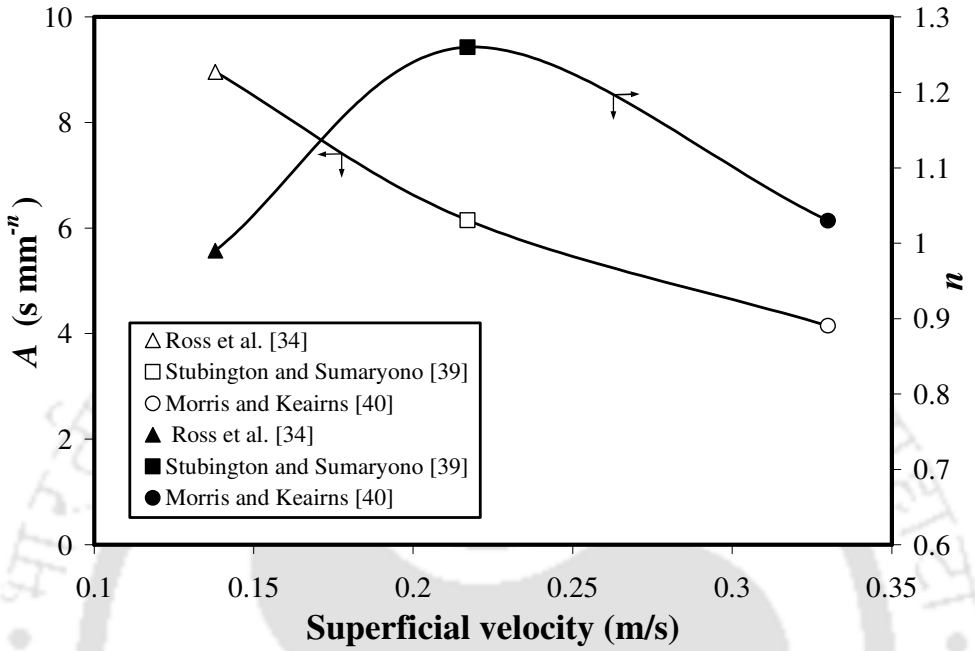

Figure 2.11 Effect of superficial velocity on parameters *A* and *n* in inert atmosphere.

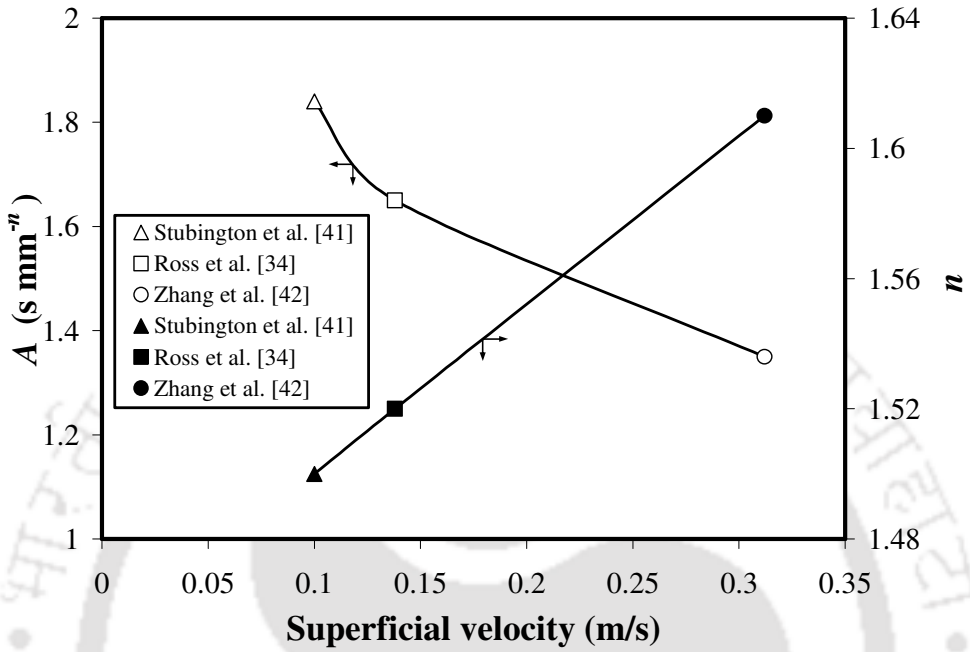

Figure 2.12 Effect of superficial velocity on the parameters *A* and *n* in air.

Table 2.3 Correlations for the devolatilization time at different oxygen concentrations

Colliery/ Coal type	Particle diameter (mm)	Bed temp. (K)	Oxygen mole fraction (x_o)	Fluidizing velocity (m/s)	Correlation* for t_v (s)
Evans/Bituminous [46]	6.7–25.5	1123	0.21	0.3–0.6	$1.31d^{1.6}$
Highvale/Bituminous [46]	8.2–34.8		0.01–0.14	0.3–0.7	$0.91d^{1.6}x_o^{-0.086}$
Lignite/Lignite [46]	10.2–36.1		0.21	0.3–0.6	$2.36d^{1.26}$
Lingan/Bituminous [46]	8.1–33.0				$1.35d^{1.6}$
Lingan/Bituminous [46]	8.1–33.0		0.0–0.14		$1.32d^{1.6}x_o^{-0.029}$
Minto/ Bituminous [46]	6.0–19.9		0.21		$1.29d^{1.6}$
Thorsby/Bituminous [47]	9.0–16.3		0.03	0.435	$21.01d^{0.75}$
			0.01		$5.17d^{1.3}$
			0.21		$2.59d^{1.36}$

* x_o represents the mole fraction of oxygen in the fluidizing gas, d represents the diameter of the coal particle, and t_v represents the devolatilization time.

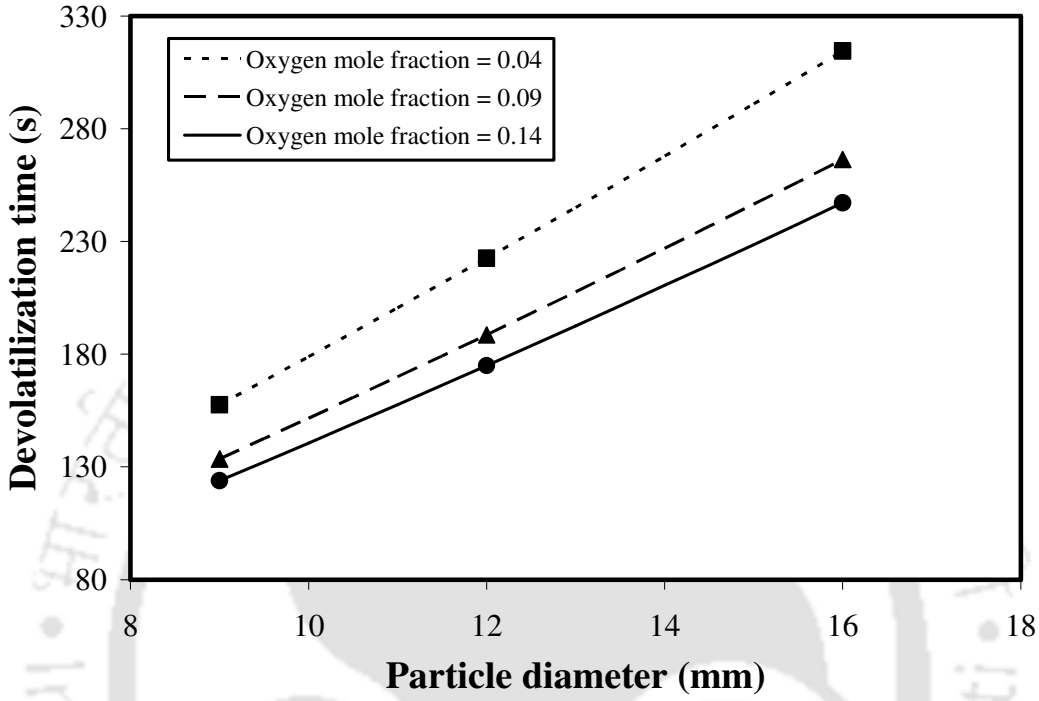

Figure 2.13 Comparison of devolatilization time at different concentrations of oxygen in the fluidizing gas [47].

2.2.3.7 Specific heat

The specific heat of coal has a direct relationship with its volatile content [48]. It can be observed from Figure 2.14 and Table 2.4 that the specific heat increases with increase in the volatile content. Specific heat can be a significant factor in the devolatilization of coal because it plays an important role in the rate of heating of coal. Increase in the heating rate induces a more rapid release of the volatile matter. The secondary reactions are reduced when there is rapid release of volatile matter. This increases the volatile yield beyond the proximate volatile content. There can be variation in the yield of volatile matter during devolatilization depending on the volatile content of the coal.

2.2.4 Implications of devolatilization for fluidized bed pyrolysis, gasification and combustion

A fluidized bed consists of a collection of particles suspended in a gas stream flowing upward at such a velocity that the particles are not carried out of the vessel but continue to circulate vigorously within the vessel. Cavities (called "bubbles") move through the suspended mass. These facilitate the vigorous circulation of the bed material. Because the bed offers resistance to flow, the drag forces, as given by the pressure drop across the bed, are sufficient to support the weight of the bed. The bed has a pseudo density and has many attributes of a liquid [49].

In combustion applications, fuel is continuously fed to a fluidized bed consisting of non-combustible particles. For solid fuels such as coal, the carbon content of the bed is no more than a few percent.

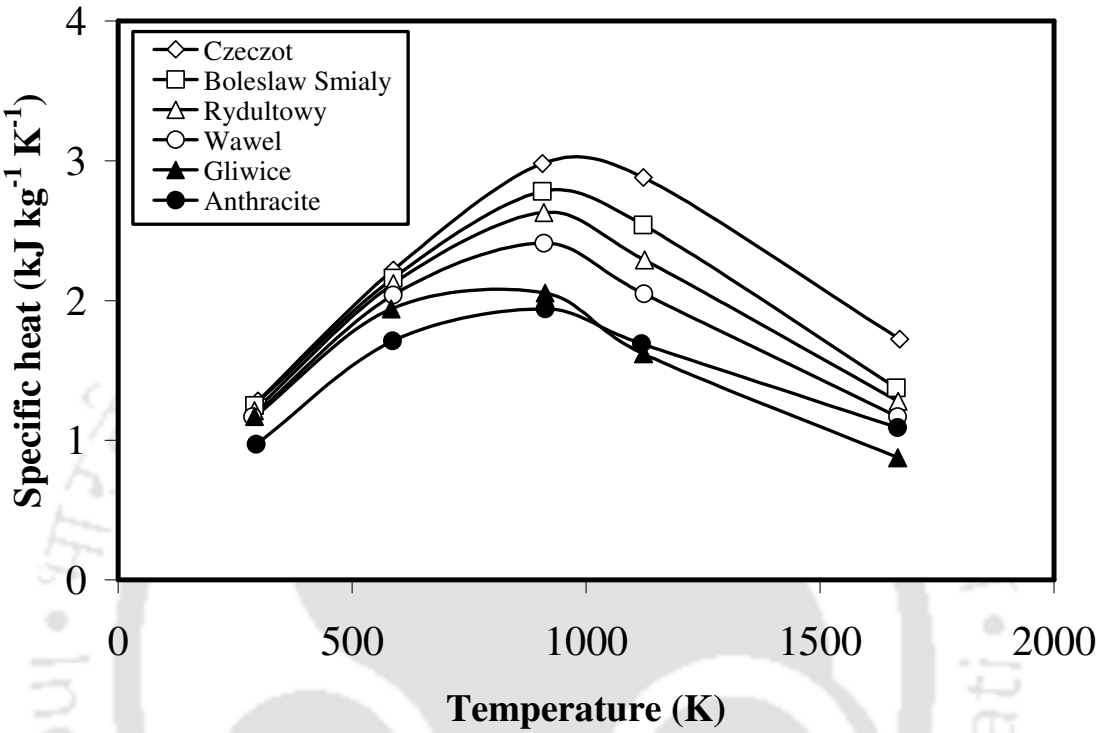

Figure 2.14 Specific heat of enriched coals having different volatile content [48]

(adapted by permission from Elsevier Ltd., © 1996).

Table 2.4 Analysis (% by wt.) of coals [48] (adapted by permission from Elsevier Ltd., © 1996)

Coal	Raw*	Enriched (by washing)*				
	A_d (%)	A_d (%)	V_{daf} (%)	C_{daf} (%)	H_{daf} (%)	O_{daf} (%)
Czeczot	32.2	3.9	41.0	69.8	4.6	22.9
Boleslaw Smialy	29.1	3.2	39.2	80.5	5.9	11.1
Rydultowy	32.5	7.2	36.0	77.2	4.8	15.1
Wawel	20.1	4.5	33.4	85.2	5.2	7.6
Gliwice	13.0	5.2	20.1	86.6	4.5	4.1
Anthracite	–	4.7	7.9	93.6	3.0	1.0

* A_d = ash content on dry basis; V_{daf} = volatile matter content on dry ash free basis; C_{daf} = carbon content on dry ash free basis; H_{daf} = hydrogen content on dry ash free basis; O_{daf} = oxygen content on dry ash free basis.

The hot bed particles act as a heat reservoir and stabilize combustion, making the fluidized bed a very desirable device for burning low-grade coals and waste materials.

The bed material consists of coal ash, limestone or sand of ~1 mm diameter. The superficial velocity through the bed is ~2–3 m/s depending on the size of the bed material and the turbulence requirement. The bed temperature is usually kept between 1000 and 1300 K. Lumped coal having a top size of 10–20 mm is fed by a screw or a spreader above the bed. Crushed coal with a top size of 6 mm is fired pneumatically under the bed. Heat is extracted through the heat exchange surfaces placed within and above the bed. The hot gases leaving the combustor contain considerable sensible heat, which can be recovered in various passes through the boiler.

Coal passes through several interactive stages before and during the burning process. These processes are: drying (with or without shrinkage), devolatilization (with or without swelling and fragmentation), combustion of volatile matter, combustion of residual char, and attrition of coal particles. Fluidized bed combustion technology offers a flexible method for coping with the solid fuels of variable quality. One of the advantages of fluidized bed combustion is that large particles can be used, which saves the cost of washing, crushing, drying and grinding. Fluidized bed combustion can handle coals having high amounts of sulfur and ash as well as the rejects from the coal washeries.

When a high-volatile coal is introduced into a fluidized bed combustor, the coal particles mix with the bed material, and they start to devolatilize simultaneously [50,51]. Coal particles undergo two overlapping stages of reaction in the fluidized bed, viz., devolatilization and char combustion. The volatile fraction of the coal contributes a significant proportion to the total amount of heat released during

combustion. The rate of heat released from the volatile combustion is determined by the rate at which they can escape from the particles and combine with the oxygen in the gas phase. Therefore, it is important to understand where and how the volatiles are released from the coal. The importance of volatile matter in the fluidized bed combustion of coals has been discussed by La Nauze [49]. Stubington et al. [41] noted that the combustion of volatiles in a fluidized bed combustor influences the design and operation via several means. It affects (i) the distribution of oxygen across the bed, (ii) the spacing of the feed points of the coal particles, (iii) the split in heat release and hence the heat transfer between the bed and the freeboard, and (iv) the release of nitrous oxide from the bed. Stubington and Linjewile [52], and Stubington et al. [45] have noted that inefficient in-bed combustion of volatile matter resulted in undesirably-high freeboard temperatures, and hence facilitated the need for larger heat transfer surfaces in the freeboard region. The evolution of volatiles within the bed is dependant upon the mixing of the coal particles [41,53]. These factors also determine the split between the volatile matter released in the bed and in the freeboard.

Borghi et al. [54] noted that the oxygen and temperature profiles in the bed were dependant on the release of volatile matter because the evolution of concentrated volatile matter in certain regions of the bed can result in areas of oxygen depletion, and possibly cause hot spots within the bed.

From the foregoing discussion, it is evident that the volatile matter should burn inside the bed so that maximum heat transfer can occur within the bed (which is the main advantage of fluidized bed combustion), and not in the freeboard region. In addition to combustion and heat transfer, evolution of polluting volatiles from the devolatilization of coal is also important from the environmental perspective. Based

on their pilot plant and laboratory-scale studies, Borghi et al. [54] reported that a major portion of the CO emission from fluidized bed is related to the release of volatile matter, and that most of the NO formed originated from the oxidation of nitrogenous groups present in the volatile matter. Borah et al. [55] have also reported high release of CO in a pilot plant study, which was reduced by the introduction of secondary air for combustion in the freeboard. Agarwal and Wildegger-Gaissmaier [56] have suggested that the volatile products contribute significantly to the release of CO and NO in the fluidized beds. The relation between the volatile matter present in coal and the emission of NO_x has been supported by Stubington and Chan [57]. Johnson [58] emphasized this by stating that the secondary reactions are quite different for the nitrogen present in the char and the nitrogen present in the volatile matter. Garcia-Labiano et al. [59] noted that a large part of the sulfur present in the parent coal is released during devolatilization. The forms of sulfur present in the coal and the atmosphere during pyrolysis dictate the volatile matter evolved during devolatilization. Hence it is apparent that the optimal design of fluidized bed combustor and development of pollution control strategy depend upon the proper understanding of the mechanism of devolatilization in fluidized bed.

2.2.5 Devolatilization experiments in inert conditions

Several investigators have examined devolatilization of large coal particles in an inert atmosphere. Zhang et al. [42] studied devolatilization and combustion of single coal particles having size in the range of 5–50 mm in a laboratory-scale fluidized bed reactor. They employed the minimum fluidization velocity corresponding to 0.5 mm diameter sand particles. Nitrogen and air were used as the gaseous media. They concluded that devolatilization of large coal particles is a strongly non-isothermal

process. The total mass-loss during devolatilization differed significantly from the proximate volatile content of the original coal. They also observed that the entire volatile matter present in the coal did not release during devolatilization.

Peeler and Poynton [60] studied devolatilization of single coal particles of size in the range of 1.4 to 29 mm under simulated fluidized bed conditions at 1173 K in nitrogen atmosphere. The superficial gas velocity was maintained at 0.25 m/s. They studied nine coals ranging from sub-bituminous to semi-anthracite. The devolatilization rate was represented by a reaction having order in the range of 0.4–0.6.

Stubington and Sumaryono [39] showed that the ratio of the extent of devolatilization/proximate volatile content varied between 0.95 and 1.15 for 3−11 mm diameter coal particles. They studied three Australian coals of volatile matter ranging from 19.4 to 43.5% (by weight) in nitrogen atmosphere at 1023, 1123 and 1223K. Zhang et al. [61] have reported similar results regarding the yield of volatile matter at 1123 K in a fluidized bed for 5–28 mm diameter Canadian coals.

From the survey of literature presented in this section, it is evident that the yield of volatile matter for the large particles is higher than the proximate volatile content of the coal. To determine the devolatilization time, it is necessary to consider the total loss of volatile matter of each particle (after deduction of the moisture content of the coal), and the time taken for the loss.

2.2.6 Devolatilization experiments in combustion conditions

Saito et al. [62] studied devolatilization of single coal particles of diameter

ranging from 2 to 4 mm in inert and combustion atmospheres in a porcelain tube-furnace at temperatures between 1123 and 1373 K. They found that the rate of evolution of volatile matter in air was nearly double of that in nitrogen. In addition, the final loss of mass due to the release of volatile matter was much greater in air than in nitrogen. The reason proposed by them was that in combustion condition, the coal particle is closely surrounded by a cloud of volatile matter that burns in oxygen. Therefore, the coal particle is additionally heated by the surrounding flame, and the resulting higher heating rate causes increase in the amount of volatile matter released. Stubington et al. [45] studied devolatilization of single coal particles of size in the range of 1 to 5 mm in a thermogravimetric apparatus. The particle was inserted into a preheated furnace, and the flow rate of the nitrogen gas was maintained at 0–100 cm^3 per minute. These results show that the devolatilization time decreases with increase in the oxygen concentration.

Winter et al. [44] studied devolatilization and combustion of two sub-bituminous coals in three different laboratory-scale fluidized bed combustors. The particle size was 10 mm. The temperature was varied between 973 and 1223 K, the partial pressure of oxygen was varied between 0 and 10 kPa, and the fluidizing velocity was varied from 0.3 to 0.9 m/s. They have reported that the release volatile matter during devolatilization was slightly higher at the higher superficial velocities. Also, more carbon was lost with increasing fluidization velocity during devolatilization and the combustion of char was faster. These observations have been explained by the fact that at the higher fluidization velocities, there is more convective heat transfer. High oxygen concentration slightly increases the ultimate yield of

volatile matter as well as the rate of devolatilization, due to the high temperature in the volatile flame surrounding the particle. Higher fluidization velocity is likely to increase the rate of mass transfer by rapidly regenerating the film surrounding the particle. At a high fluidization velocity, the bulk concentration of volatile matter can be assumed to be equal to zero, and the concentration (of volatile matter) is equal to the concentration at the surface, which signifies more mass transfer. From the foregoing discussion, it is evident that the devolatilization time in fluidized bed is dependant on temperature, fluidization velocity, oxygen concentration and particle size.

2.2.7 Definition of devolatilization time and the different methods employed for its evaluation

Devolatilization is a general term that means removal of volatile matter from the coal matrix. No distinction is made regarding the nature of the gaseous surroundings, i.e., inert (pyrolysis) or oxidizing (combustion) atmosphere. Even under oxidizing conditions pyrolysis-like condition prevails at the initial stage when the devolatilization rate is much higher than the oxidation of the char particle. Hence this period can be called devolatilization. The time taken for devolatilization in a fluidized bed combustor is very significant. The devolatilization time must be compared with the particle mixing time in order to decide the appropriateness of the various models proposed for combustion of volatile matter [50]. Most of the workers have inferred devolatilization time from the occurrence of a volatile diffusion flame around the individual particles [63–66]. However, these methods underestimate the total devolatilization time because devolatilization may still occur after the extinction of the flame. Devolatilization time has also been measured from the concentration

profiles of the evolved gases [40]. But there exists a time lag between the volatile evolution and its measurement. Also, the trace amounts of volatile matter during the end of devolatilization may be undetected due to the dilution affect. Since direct measurements of weight cannot be made if the particle is surrounded by the inert particles, thermogravimetric techniques have been applied to the stationary particles [42,56,62]. From these data, the devolatilization time has been defined in different ways (e.g., as the time for 90% devolatilization [45], or the time for 95% devolatilization [60].

Earlier works on the determination of devolatilization time may be divided into two categories depending upon the mobility of the particles in the reactor. In the first category of works, the particles were injected into a hot fluidized bed and allowed to move freely within the bed. Therefore, their immediate environment was similar to the environment in a fluidized bed combustor. In the second category, the particles were dropped into a hot reactor, and the particle either remained stationary in the hot zone on a fixed support, or was suspended in a hot gas stream. Therefore, there were no fluidized particles in contact with the devolatilizing coal particle. In the works belonging to the first category in inert atmosphere, intermittent quenching and removal of coal particles from the bed and determination of volatile matter have been employed [40]. In this procedure, the devolatilization continues during quenching till its temperature comes down significantly. In air, the flame extinction time was taken into consideration. It is defined as the time counted from the injection of the particle into the bed up to the moment a visible volatile flame is extinguished above the bed. The flame extinction time is possible only at the lower gas velocities. At the high gas velocities, the diffusion flame may not be visible. Moreover, the end point may not be

visible as the evolution of volatile matter considerably reduces during the end of devolatilization.

2.3 Models of coal devolatilization

There are two types of model which are employed to describe coal devolatilization, viz. “empirical” and “structural” models. In the literature, the empirical models have been extensively developed for both pulverized and large coal particles. An empirical model is generally useful in predicting the rate of volatile evolution and the composition of the devolatilization products for the coals for which it has been developed. On the other hand, the structural models are based upon the thermal decomposition process. These models deal with the structure of the parent coal, and require the knowledge of the functional groups present in the coal and their nature. The structural models are generally complex, because they depend on the chemical structure of the parent coal.

2.3.1 Structural models for coal devolatilization

A number of structural models have been developed such as the “Chemical Percolation Devolatilization (CPD) model” [67–69] and “Functional Group-Depolymerization, Vaporization and Cross-linking (FG-DVC) model” [3,70,71].

2.3.1.1 Chemical Percolation Devolatilization (CPD) model

The CPD model describes the coal conversion behavior based on the chemical structure of the parent coal [67]. Using the structure as the starting point, percolation lattice statistics is employed to estimate the yield and mass distribution of the devolatilization products evolved from the break-up of the macromolecular coal

network. The model requires three groups of input parameters: (i) coal-independent kinetic parameters, which are the rate parameters, (ii) coal-dependent parameters, which are used to define the chemical structure of the parent coal, and (iii) an elemental analysis of the parent coal. The kinetic parameters in the model are assumed to be identical for all coals, and the variation in the devolatilization behavior for different coals is dependant on the structural parameters [68,69].

The kinetic rate parameters for the CPD model are derived from experimental techniques such as TG-FTIR and GC-MS, and from thermochemical kinetics. Coal structure parameters are derived directly from the NMR data, except for the initial fraction of char bridges, which is assumed to be zero for high-rank coals, and determined empirically for low-rank coals by comparing the CPD model predictions with experimental tar yields [69]. In order to simulate the breakdown of the coal structure, bonds are randomly broken within the coal macromolecule depending upon the thermal treatment of the coal and the corresponding probability of the given bond being ruptured. In this manner, the formation of loose aromatic ring clusters, which lead to tars, and light gases from the labile bridges and side chains, which result in the formation of light gas can be predicted [71].

2.3.1.2 Functional Group-Depolymerization, Vaporization and Cross-linking (FG-DVC) model

The FG-DVC model starts with the parent coal structure as in the CPD model, but the tar formation and the behavior of the char produced during devolatilization are more extensively treated. In the FG-DVC model, linear oligomers of aromatic ring clusters (having a molecular weight distribution defined by an average and a standard deviation) are linked by cross-links per monomer. Cross links are defined as the

points at which more than two attachments connect one cluster to another. During thermal decomposition, bridges are broken and the cross-links are formed. The molecular weight of the resultant oligomers is calculated by randomly distributing these changes [71].

The devolatilization products as per the FG-DVC and CPD models differ. The CPD model assumes that all molecules which are not attached to the macromolecular network are essentially evolved as tars. In the FG-DVC model, mass transport equations have been included. It has been assumed that the molecular weight-dependent vapor pressure controls whether the molecules are released into the gas phase or not. These gases escape by convective transport from the coal particle. Thus, the tar fraction comprises of aromatic ring clusters, which are released during decomposition, and this belongs to the lower molecular weight region with sufficiently high vapor pressures. The remaining fraction is trapped within the coal as either solvent-extractable material or as liquids.

2.3.1.3 Advantages and disadvantages of structural models

Structural models such as the CPD and FG-DVC models are useful in predicting the production of tar, char and evolution of light gas during the devolatilization of coal [3,4,68,69,71]. The FG-DVC model is able to predict behavior such as cross-linking, hydrogen utilization and fragmentation during devolatilization [3,4,71]. It can also predict the swelling and solubility of coals, and can distinguish between the evolved tars and solvent-extractable liquid products generated during devolatilization with reasonable success [3,4,71]. Both of these models utilize data generated by instrumental analysis. The quantity of data required is significant and these are highly coal specific. This restricts the scope of the model to a unique type of

coal, which corresponds to the input data. The major success of these models is in the prediction of the trends of tar and char production with operating conditions. This is due to their ability to consider the structural aspects of coal. With the inclusion of mass transfer process, the FG-DVC model has become more complex. The CPD model is computationally more efficient than the FG-DVC model in its treatment of coal structure [71], and it is also less complex.

2.3.2 Empirical models for coal devolatilization

Empirical models adopt a less sophisticated approach than the structural models. They refer to a global approach to the modeling of devolatilization. Empirical models were originally developed to model the devolatilization of pulverized bituminous coal particles. A general review of the empirical modeling approaches is given in the following sections.

2.3.2.1 Single first-order Arrhenius models

Since the complex chemical reactions and transport processes occurring within the coal particle are not well understood, a number of simple first-order Arrhenius-type models have been developed. Such models have been used by van Krevelin et al. [72], Stone et al. [73], Howard and Essenhigh [74], Wiser et al. [75], Badzioch and Hawksley [76], Anthony et al. [30], Kobayashi et al. [77], Maloney and Jenkins [78], Niksa et al. [23], Sandhu and Hashemi [79], Gokhale et al. [22], Fu et al. [80], and Sharma et al. [81] for coals ranging from bituminous to brown types. The general form of the model can be represented by the following equation.

$$\frac{dV}{dt} = k(V^* - V) \tag{2.1}$$

where V^* is the ultimate yield of volatile matter (kg/kg dry coal). $V \to V^*$ as $t \to \infty$. The kinetic rate constant k varies with temperature following the Arrhenius equation,

$$k = k_0 \exp(-E/RT) \tag{2.2}$$

Experimental support for these models has been presented in a number of works. The kinetic parameters of these models are extremely sensitive to the operating conditions, and vary significantly to produce a reasonably good fit. These models are therefore limited in their application to the conditions at which supporting experimental data are available.

2.3.2.2 Models with m^{th}-order kinetics

The m^{th}-order reaction models use the following devolatilization equation.

$$\frac{dV}{dt} = k(V^* - V)^m \tag{2.3}$$

According to Peeler and Poynton [60], the m^{th}-order model is extremely useful in predicting the mass-loss data for particles in the size range of 1.4 to 29 mm, and ranging from sub-bituminous to semi-anthracite coals. In their work, the data were recorded by suspending the coal particles from a microbalance into a hot stream of nitrogen gas, and the transient weight loss profiles were analyzed. The experiments were conducted at 1173 K and the rate constant, k, was related to the particle size as,

$$k = p\hat{d}^q \tag{2.4}$$

where $\hat{d}$ is the geometric mean coal particle diameter, and p and q are coal-dependant parameters. The reaction-order was reported to vary between $m = 0.4$ and $m = 0.6$ depending upon the type of coal [60].

In contrast to the reaction orders reported by Peeler and Poynton [60], Li et al. [82] have reported reaction orders between $m = 1.27$ and $m = 4.5$. However, the particles studied by them were small. In addition, they had used a thermogravimetric apparatus with a varying heating rate. The lower reaction orders seems to indicate that devolatilization of large coal particles becomes less kinetically controlled as the particle size increases, and phenomena such as heat and mass transfer become increasingly important.

2.3.2.3 Competing reaction models

The inability of the single first-order and m^{th}-order reaction models to describe the devolatilization behavior of coals over a wide range of operating conditions has led to the use of more sophisticated reaction models such as the "competing reaction" models. Doolan et al. [83] combined the single first-order volatile evolution model with a similar term describing the decomposition of volatile matter according to the following equation.

$$\frac{dV_i}{dt} = k_{vi}\left(V_i^* - V_i\right) - k_{di}V_i \tag{2.5}$$

where V_i represents the yield of species i and V_i^* represents the ultimate yield of the same species. k_{vi} denotes the rate of evolution of species i, which is proportional to

the amount of species i remaining in the coal, i.e., $\left(V_i^* - V_i\right)$. k_{di} refers to the decomposition rate of species i, which is related to the amount of species i which formed V_i. A similar approach was used by Cliff et al. [19], and Yang and Wang [84]. Jamaluddin et al. [85] have compared the effectiveness of several models. They have reported that the competing reaction model was able to provide better predictions over a range of heating rates. It predicted the final temperature more accurately than the single first-order reaction model. It also performed better in predicting the yields of various volatile species at the higher temperatures.

2.3.2.4 Multiple parallel reaction models

In multiple parallel reaction models, a particular volatile species is evolved via a number of simultaneous, independent, first-order reactions. Each species is derived from a number of sources within the coal structure, each of which yields the species according to differing kinetics. Tomeczek and Kowol [86] proposed that individual volatiles can be derived via several (e.g., four to six) simultaneous, independent, first-order reactions. Several models have been developed in which coal devolatilization has been described by infinite number of simultaneous, independent, first-order reactions [31,54,87–96]. A significant amount of work has been done using the multiple parallel reaction models for large particles. Agarwal et al. [87] concluded that the modeling approach involving multiple parallel reactions was able to predict both mass-loss and evolution of individual gaseous species from large coal particles with reasonable accuracy. However, as the time increases, the computational time necessary for calculating the volatile yield becomes increasingly larger.

2.3.2.5 Shrinking-core model

It has been demonstrated in the literature [97] that devolatilization of coal can be explained by the shrinking-core model assuming no change in the size of the particles. Chern and Hayhurst [97] performed devolatilization studies with bituminous and lignite coals in a fluidized bed in nitrogen atmosphere by withdrawing coal particles from the hot bed before any fragmentation could occur. The particle was then quenched in nitrogen, weighed, sectioned and examined in a microscope. Apart from the final stages of devolatilization, these particles had a central core of virgin coal, surrounded by the char. The boundary between these two regions was sharp, indicating a shrinking core. The velocity of the movement of the boundary was found to be constant. This conclusion was confirmed by the measurement of the particle's mass with time. They developed a model involving heat transfer from the fluidized bed to the exterior of the coal particle, followed by heat conduction through the outer layer of the char to provide the enthalpy required for the endothermic thermal decomposition in the moving reaction zone. This model predicts that apart from the very beginning and the end of devolatilization, there is an almost constant velocity of the shrinking core of the raw coal. They concluded that it is possible to describe the generation of volatile matter with a simple shrinking-core model, at least for the early stages of pyrolysis. They also concluded that although their model matched and described the observations well for bituminous and lignite coals, it is not suitable for the anthracite coals, which chatter into many pieces soon after entering the hot fluidized bed.

Chern and Hayhurst [97] showed that for $k_t/(ah) = 0.5$ (where k_t is the thermal conductivity of coal, a is the radius of the coal particle and h is the convective

heat transfer coefficient), the ratio of the reacting core radius/initial radius varied linearly with the ratio of time/time of devolatilization. This indicates that at $k_t/(ah) = 0.5$, the reaction front proceeds at a constant velocity, and the intercept of the linear portion of the curve of r_c/a versus t/t_v is unity at $t = 0$. For $k_t/(ah) < 0.5$, the plot gives a negative intercept at $t = 0$. For $k_t/(ah) > 0.5$, the plot gives a positive intercept at $t = 0$. The swelling of coal has not been considered in their work. Also, the sensible heat to raise the temperature of the coal particle to the point of devolatilization was not considered because it is a rather small quantity in comparison with the enthalpy of devolatilization.

2.3.2.6 Advantages and disadvantages of empirical models

The simplicity of the empirical coal devolatilization models is due to the assumption that the entire process can be represented by a simplified overall reaction rate on a global scale, rather than consideration of the breaking of individual bonds within the coal macromolecule. The second advantage is that extensive data related to the structure of the coal is not required in these models. The data necessary to supplement the empirical models can be obtained with far simpler techniques than that required for the structural models (mainly due to the type of data involved).

Empirical models have no distinct relation with the parent coal structure, which is a limitation of these models for rigorous modeling of devolatilization. Other coal properties related to the structural changes occurring during devolatilization (e.g., solvent swelling) cannot be predicted by these models. Empirical models are less effective in predicting the yields of tar, char and volatile gases.

2.4 Modeling of devolatilization of large coal particles

Modeling of large coal particles differs from that of the pulverized coal particles because the temperature of the particles can no longer be assumed to be uniform during heating. This is particularly relevant in fluidized bed systems where high heat transfer rates deliver heat rapidly to the particle surface. Longer devolatilization time may result due to the internal heat conduction limitation, which results in a slower transfer of heat to the center of the particle.

2.4.1 Kinetic modeling

The most significant change in the devolatilization mechanism for large particles relevant to fluidized bed pyrolysis is due to the secondary devolatilization reactions. During this stage, the primary volatiles undergo cracking, condensation, polymerization and char formation reactions while transported out of the particle. The FG-DVC model for coal devolatilization is the most comprehensive structural model which incorporates the transport processes into the overall model. However, it has a major limitation because of the complexity of the model. Empirical models present less complicated solution, and therefore, may be suitable for integration into the devolatilization models for large particles. This has been done in several studies [39,59,60,80,86–89,91,94,98]. These studies have shown reasonable success in predicting the total mass-loss and evolution of individual volatile species from the large coal particles during devolatilization. This indicates their suitability for this application.

2.4.2 Modeling of mass transfer

Winter et al. [44] have studied devolatilization of coal at fluidization velocities

in the range of 0.3 to 9 m/s. They reported that with increase in the fluidization velocity, there is increase in the loss of carbon during devolatilization. This has been attributed to the higher rate of transfer of oxygen to the surface of the particle. Relatively few studies on mass transfer in the devolatilization of large particles have been reported. Peters and Bertling [24] studied the pyrolysis of coking coals in the size range of 1 to 15 mm. They pointed out that larger temperature gradients could exist within the particle for high external heat transfer co-efficient (as would be encountered in fluidized beds). They interpreted their results by comparing the devolatilization process to the drying of coke, and developed a correlation for fractional release of volatile matter by relating it with the temperature of pyrolysis and particle size as shown by the following equation.

$$\frac{V}{V^*} = 3\times10^{-4}\left(T_b - 330\right)d^{-0.26}t \tag{2.6}$$

where T_b is the temperature of the fluidized bed, d is the particle diameter, t represents time, V is the volatile matter evolved at time t, and V^* is the total volatile matter evolved. Essenhigh [63] studied the devolatilization of particles having diameter in the range of 0.295 to 4.76 mm in a non-fluidized combustion system. As per this model, the volatiles form a drop, and the volatile matter transfers from the drop surface to the outside. Assuming mass transfer as the rate-limiting step, he proposed that the time required for devolatilization could be predicted by the following equation.

$$t_v = \sigma_d\left(\frac{\eta}{8Pc_a}\right)\left(\frac{V^*}{100}\right)d^2 \tag{2.7}$$

where P is the permeability of the char, η is the viscosity of the flowing volatiles, σ_d is the density of the drop liquid, and c_a is the constant of proportionality between the rate of transformation of liquid to vapor at the surface of the drop of volatile matter (per unit area) and the rate of shrinkage of the drop.

La Nauze [49] has proposed a model for devolatilization assuming internal mass transfer as the rate-controlling step. The total time for volatile evolution was shown to follow the equation,

$$t_v = \frac{\rho_v d^2}{24Dc} \tag{2.8}$$

where ρ_v is the molar density of volatile matter in the particle, D is the effective diffusivity of the volatiles through the char of diameter d, and c is the mean value of concentration of volatiles assuming a uniform distribution of potential volatile species throughout the particle. The approach of LaNauze [49] is similar to that of Essenhigh [63], except in the treatment of the diffusion process. Gavalas [31] has studied the effect of mass transfer limitation on the pyrolysis of coal. Jüntgen and van Heek [99] have presented two different models that take into account the transitions from reaction-controlled pyrolysis (independent of particle size) to diffusion or heat transfer-controlled pyrolysis (dependant on particle size and rate of heating). They suggested that under fluidized bed combustion process, where the rate of heating is ~1273–10273 K/min, the process is reaction-controlled when the particle is < 0.6 mm.

2.5 Conclusions

1. The devolatilization process is related to the structure of the coal. The influence of various operating parameters on devolatilization can be analyzed based on the structural and mechanistic models.
2. The trends observed in the yield and distribution of the products of devolatilization with variation of temperature can be rationalized using the mechanisms proposed by Solomon et al. [3], and Hesp and Waters [10].
3. Higher heating rates are expected in a fluidized bed rig, which suggests that such heating favors tar evolution and limits the secondary reactions. It is likely that the increased heating rate induces a more rapid release of volatile matter from the particles, and accordingly there is a greater internal pressure build-up within the pore structure. This pressure build-up causes the products to be expelled from the particles more rapidly, and reduces their residence time in the pore structure. This limits secondary tar cracking and condensation reactions.
4. There are reports in the literature on devolatilization time at the low gas velocities. The devolatilization rate increases with the increase in superficial gas velocity. In commercial fluidized beds, higher fluidization velocities are employed. Therefore, this aspect needs systematic investigation.
5. Larger particles do not heat rapidly or uniformly. Therefore, a single temperature cannot be used to characterize the entire particle. The devolatilization of large coal particles is a complicated process because no single parameter such as temperature, heating rate or pressure can explain the trends observed in the evolution of volatile matter. Hence, further investigation into the devolatilization process will require careful selection of the parameters.

6. The devolatilization time decreases with increase in temperature and oxygen concentration. This provides evidence that the presence of oxygen in the gaseous medium helps to reduce the devolatilization time. So far, devolatilization has not been studied at oxygen concentrations higher than that is present in air. There is a possibility of reduction in devolatilization time and increase in combustion efficiency in presence of extra oxygen.
7. It is evident from these studies that the yield of volatile matter for large particles is higher than the proximate volatile content of the coal. But there is no report on how the extent of devolatilization depends on particle size and volatile matter content.
8. The simplicity of the empirical coal devolatilization models is due to the assumption that the entire process can be represented by a simplified overall reaction rate on a global scale, rather than consideration of the breaking of individual bonds within the coal macromolecule. The second advantage is that extensive data related to the structure of the coal is not required to apply in these models. The data necessary to supplement the empirical models can be obtained with simpler techniques than that required for the structural models (mainly due to the type of data involved).
9. Empirical models have no distinct relation with the parent coal structure, which is a limitation of these models for rigorous modeling of devolatilization. Other coal properties related to the structural changes occurring during devolatilization (e.g., solvent swelling) cannot be predicted by these models. Empirical models are less effective in predicting the yields of tar, char and volatile gases.
10. The shrinking-core model predicts that apart from the very beginning and the end of devolatilization, there is an almost constant velocity of the movement of the

shrinking-core of the raw coal. Chern and Hayhurst [97] have concluded that although their shrinking-core model matched and described the observations well for bituminous and lignite coals, it was not suitable for the anthracite coals, which chatter into many pieces soon after entering the hot fluidized bed.

Notations

a	radius of coal particle, m
A	correlation constant, s mm^{-n}
A_d	ash content on dry basis, %
c	mean value of concentration of volatiles assuming a uniform distribution of potential volatile species throughout the particle, mol/m^3
c_a	constant of proportionality between the rate of transformation of liquid to vapor at the surface of the drop of volatile matter (per unit area) to the rate of shrinkage of the drop of volatile matter, $kg^2\ m^{-2}\ s^{-2}$
C_{daf}	carbon content on dry ash free basis, %
d	diameter of the coal particle, m
$\hat{d}$	geometric mean diameter of coal particle, m
D	effective diffusivity of the volatile matter, m^2/s
E	activation energy, J/mol
h	convective heat transfer coefficient, W m^{-2} K^{-1}
H_{daf}	hydrogen content on dry ash free basis, %
k	rate constant, s^{-1}
k_0	frequency factor, s^{-1}
k_{di}	decomposition rate of species i, s^{-1}
k_t	thermal conductivity of coal, W m^{-1} K^{-1}

k_{vi}	rate of evolution of species i, s^{-1}
m	reaction order
n	correlation parameter
O_{daf}	oxygen content on dry ash free basis, %
p	constant, s^{-1} m^{-q}
P	permeability of the char, m^2
q	constant
r_c	radius of the unreacted core of the coal particle, m
R	universal gas constant, J mol^{-1} K^{-1}
t	time, s
t_v	devolatilization time, s
T	temperature, K
T_b	temperature of the fluidized bed, K
V	volatile matter content at time t, kg/kg of dry coal
V^*	ultimate yield of volatile matter, kg/kg of dry coal
V_{daf}	volatile matter content on dry ash free basis, %
V_i	yield of species i, kg/kg of dry coal
V_i^*	ultimate yield of species i, kg/kg of dry coal
x_o	mole fraction of oxygen

Greek symbols

η	viscosity of the flowing volatile matter, Pa s
σ_d	drop density, kg/m^3

ρ_v	molar density of volatiles in the particle, mol/m^3

Reference

1. E. Stach, M.-Th. Mackowsky, M. Teichmüller, G.H. Taylor, D. Chandra, R. Teichmüller, Stach's Textbook of Coal Petrology, Gebrüder Borntraeger, Berlin, 1982.
2. J.H. Shinn, From coal to single-stage and two-stage products: a reactive model of coal structure, Fuel 63 (1984) 1187–1196.
3. P.R. Solomon, D.G. Hamblen, M.A. Serio, Z.-Z. Yu, S. Charpenay, A characterization method and model for predicting coal conversion behaviour, Fuel 72 (1993) 469–488.
4. P.R. Solomon, T.H. Fletcher, R.J. Pugmire, Progress in coal pyrolysis, Fuel 72 (1993) 587–597.
5. K.H. van Heek, W. Hodek, Structure and pyrolysis behaviour of different coals and relevant model substances, Fuel 73 (1994) 886–896.
6. H. Jüntgen, Review of the kinetics of pyrolysis and hydropyrolysis in relation to the chemical constitution of coal, Fuel 63 (1984) 731–737.
7. M.A. Serio, D.G. Hamblen, J.R. Markham, P.R. Solomon, Kinetics of volatile product evolution in coal pyrolysis: experiment and theory, Energy and Fuels 1 (1987) 138–152.
8. J. Hayashi, K. Nakagawa, K. Kusakabe, S. Morooka, Change in molecular structure of flash pyrolysis tar by secondary reaction in a fluidized bed reactor, Fuel Processing Technology 30 (1992) 237–248.
9. T.S. Pather, W.A. Al-Masry, The influence of bed depth on secondary reactions during slow pyrolysis of coal, Journal of Analytical and Applied Pyrolysis 37 (1996) 83–94.
10. R. Hesp, P.L. Waters, Thermal cracking of tars and volatile matter from coal carbonization, Industrial and Engineering Chemistry Product Research and Development 9 (1970) 194–202.
11. S. Niksa, Modeling the devolatilization behavior of high-volatile bituminous coals, Proceedings of the 22nd International Symposium on Combustion, The Combustion Institute, Pittsburgh, 1988, pp. 105–114.

12. W.-C. Xu, A. Tomita, The effects of temperature and residence time on the secondary reactions of volatiles from coal pyrolysis, Fuel Processing Technology 21 (1989) 25–37.
13. H.N. Stiles, R. Kandiyoti, Secondary reactions of flash pyrolysis tars measured in a fluidized bed pyrolysis reactor with some novel design features, Fuel 68 (1989) 275–282.
14. A. Jess, Mechanisms and kinetics of thermal reactions of aromatic hydrocarbons from pyrolysis of solid fuels, Fuel 75 (1996) 1441–1448.
15. W.-C. Xu, A Tomita, Effect of temperature on the flash pyrolysis of various coals, Fuel 66 (1987) 632–636.
16. R.J. Tyler, Flash pyrolysis of coals. 1. Devolatilization of a Victorian brown coal in a small fluidized-bed reactor, Fuel 58 (1979) 680–686.
17. E.M. Suuberg, W.A. Peters, J.B. Howard, Product compositions and formation kinetics in rapid pyrolysis of pulverized coal – implication for combustion, Proceedings of the 7th International Symposium on Combustion, The Combustion Institute, Pittsburgh, 1979, pp. 117–130.
18. R.J. Tyler, Flash pyrolysis of coals. Devolatilization of bituminous coals in a small fluidized-bed reactor, Fuel 59 (1980) 218–226.
19. D.I. Cliff, K.R. Doolan, J.C. Mackie, R.J. Tyler, Products from rapid heating of a brown coal in the temperature range 400–2300^{o}C, Fuel 63 (1984) 394–400.
20. W.H. Calkins, H. Hagaman, H. Zeldes, Coal flash pyrolysis. 1. An indication of the olefin precursors in coal by CP/MAS ^{13}C n.m.r. spectroscopy, Fuel 63 (1984) 1113–1118.
21. W.R. Ladner, The products of coal pyrolysis: properties, conversion and reactivity, Fuel Processing Technology 20 (1988) 207–222.
22. A.J. Gokhale, T.V. Vasudevan, R. Mahalingam, Parametric studies on devolatilization of a subbituminous coal in a reactive gas environment, Fuel 65 (1986) 1670–1676.
23. S. Niksa, L.E. Heyd, W.B. Russel, D.A. Saville, On the role of heating rate in rapid coal devolatilization, Proceedings of the 20th International Symposium on Combustion, The Combustion Institute, Pittsburgh, 1985, pp. 1445–1453.
24. W. Peters, H. Bertling, Kinetics of the rapid degasification of coals, Fuel 44 (1965) 317–331.

25. R. Loison, R. Chauvin, Rapid pyrolysis of coal, Chimie et Industrie 91 (1964) 269–275.
26. J.F. Jones, M.R. Schmid, R.T. Eddinger, Fluidized-bed pyrolysis of coal, Chemical Engineering Progress 60 (1964) 69–73.
27. R.T. Eddinger, L.T. Friedman, E. Rau, Devolatilization of coal in a transport reactor, Fuel 45 (1966) 245–252.
28. E. Rau, J.A. Robertson, The use of the microsample strip furnace in coal research, Fuel 45 (1966) 73–80.
29. M. Mentser, H.J. O'Donnell, S. Ergun, Rapid thermal decomposition of bituminous coals, American chemical Society (preprint of papers), Division of Fuel Chemistry 14 (1970) 94–100.
30. D.B. Anthony, J.B. Howard, H.C. Hottel, H.P. Meissner, Rapid devolatilization of pulverized coal, Proceedings of the 15th International Symposium on Combustion, The combustion Institute, Pittsburgh, 1975, pp. 1303–1317.
31. G.R. Gavalas, Coal Pyrolysis [in Coal Science and Technology (Editor: L. L. Anderson), vol. 4], Elsevier, New York, 1982, pp. 66–69.
32. J.F. Stubington, D. Sasongko, On the heating rate and volatile yield for coal particles injected into fluidised bed combustors, Fuel 77 (1998) 1021–1025.
33. P. Arendt, K.-H. van Heek, Comparative investigations of coal pyrolysis under inert gas and H_2 at low and high heating rates and pressures up to 10 MPa, Fuel 60 (1981) 779–787.
34. D.P. Ross, C.A. Heidenreich, D.K. Zhang, Devolatilization times of coal particles in a fluidised-bed, Fuel 79 (2000) 873–883.
35. L.D. Smoot, P.J. Smith, Coal Combustion and Gasification, Plenum Press, New York, 1985.
36. R.M. Morris, Effect of particle size and temperature on evolution rate of volatiles from coal, Journal of Analytical and Applied Pyrolysis 2 (1993) 97–107.
37. R.M. Morris, Effect of particle size and temperature on volatiles produced from coal by slow pyrolysis, Fuel 69 (1990) 776–779.
38. T.P. Griffin, J.B. Howard, W.A. Peters, An experimental and modeling study of heating rate and particle size effects in bituminous coal pyrolysis, Energy and Fuels 7 (1993) 297–305.

39. J.F. Stubington, Sumaryono, Release of volatiles from large coal particles in a hot fluidized bed, Fuel 63 (1984) 1013–1019.
40. J.P. Morris, D.L. Keairns, Coal devolatilization studies in support of the Westinghouse fluidized-bed coal gasification process, Fuel 58 (1979) 465–471.
41. J.F. Stubington, K.W.K. Ng, B. Moss, P.K. Peeler, Comparison of experimental methods for determining coal particle devolatilization times under fluidized bed combustor conditions, Fuel 76 (1997) 233–240.
42. J.Q. Zhang , H.A. Becker, R.K. Code, Devolatilization and combustion of large coal particles in a fluidized bed, The Canadian Journal of Chemical Engineering, 68 (1990) 1010–1017.
43. J.F. Stubington, T.Y. Chui, S. Saisthidej, Experimental factors affecting devolatilization time in fluidized bed combustion, Fuel Science and Technology International, 10 (1992) 397–419.
44. F. Winter, M.E. Prah, H. Hofbauer, Temperature in a fuel particle burning in a fluidized bed: the effect of drying, devolatilization, and char combustion, Combustion and Flame 108 (1997) 302–314.
45. J.F. Stubington, G. Huang, A.W. Scaroni, Devolatilization times of mm-size coal particles, Fuel 70 (1991) 1105–1108.
46. L. Jia, H.A. Becker, R.K. Code, Devolatilization and char burning of coal particles in a fluidized bed combustor, The Canadian Journal of Chemical Engineering 71 (1993) 11–19.
47. T.F. Salam, X.L. Shen, B.M. Gibbs, A technique for determining devolatilization rates of large coal particles in a fluidized bed combustor, Fuel 67 (1988) 414–419.
48. J. Tomeczek, H. Palugniok, Specific heat capacity and enthalpy of coal pyrolysis at elevated temperatures, Fuel 75 (1996) 1089–1093.
49. R.D. LaNauze, Coal devolatilization in fluidized bed combustors, Fuel 61 (1982) 771–774.
50. J.F. Stubington, The role of coal volatiles in fluidized bed combustion, Journal of the Institute of Energy 53 (1980) 191–195.
51. R.J. Bywater, The effects of devolatilization kinetics on the injector region of fluidized beds, Proceedings of the 6th International Conference on Fluidized Bed Combustion, Atlanta, 1980, pp. 1092–1102.

52. J.F. Stubington, T.M. Linjewile, The effects of fragmentation on devolatilization of large coal particles, Fuel 68 (1989) 155–160.
53. P.K. Agarwal, R.D. LaNauze, Transfer processes local to the coal particle: a review of drying, devolatilization and mass transfer in fluidized bed combustion, Chemical Engineering Research and Design 67 (1989) 457–480.
54. G. Borghi, A. Sarofim, J.M. Beer, A model of coal devolatilization and combustion in fluidized beds, Combustion and Flame 61 (1985) 1–16.
55. R.C. Borah, B. Mazumder, M.M. Bora, Atmospheric fluidized bed combustion of high sulphur high volatile N.E. Region coals of India, Research and Industry 40 (1995) 315–321.
56. P.K. Agarwal, A.E. Wildegger-Gaissmaier, Combustion of coal volatiles in gas fluidized beds, Chemical Engineering Research and Design 65 (1987) 431–441.
57. J.F. Stubington, S.W. Chan, On the phase location and rate of volatiles combustion in bubbling fluidized bed combustors, Chemical Engineering Research and Design 68 (1990) 195–201.
58. J.E. Johnsson, Formation and reduction of nitrogen oxides in fluidized-bed combustion, Fuel 73 (1994) 1398–1415.
59. F. García-Labiano, J. Adánez, E. Hampartsoumian, A Williams, Sulfur release during the devolatilization of large coal particles, Fuel 75 (1996) 585–590.
60. J.P.K. Peeler, H.J. Poynton, Devolatilization of large coal particles under fluidized bed conditions, Fuel 71 (1992) 425–430.
61. J.Q. Zhang, H.A. Becker, R.K. Code, Experimental study on devolatilization of large coal particles in a fluidized bed, Proceedings of 9th International Conference on Fluidized Bed Combustion, vol. 2, ASME, New York, 1987, pp. 1203–1210.
62. M. Saito, M. Sadakata, T. Saka, Measurements of surface combustion rate of single coal particles in laminar flow furnace, Combustion Science and Technology, 51 (1987) 109–128.
63. R.H. Essenhigh, Influence of coal rank on the burning times of single captive particles, Journal of Engineering for Power 85 (1963) 183–190.
64. K. Jung, B.R. Stanmore, Fluidized bed combustion of wet brown coal, Fuel 59 (1980) 74–80.
65. K.K. Pillai, Influence of coal type on devolatilization and combustion in fluidized beds, Journal of the Institute of Energy 54 (1981) 142–150.

66. K.W. Ragland, C.A. Weiss, Combustion of single coal particle in a jet, Energy 4 (1979) 341–348.
67. D.M. Grant, R.J. Pugmire, T.H. Fletcher, A.R. Kerstein, Chemical model of coal devolatilization using percolation lattice statistics, Energy and Fuels 3 (1989) 175–186.
68. T.H. Fletcher, M.S. Solum, D.M. Grant, S. Critchfield, R.J. Pugmire, Solid state ^{13}C and ^{1}H NMR studies of the evolution of the chemical structure of coal char and tar during devolatilization, Proceedings of the 23rd International Symposium on Combustion, The Combustion Institute, Pittsburgh, 1990, pp. 1231–1237.
69. T.H. Fletcher, A.R. Kerstein, R.J. Pugmire, M.S. Solum, D.M. Grant, Chemical percolation model for devolatilization. 3. Direct use of ^{13}C NMR data to predict effects of coal type, Energy and Fuels 6 (1992) 414–431.
70. P.R. Solomon, D.G. Hamblen, R.M. Carangelo, M.A. Serio, G.V. Deshpande, A general model of coal devolatilization, Energy and Fuels 2 (1988) 405–422.
71. P.R. Solomon, D.G. Hamblen, Z.Z. Yu, M.A. Serio, Network models of coal thermal decomposition, Fuel 69 (1990) 754–763.
72. D.W. van Krevelen, F.J. Huntjens, H.N.M. Dormans, Chemical structure and properties of coal. XVI. Plastic behavior on heating, Fuel 35 (1956) 462–475.
73. H.N. Stone, J.D. Batchelor, H.F. Johnstone, Low-temperature carbonization rates in a fluidized bed, Journal of Industrial and Engineering Chemistry 46 (1954) 274–278.
74. J.B. Howard, R.H. Essenhigh, Pyrolysis of coal particles in pulverized fuel flames, Industrial and Engineering Chemistry Process Design and Development 6 (1967) 74–84.
75. W.H. Wiser, G.R. Hill, N.J. Kertamus, Kinetic study of the pyrolysis of a high-volatile bituminous coal, Industrial and Engineering Chemistry Process Design and Development 6 (1967) 133–138.
76. S. Badzioch, P.G.W. Hawksley, Kinetics of thermal decomposition of pulverized coal particles, Industrial and Engineering Chemistry Process Design and Development 9 (1970) 521–530.
77. H. Kobayashi, J.B. Howard, A.F. Sarofim, Coal devolatilization at high temperatures, Proceedings of the 16th International Symposium on Combustion, The combustion Institute, Pittsburgh, 1976, pp. 411–425.

78. D.J. Maloney, R.G. Jenkins, Coupled heat and mass transport and chemical kinetic rate limitations during coal rapid pyrolysis, Proceedings of the 20th International Symposium on Combustion, The Combustion Institute, Pittsburgh, 1984, pp. 1435–1443.
79. S.S. Sandhu, H.R. Hashemi, A model for simultaneous heating and devolatilization of a single coal particle in a hot gas stream in the presence of a thermal radiative field, American Institute of Chemical Engineers Journal 31 (1985) 1714–1717.
80. W. Fu, Y. Zhang, H. Han, Y. Duan, A study on devolatilization of large coal particles, Combustion and Flame 70 (1987) 253–266.
81. D.K. Sharma, M.K. Sarkar, M. Ganapathi, Kinetics studies of the devolatilization of Indian coals in isothermal and nonisothermal conditions in thermobalance and in a batch reactor, Fuel Science and Technology International 12 (1994) 795–811.
82. Y. Li, G.Q. Lu, V. Rudolph, A kinetic study on pyrolysis of Australian coals by thermogravimetric analysis, Proceedings of the 24th Australian and New Zealand Chemical Engineering Conference and Exhibition (Chemeca 96), vol. 3, ISBN 0858256584, Sydney, 1996, pp. 143–148.
83. K.R. Doolan, J.C. Mackie, M.F.R. Mulcahy, R.J. Tyler, Kinetics of rapid pyrolysis and hydropyrolysis of a sub-bituminous coal, Proceedings of 19th International Symposium on Combustion, The Combustion Institute, Pittsburgh, 1982, pp. 1131–1138.
84. J.T. Yang, G.G. Wang, The effect of heat transfer on coal devolatilization, Journal of Heat transfer 112 (1990) 192–200.
85. A.S. Jamaluddin, J.S. Truelove, T.F. Wall, Modeling of coal devolatilization and its effect on combustion calculations, Combustion and Flame 62 (1985) 85–89.
86. J. Tomeczek, J. Kowol, Temperature field within a devolatilizing coal particle, Canadian Journal of Chemical Engineering 69 (1991) 286–293.
87. P.K. Agarwal, W.E. Genetti, Y.Y. Lee, Model for devolatilization of coal particles in fluidized beds, Fuel 63 (1984) 1157–1165.
88. P.K. Agarwal, W.E. Genetti, Y.Y. Lee, Devolatilization of large coal particles in fluidized beds, Fuel 63 (1984) 1748–1752.
89. P.K. Agarwal, Distributed kinetic parameters for methane evolution during coal pyrolysis, Fuel 64 (1985) 870–872.

90. P.K. Agarwal, A single particle model for the evolution and combustion of coal volatiles, Fuel 65 (1986) 803–810.
91. P.K. Agarwal, J.B. Agnew, N. Ravindran, R. Weimann, Distributed kinetic parameters for the evolution of gaseous species in the pyrolysis of coal, Fuel 66 (1987) 1097–1106.
92. A.E. Wildegger-Gaissmaier, P.K. Agarwal, Drying and devolatilization of large coal particles under combustion conditions, Fuel 69 (1990) 44–52.
93. W. Jie, Y. Cao, Y. Yan, J. Gao, Heat transfer and kinetics of lignite devolatilization in wire-mesh apparatus, Fuel Processing Technology 38 (1994) 57–67.
94. B.A. Adesanya, H.N. Pham, Mathematical modeling of devolatilization of large coal particles in a convective environment, Fuel 74 (1995) 896–902.
95. K. Miura, A new and simple method to estimate $f(E)$ and $k_0(E)$ in the distributed activation energy model from three sets of experimental data, Energy and Fuels 9 (1995) 302–307.
96. T. Maki, A. Takatsuno, K. Miura, Analysis of pyrolysis reactions of various coals including Argonne Premium coals using a new distributed activation energy model, Energy and Fuels 11 (1997) 972–977.
97. J.S. Chern, A.N. Hayhurst, Does a large coal particle in a hot fluidised bed lose its volatile content according to the shrinking core model? Combustion and Flame 139 (2004) 208–221.
98. S. Tia, S.C. Bhattacharya, P. Wibulswas, Pyrolysis and volatile combustion of a single large lignite particle, Energy 16 (1991) 1131–1146.
99. H. Jüntgen, K.H. van Heek**,** An update of German non-isothermal coal pyrolysis work, Fuel Processing Technology 2 (1979) 261–293.

CHAPTER 3

EXPERIMENTAL WORK

3.1 Introduction

Devolatilization is an important step in the fluidized bed combustion and gasification of coal. A practical knowledge of the behavior of high-volatile coals during devolatilization is essential for improving the efficiency of the process as well as to gain control of the gaseous emission from the process. In this section, the experimental procedure employed for the devolatilization of five high-volatile coals of northeastern India is described. Gaseous atmospheres of argon, air and enriched air have been used to analyze the behavior of high-volatile coals during devolatilization in purely pyrolysis, combustion, and in enhanced combustion conditions. The third situation is rather unexplored, and there is hardly any literature on it. The coals have been chosen in such a way that their volatile content is high and it varies over a wide range. This enabled us to record and analyze the devolatilization characteristics easily.

There are reports of experimental studies for total devolatilization time, 95% devolatilization time and 90% devolatilization time in inert atmosphere and in air in various equipment such as thermogravimetric apparatus, convective tube and fluidized bed [1–19]. However, very little emphasis has been given to the mass-loss characteristics during devolatilization, which is important for the optimization of particle size and bed height. Devolatilization time provides an estimate of the time required for a particle to devolatilize. It, however, does not provide any information regarding the extent of devolatilization at a particular time after the particle enters the bed. Therefore, it is not possible to ascertain the total amount of volatile matter

processed by the equipment at a particular time. It has been reported in the literature that the volatile matter can burn in the freeboard [20], which reduces the extent of heat transfer from the bed. In addition, unburned volatile matter creates air pollution.

There is discrepancy in the literature on the effect of gas velocity on the rate of devolatilization. Some authors claim that there is hardly any effect of gas velocity on devolatilization rate [10,11,14,16]. However, a few authors claim that the devolatilization rate increases with increasing velocity [21]. Therefore, the role of superficial gas velocity on the rate of devolatilization is to be explored. It is difficult to measure the mass-loss of a coal particle in a fluidized bed because the particle is in contact with the inert particles. At a higher velocity, the "flame extinction time" method cannot be employed because the diffusion flame is not visible. In the gas monitoring method, the dilution ratio of gas is large at the higher velocity, and the inaccuracy due to dilution is large. There is no other method for the measurement of mass-loss at a high velocity. Therefore, the purpose of this section is to develop a thermogravimetric set-up for collecting the mass-loss data continuously and accurately during devolatilization of a coal particle under the fluidized bed conditions. In this method, the mass-loss measurement will be carried out continuously by a sensitive and accurate microbalance during the time the sample is exposed to turbulent conditions in the freeboard of a hot fluidized bed.

The experimental set-up used in this study will be described in the Section 3.2.1. The use of this set-up for collection of data on devolatilization in inert atmosphere, air and enriched air will be described. Next, the procedure applied for the measurement of size of the particles will be explained. Calibration of the temperature measurement system will be described. The procedure adopted for the experimental determination of minimum fluidization velocity will be explained. Thereafter, the

proximate and ultimate analyses of the coals will be described and the properties of the coals will be analyzed.

3.2 Experimental studies on coal devolatilization

3.2.1 Experimental set-up

The devolatilization set-up used to carry out the experiments was similar to the apparatus reported in literature [22]. It is shown in Figure 3.1. Instead of a gas pre-heater, the fluidized bed was used to raise the temperature of the fluidizing media to the desired temperature, as described by Zabrodsky [23]. The fluidized bed consisted of a cylindrical tube made of sillimanite having 2.5 cm internal diameter and 60 cm length. It was housed inside a mild-steel casing, which was packed with insulating brick. The casing had 20 cm diameter and was 60 cm long. The total resistance of the heating element [Kanthal (UK)] was 55 Ω, which delivered a maximum of 1 kW power. The furnace had provisions for heating up to 1523 K. A digital temperature controller [Max-Thermo (Taiwan)] was used for recording and controlling the temperature of the furnace. A steel tube of 1.9 cm diameter and 10.16 cm height having perforations of 2 mm diameter at its periphery (~3% open area) was used as the gas distributor at the bottom of the cylindrical sillimanite tube. Calcined lime particles of ~0.72 mm diameter were used as the bed material for fluidization. The minimum fluidization velocity of the bed material was 53 cm/s. High-purity moisture-free argon, oxygen and air were used in the present study. High-purity moisture-free air and oxygen were mixed in the case of oxygen-enriched air such that the oxygen concentration in the mixed air was 30%. The air and oxygen were supplied to the system after mixing the two gases from the two gas cylinders. The flow rates of the

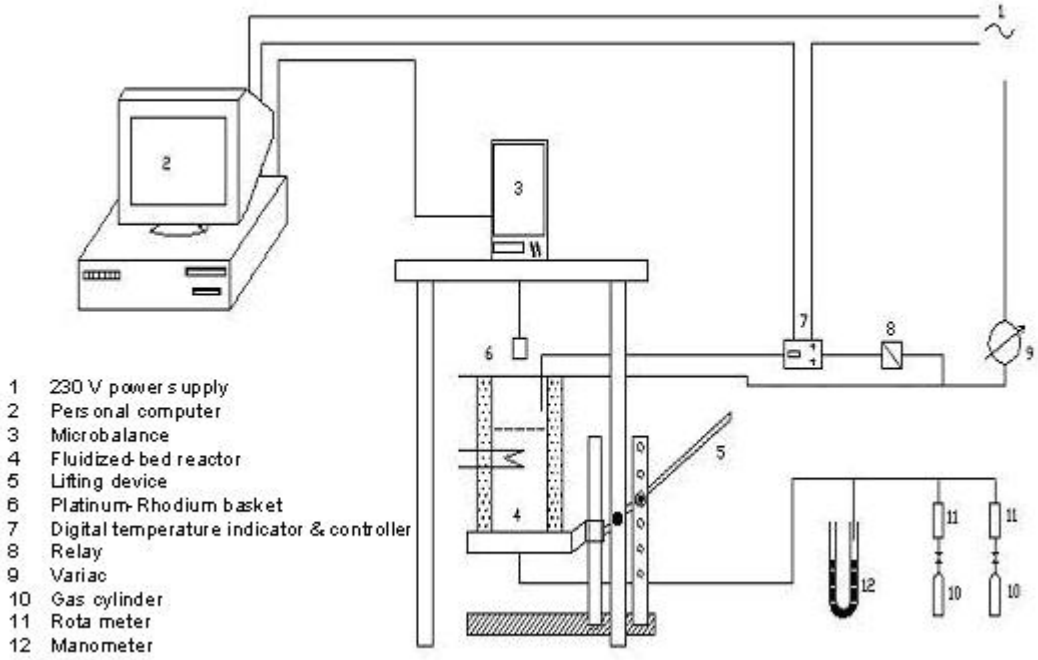

Figure 3.1 The experimental set-up.

gases were measured by rotameters. An online zirconia oxygen gas analyzer [Fuji Electric Co. (Japan)] having a response time of 10 s was used to monitor the oxygen concentration of air. A water manometer was connected to the gas line to measure the pressure drop across the rotameter.

3.2.2 Temperature measurement

In this study, the measurement of temperature was carried out using 1 mm diameter K-type chromel–alumel thermocouples. This thermocouple is capable of withstanding temperatures up to 1523 K, which makes it suitable for the present work. The thermocouple was connected to the digital temperature controller, which was connected to the personnel computer via RS-232 interface. The signal from the controller was recorded by the data-capturing software installed in the computer. The chromel–alumel thermocouple and the temperature controller assembly were calibrated with the help of a standard voltage measurement system. The chromel–alumel thermocouple was placed inside the freeboard section of the bed to measure and control the temperature. It was put into such a depth that it was positioned just above the expanded bed.

3.2.3 Minimum fluidization velocity

To determine the minimum fluidization velocity, a plot was made of the pressure drop across the bed versus the superficial gas velocity (Figure 3.2). The two linear parts of the plot were extended until they intersected. The minimum fluidization velocity is defined as the velocity at the point of intersection of two straight lines. The part on the left corresponding to low superficial velocities refers to the fully-fluidized zone, and the part on the right corresponds to a fully-static condition [24]. Pressure drop across the bed was measured with the help of water manometers. Superficial

velocity was computed from the volumetric flow rate of the fluidizing gas. Size analysis of the bed material is given in Table 3.1. The analysis of the major constituents of the bed material is given in Table 3.2.

3.2.4 Determination of particle diameter

A selection of particle mass (e.g., 0.145–0.155 g) was chosen for each of the coal samples to calculate the mass-equivalent-volumetric diameter (d_v). In each selection, about 20 coal particles were present. The diameters of the particles studied in this work were between 4 and 9 mm. The density was determined by calculating the volume of water displaced, following the procedure described in ASTM C693-93 [25]. A clean piece of coal was weighed accurately in air using a balance. The same coal sample was weighed while suspended in water. Deducting the mass of the suspension wire from the weight in water, the volume of the coal was calculated from the effect of displacement by water of known density (i.e., Archimedean principle). While calculating the volume of the displaced water, the density adjustments corresponding to the room temperature were taken into account.

About fifty coal particles for each size selection were collected and dried in an electric oven in nitrogen atmosphere for 1 hour at 378 K. The oven-dried coal particles were preserved in sealed bottles for future analysis so that the particles were not oxidized by air. The mass-equivalent volumetric diameter (assuming the coal particles to be spherical) was calculated following the procedure given by Stubington et al. [3]. Mass of the near-spherical particle was divided by the density of the coal to obtain the apparent volume of the coal particle.

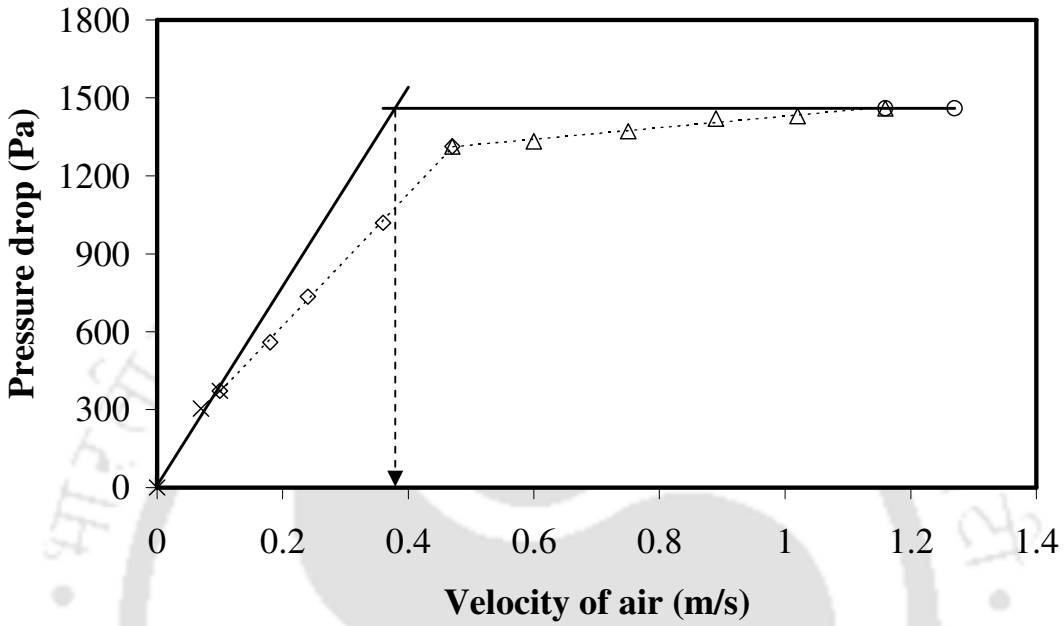

Figure 3.2 Determination of minimum fluidization velocity.

Table 3.1 Size analysis of the bed material used in the fluidized bed

Particulars of the B. S. sieve	Average size (mm)	Mass fraction retained
–4, +7	3.550	0.0862
–7, +14	1.770	0.0845
–14, +25	0.890	0.0908
–25, +36	0.510	0.0955
–52, +52	0.256	0.4285
–72	0.106	0.2145

Table 3.2 Analysis of the bed material

Constituent	Composition (%)
Calcium sulfate	48.6
Calcium oxide	37.4
Undecomposed $CaCO_3$	9.5
Unburnt carbon	0.6
Mixed oxide (e.g., MgO and FeO)	3.9

From the volume of the coal particle, the radius of the coal particle calculated, assuming it to be spherical. A typical calculation of mass-equivalent radius is given in Appendix 3.1. The mass-equivalent volumetric diameter was plotted against the average mass of the particles for all five coal samples, as shown in Figure 3.3. The data were fitted by the following polynomial equation.

$$d_v = 37.51M^3 - 46.35M^2 + 25.10M + 3.43 \tag{3.1}$$

where M is the mass of the coal particle. Equation (3.1) fitted the data well (coefficient of determination, $R^2 = 0.99$). The 95% confidence intervals for 37.1, –46.35, 25.1 and 3.43 are (14.12, 60.91), (–66.94, –25.76), (20.21, 29.98), (3.14, 3.72), respectively.

3.2.5 Mass-loss measurement procedure

In all the experiments performed in this work, the mass of the particle was recorded before it was placed inside the hot furnace. As the response time of the balance was 0.3 s, the mass of the coal particle was recorded every 0.3 s throughout the time span of the experiment with the help of the data-logging software, until the mass of the particle reached a constant value. The weight of the empty sample basket and the suspension system was determined at the test conditions.

The effect of gas flow rate was taken into consideration to allow for any possible flow-induced drag on the basket. For each particle size, duplicate devolatilization experiments have been carried out. The variation of devolatilization time from one experiment to another was less than 5%.

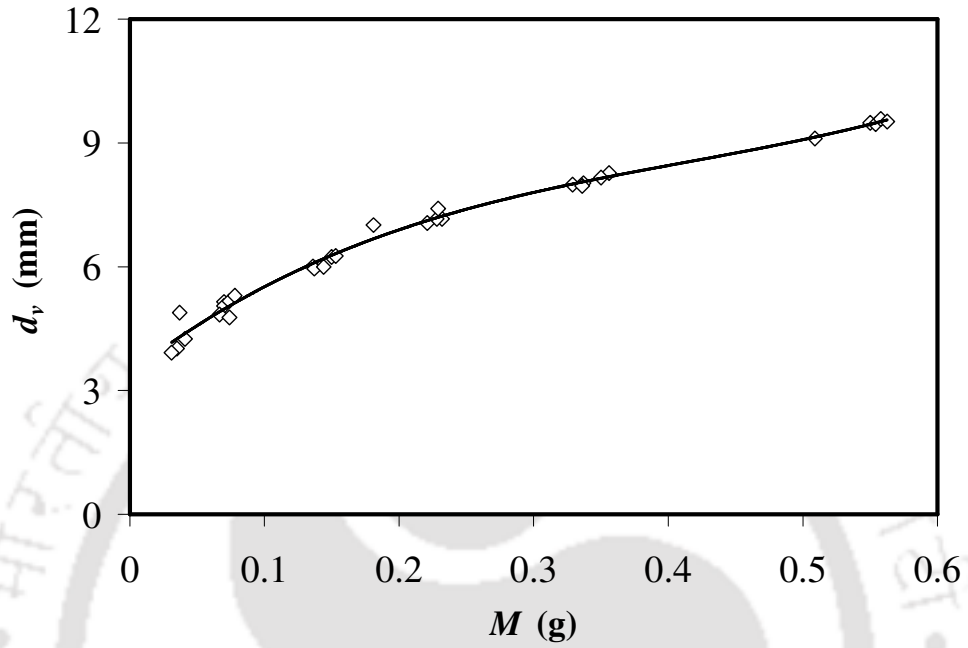

Figure 3.3 The variation of mass-equivalent volumetric diameter (d_v) with the mass of the particle (M) for the five coals.

3.2.6 Experimental procedure

The coal particle under investigation was held in a basket of 1.2 cm diameter and 2 cm height. It was made of a platinum–rhodium net, and was suspended with the help of a platinum wire from the hook of a microbalance [AND (Japan)]. The response time of the microbalance was 0.3 s. The microbalance was connected to a desktop computer via the RS-232 data interface. The data-capturing software enabled us to record the weight measured by the balance in a continuous manner. The position of the suspended basket was such that when the vertical furnace was lifted with the help of the lifting device, the coal particle in the basket was placed just above the fluidized bed, and it experienced the conditions of the hot furnace instantly, as a particle would experience in a typical fluidized bed.

Initially, the power input to the electric coil was adjusted to give a uniform temperature (1123 K) inside the furnace. After this, purging of the gas (argon, air or air–oxygen mixture) was commenced. The flow was adjusted such that the velocity of the fluidizing gas was 1 m/s. This velocity is well below the elutriation velocity of the particles of the fluidized bed. The elutriation of particles occurs when the terminal velocity exceeds the settling velocity of the bed material. The ratio of superficial velocity to the minimum fluidization velocity is >8.7 under the elutriation condition [26]. The minimum fluidization velocity of a 0.72 mm diameter bed particle is 0.38 m/s. The superficial velocity employed in our work was 1 m/s, which is far below the terminal velocity of the bed material (viz. 4.62 m/s). Therefore, there is no possibility of elutriation of the bed material under the conditions in which we conducted the experiments.

Once the velocity of the gas and the temperature were stabilized, the empty basket with the platinum wire was suspended from the balance hook and the furnace assembly was lifted with the help of the lifting device as described earlier in this section. The empty run was recorded and the furnace was lowered. As soon as the empty basket and the platinum wire assembly cooled down to room temperature, the pre-weighed coal sample was put into the basket. The furnace assembly was lifted with the help of the lever and the system was locked at that position. The weight was recorded continuously. The time versus weight data were analyzed subsequently.

3.2.7 Measurement of devolatilization time

It has been reported in the literature that the methods by which the end of devolatilization in a fluidized bed is determined can affect the results [26]. Some of these approaches and the sources of inaccuracy are explained below.

- The *flame extinction time* is measured from the time the particle comes in contact with the bed until the extinction of any visible flame at the surface of the bed. Visual detection of a visible flame around the coal particles and its disappearance at the bed surface may be erroneous because, towards the end of devolatilization, the concentration of volatile matter is very small, which may not develop a visible flame. Moreover, visual detection is possible only at a low fluidization velocity. At the high fluidization velocities, the diffusion flame is not visible.
- In another approach, the fluidized bed in inert atmosphere is quenched instantly after a certain period of time, and the volatile matter of the removed particles is determined. The process continues with different intervals for the same particle size until the volatile content of the char is

zero. The time required to remove 95% of the volatile matter is taken as the devolatilization time. The measurement of mass of the particle by interrupting the process can lead to erroneous results because the devolatilization process continues up to the moment of the actual measurement.

- In the *carbon dioxide evolution time* approach, the coal particle is introduced into a hot bed and the carbon dioxide in the flue gas is monitored by the gas analyzer. The devolatilization time is taken as the time when the CO_2 concentration in the flue gas reaches the minimum. When the evolved volatile gases are monitored, there can be errors due to the time lag in the gas evolution in the fluidized bed, and detection in the gas analyzer. The error can be more severe at the high fluidization velocities.

Direct measurement of the mass of a coal particle cannot be made because the coal particle is surrounded by inert particles in a fluidized bed. Thermogravimetric techniques have been extensively used to study devolatilization [8,10,22]. From these results, the devolatilization time has been defined in various ways depending upon the atmosphere. In case of air as the fluidizing medium, the devolatilization time is defined as the point of intersection of the two linear portions of the mass versus time curve [10]. This gives the time for ~90% devolatilization. This procedure was adopted in this work for the determination of devolatilization time in air and in oxygen-enriched air. A typical example has been shown in Figure 3.4. In the inert atmosphere, the rate of devolatilization slows down towards the end. Therefore, the time required for 95% of the ultimate mass loss was taken as the devolatilization time [22]. In this work, total as well as 95% devolatilization time were considered.

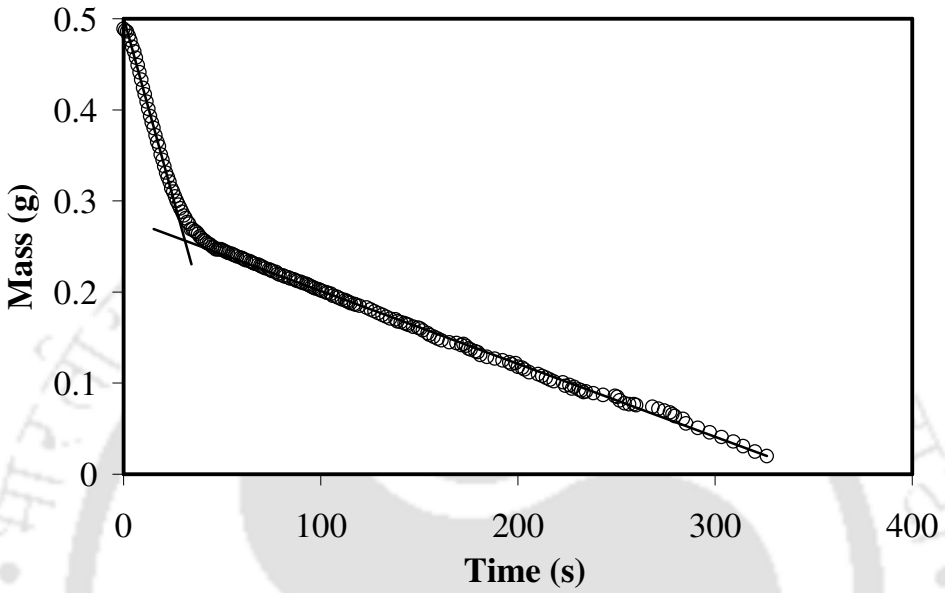

Figure 3.4 Determination of devolatilization time in air from the experimental data for a Baragolai coal particle of 9 mm diameter.

3.2.8 Error

The root mean square error (RMSE) is a measure of the difference between the values predicted by the model and the values observed experimentally. It is defined as,

$$\text{Error} = \text{RMSE} = \left[\frac{(\text{Experimental data} - \text{Predicted data})^2}{\text{Total number of observations}} \right]^{1/2} \quad (3.2)$$

The RMSE has been used to optimize the correlations developed in this work. A typical error calculation has been given in Appendix 3.2.

3.3 Characterization of coal

Coal combustion is a complex process which cannot be characterized by a set of simple principles because of the wide variety of the physical and chemical properties of coal. As a consequence, it must be considered in those terms which relate to the overall system design. The user is interested not only in the amount of energy generated by burning the coal, but he must also address other related aspects such as fuel handling, ash removal, emissions, and the environmental control techniques. The properties of coal can provide an indication of its performance during burning under specific conditions.

The analysis of coal is therefore very important for its use. The data obtained from the various analyses establish the value of the coal. In commercial operations, the price of coal not only reflects the quantity of the coal, but also reflects the relationship of a desirable property (or a combination of properties) to the performance of the coal under service conditions. Measurements of the desired properties are usually grouped together under the general title “specifications”. The

accuracy of these measurements is of utmost importance. Inaccurate data may have serious scientific, economic and quality-related consequences.

There are many problems associated with the analysis of coal. One of these problems is the heterogeneous nature of coal. Other problems include the tendency of coal to gain or lose moisture, and to undergo oxidation when exposed to the atmosphere [27]. Many of the test methods applied to coal analysis are empirical in nature, and strict adherence to the procedural guidelines is necessary to obtain reproducible results. The type of analysis requested by the coal industry may be either a proximate analysis or an ultimate analysis, or sometimes both. Proximate and ultimate analyses are the important quality control parameters for coal.

The proximate analysis covers the determination of moisture, volatile matter, fixed carbon and ash in coals. It is often used to establish the rank of coals, and to show the ratio of combustible to incombustible constituents. The ultimate analysis of coal involves the determination of carbon, sulfur, hydrogen, nitrogen and oxygen (usually calculated by difference). Trace elements which occur in coal are often included in the ultimate analysis. The determination of carbon includes the carbon present as organic carbon occurring in the coal substance, and any carbon present as mineral carbonate. The determination of hydrogen includes hydrogen present in the organic materials as well as the hydrogen in all forms of water associated with the coal. All the nitrogen is assumed to occur within the organic matrix of coal. On the other hand, sulfur occurs in three forms in coal: organic sulfur compounds, inorganic sulfides (e.g., iron sulfide pyrite and marcasite), and as inorganic sulfates (e.g., sodium sulfate and calcium sulfate). The amount of sulfur reported in the ultimate analysis may include inorganic as well as organic sulfur.

A very important task in the testing of coal is the need for obtaining a representative sample, which is a difficult task. Generally, the entire quantity of material is incrementally sampled such that equal portions comprise the gross sample. Equal amount of sample from each increment is collected. The number of increment will depend upon the total amount of coal available.

This section presents sample collection and preparation methods, and the proximate and ultimate analyses of the coal samples. It also describes the storage of the samples so that they do not oxidize.

3.3.1 Sample collection and preparation

The samples were collected from five collieries of northeastern India, and thereafter processed in the laboratory for characterization, following the procedures given in IS 436 (Part I)-1964 [28].

3.3.1.1. Sample collection

Samples collected from the collieries are called "gross samples". They are defined as the samples as collected from a "sub-lot" (i.e., the quantity of coal obtained by aggregating together all the increments of equal proportions drawn from the same sub-lot). A "lot" is the quantity of coal available for disposal at one time. It is divided into a number of sub-lots for sampling, depending upon the quantity in the lot. For up to 5×10^5 kg of coal, the number of sub-lots will be two and therefore, the number of gross sample will be two.

The Indian coals are divided into three size groups as described in Table 3.3 [28]. The minimum amount of gross sample was 350 kg [28]. For our work, the amount was reduced to 40 kg by applying the coning and quartering method

(described in Section 3.2.2). This amount was divided further into two equal parts. From one part, different size fractions of coal were separated by sieving. Each fraction was preserved under sealed conditions. The other part was processed for the preparation of sample for characterization, as described in Section 3.3.1.2.

3.3.1.2 Sample preparation for the characterization of coal

A gross sample of 20 kg of coal was crushed to 5 cm by mechanical method. The crushed portion was mixed thoroughly and quartered. Two opposite quarters were retained and the rest were rejected as explained in Figure 3.5. The retained material was further mixed together, and the process was repeated until one quarter of the original mass was retained and the rest was rejected. The material so obtained was crushed to 12.5 mm by a jaw crusher, and then to 3.35 mm by a roll crusher. The crushed material was reduced by coning and quartering. The procedure adopted for coning and quartering was as follows. The material that was crushed to 3.35 mm was heaped into the shape of a cone by pouring scoopfuls of the material one after another at the apex of a cone until the entire sample was transformed into a conical form. The material was allowed to slide down the sides of the cone under the influence of gravity. Then the cone was flattened evenly so that it formed a low circular pile. The pile was cut into four quarters along two diameters, which intersected at right angles. Opposite quarters were retained and the other was rejected. The process was repeated until 1.25 kg of sample was prepared.

The sample was ground to pass through a 212 μm sieve. The particle size range of the ground coal is given in Table 3.4. Grinding to ultra-fine particles was avoided.

Table 3.3 Divisions of Indian coals into different size groups

Name	Nominal size
Run-of-mine (ROM) coal	23 to 0 cm
Coal, large	23 to 5 cm
Coal, small	5 to 0 cm

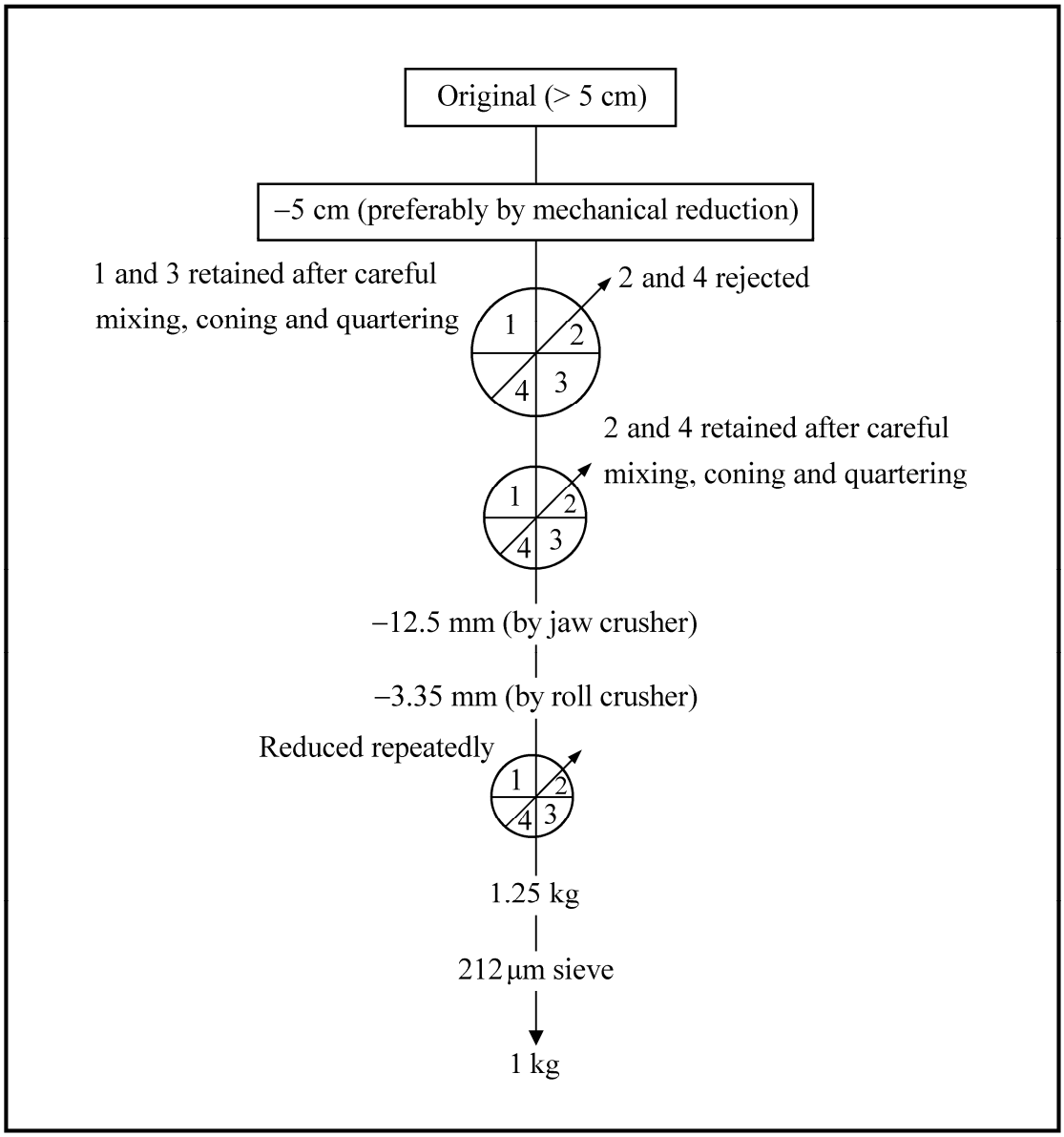

Figure 3.5 Reduction of the gross sample.

Table 3.4 Particle size distribution of a ground coal sample used for characterization

Size range	Weight %
Passing 212 µm sieve, and retained on 125 µm sieve	35
Passing 125 µm sieve, and retained on 63 µm sieve	30 to 35
Passing 63 µm sieve	Remainder

3.3.2 Proximate and ultimate analyses of the coal samples

The proximate analysis of the coal samples was carried out by the method outlined in IS: 1350 (Part I) [29]. The ultimate analysis of the coal samples was carried out by the methods outlined in IS: 1350 (Part IV/Section 1) [30] for determination of carbon and hydrogen, IS: 1350 (Part IV/Section 2) [31] for determination of nitrogen, and IS: 1350 (Part III) [32] for determination of sulfur.

3.3.2.1. Proximate analysis

Coals, especially those of low-rank, are hygroscopic in nature. They absorb or lose moisture according to the humidity and temperature to which they are exposed. The results of proximate analysis are generally recorded as a percentage of the air-dried material. The ash may be expressed on the dry basis. Volatile matter and fixed carbon may be expressed on a dry basis, dry-ash-free (daf) basis or dry-mineral-matter-free (dmf) basis. Such figures are arrived at by calculation from the results on an air-dried basis.

Gross samples collected from the colliery were air-dried inside a room by laying in a single layer, stirring from time to time for approximately 24 hours, or until the sample attained a constant weight. The results of the proximate analysis are presented in Table 3.5.

3.3.2.1.1 Determination of moisture

Water expelled in its various forms when tested under the specific conditions is expressed as the *moisture content* of the coal. The moisture present in the coal sample is important both in the proximate analysis and in calculating other analysis results. Coal that has been exposed to water in the seam, in washery, or wetted by

rain, may carry free or visible water. The total of this water and the moisture within the material is expressed as *total moisture*.

At the beginning, a moisture crucible made of silica having 10 cm^2 area with ground edges and fitted with ground covers, was heated at 378 ± 2 K for 1 hour. It was weighed after cooling for 20 minutes in a desiccator. Then 1.5 g of crushed coal (which passed through a 212 μm sieve) was taken into the crucible and spread in a manner such that there was not more than 150 mg of the material per cm^2 area. It was weighed again. The cover of the crucible was removed in the drying oven and heated at 378 ± 2 K until no further loss in mass took place. This normally took 1–1.5 hours. Then the cover was replaced, the crucible was cooled in a desiccator for 20 minutes, and weighed.

The results of duplicate determinations agreed within the limits given in Table 3.6. The loss in mass was expressed as the percentage moisture in the sample. The calculation procedure is given in Appendix 3.3. The moisture contents of the five coals are given in Table 3.5.

3.3.2.1.2 Determination of volatile matter

The volatile content of a coal is the loss in mass, less the loss due to moisture, when the coal is heated under standard conditions. The test is empirical and in order to ensure accurate results, it is essential that the rate of heating, the final temperature, and the overall duration of the test should be carefully controlled. It is also essential to exclude air from the crucible during heating to prevent oxidation. Therefore, the fit of the lid of the crucible is critical. The moisture content of the sample should be determined at the same time as the volatile matter so that appropriate corrections can be made.

Table 3.5 Proximate analysis of the coal samples

Parameter (%)	Colliery				
	Baragolai	Ledo	Tikak	Baragolai A	Tirap
Volatile matter	31.20	40.80	37.8	35.4	38.10
Fixed carbon	36.50	46.90	43.8	43.0	45.60
Ash	28.80	10.10	16.7	19.3	14.40
Moisture	3.50	2.20	1.7	2.3	1.90

A standard crucible (used for volatile matter test) made of silica having 25 mm diameter and 38 mm depth, and provided with a fitting lid of same material was heated at 1173 ± 10 K, cooled for 5 minutes by keeping it on a metal plate, and then placed in a desiccator for 10 minutes. Then 1.00–1.01 g of sample was taken into the empty crucible. The crucible was tapped on a clean hard surface so that the sample formed a layer of uniform thickness. The crucible with sample (including the lid) was placed in the furnace and kept for 7 minutes. Then it was taken out, cooled and weighed as described for the empty crucible. The difference in weight after the deduction of moisture content gave the volatile matter content of the coal. The results of duplicate determinations agreed within the limits given in Table 3.7.

The calculation procedure involved in the determination of volatile matter is described in Appendix 3.4. The volatile contents of the five coals are given in Table 3.5.

3.3.2.1.3 Determination of ash

The *ash content* of coal is defined as the inorganic residue left when coal is burnt in air under specified conditions to constant weight. The following procedure was adopted for the determination of ash content.

An empty dish (made of silica), 15 mm deep and 45 mm diameter with a lid was weighed. One gram of the thoroughly-mixed coal powder was taken into the dish. Then the powder was spread so that it did not exceed 150 mg per square centimeter area. Then the dish was uncovered and put into the muffle furnace at room temperature. Thereafter, it was heated to 773 K in 30 minutes, and further to 1088±10 K in 30 minutes. It was kept at this temperature for 60 minutes. Then the dish was removed from the muffle furnace and allowed to cool on a cold metal slab for ten

Table 3.6 Precision in the moisture-determination experiments

Moisture (%)	Precision	
	Repeatability	Reproducibility
Upto 3.0	0.1 units	0.2 units
Over 3.0	3.0% of the arithmetic mean of the duplicate values	6.0% of the arithmetic mean of the duplicate values

Table 3.7 Precision in the experiments for the determination of volatile matter

Precision	
Repeatability	Reproducibility
1.0% of the arithmetic mean of the duplicate values	1.5% of the arithmetic mean of the duplicate determinations

minutes, and finally placed in a desiccator. The weight of the dish was taken after keeping it in the desiccator for 15 minutes. Then the ash was brushed out of the dish and the weight of the empty dish was recorded. The mass of ash was calculated by the difference. The computation procedure for the determination of ash is given in Appendix 3.5. The results of duplicate determinations agreed within the limits given in Table 3.8. The ash contents of the five coals are given in Table 3.5.

3.3.2.1.4 Reporting of results

The results of analysis are reported on the air-dried basis as explained below. Let M_0 be the percentage of moisture in the sample, A be the percentage of ash in the sample, V_m be the percentage of volatile matter in the sample, and F be the percentage of fixed carbon in the sample. It has been noted in Section 3.3.2.1.2 that the volatile matter (V_m) is the total loss recorded during the determination of volatile matter, less the moisture given off upon drying the coal sample. The amount of fixed carbon (F) is calculated after deducting the sum of moisture, ash and volatile matter from 100 percent. Therefore,

$$F = 100 - (M_0 + A + V_m) \tag{3.3}$$

3.3.2.2 Ultimate analysis of coal

The ultimate analysis of coal comprised of the determination of the constituent elements, viz. carbon, hydrogen, nitrogen and sulfur. The ultimate analyses of the five coals used in this work are summarized in Table 3.9.

Table 3.8 Precision in the experiments for ash determination

Ash (%)	Precision	
	Repeatability	Reproducibility
Up to 10.0	0.2 units	0.4 units
Over 10.0	2.0% of the arithmetic mean of the duplicate values	3.0% of the arithmetic mean of the duplicate values

3.3.2.2.1 Determination of carbon and hydrogen [30]

For determining the amounts of carbon and hydrogen, the coal sample was burnt in a current of oxygen. All hydrogen was converted to water and all carbon was converted to carbon dioxide. These products were absorbed by suitable reagents and determined gravimetrically. Sulfur products were captured by lead chromate and chlorine by silver gauge. The results comprise of the carbon that may be obtained from the carbonates, and the hydrogen in the moisture and in the water of hydration of silicates, which are found to be associated with coals. The estimation procedure is described in Appendix 3.6. The percentages of carbon and hydrogen present in the five coals are given in Table 3.9.

3.3.2.2.2 Determination of nitrogen

The amount of nitrogen in coal was determined by the Kjeldahl method [31]. The coal powder was treated with concentrated sulphuric acid in presence of a suitable catalyst (viz. 10 g of potassium sulfate +0.2 g of the selenium powder) to convert the nitrogen into ammonium sulfate. The ammonia gas released by distillation with sodium hydroxide was absorbed in boric acid and then titrated with standard sulphuric acid. The calculation procedure is described in Appendix 3.7. The nitrogen contents of the five coals are given in Table 3.9.

3.3.2.2.3 Determination of sulfur

The amount of sulfur in coal was determined by the Eschka's method [32]. The coal sample was heated in intimate contact with the Eschka's mixture in an oxidizing atmosphere to remove the combustible matter, and to convert the sulfur into sulfate. It was then extracted and determined by gravimetric method in which barium

Table 3.9 Ultimate analysis of the coal samples

Parameter (%)	Colliery				
	Baragolai	Ledo	Tikak	Baragolai A	Tirap
Carbon	81.00	79.90	81.0	80.4	81.60
Hydrogen	5.70	5.70	5.8	6.0	5.30
Nitrogen	1.50	1.40	1.1	1.3	1.30
Sulfur	4.00	4.60	3.5	5.4	4.90
Oxygen (by difference)	7.80	8.40	8.6	6.9	6.90

sulfate was precipitated.

The weight of sample required for the determination of total sulfur varied according to the expected sulfur content of the coal. It is described in Table 3.10. The Eschka's mixture was prepared by mixing two parts by weight of light calcined magnesia with one part of anhydrous sodium carbonate. The mixture entirely passed through the 212 μm sieve and its bulk density was less than 0.5 g/cm^3. A blank determination with only Eschka's mixture under the same condition was carried out without the coal sample. The results of duplicate determinations agreed with the limits given in Table 3.11. The procedure of calculation of the amount of sulfur is given in Appendix 3.8. The sulfur contents of the five coals are given in Table 3.9.

3.3.2.2.4 Oxygen in coal

The percentage of oxygen was determined by subtracting the sum of the percentages of moisture, mineral matter, carbon, hydrogen, nitrogen and sulfur (total) from 100. The oxygen contents of the five coals are given in Table 3.9.

3.3.2.3 Calorific value of coal

The calorific values of the coals were determined by using the methods prescribed in IS: 1350 (Part II) [33]. In the determination of gross calorific value, air-dried powdered coal sample was burnt in a bomb calorimeter of known heat capacity. The principal parameter was the rise in temperature which, when rectified for the inaccuracies of the thermometer and multiplied by the effective heat capacity at the mean temperature of the chief period (defined as the period from the instant of firing until the time after which the rate of change of temperature becomes constant), gave the heat release. In addition, allowance was necessary for, (a) the cooling loss, (b) the

Table 3.10 Requirement of the amount of sample based on the expected sulfur content of the coal sample

Expected sulfur content (%)	Quantity of sample (g)
0.1 and up to and including 5	1
Above 5 and up to and including 10	0.5

Table 3.11 Precision in the sulfur determination experiments

Sulfur content (%)	Tolerance
Up to 2	±0.02
2 to 10	±0.04

heat gain due to the heat released by the ignition system, and (c) the heat of formation of sulfuric and nitric acids from sulfur dioxide and nitrogen. The results of duplicate determinations agreed within 125.6 J/g. The calculation of gross calorific value of coal and the corrections are described in Appendix 3.9. The values of gross calorific values of the five coals are given in Table 3.12.

Table 3.12 Gross calorific values of the five coals

Parameter (MJ/kg)	Colliery				
	Baragolai	Ledo	Tikak	Baragolai A	Tirap
Gross specific energy	21.39	28.97	27.3	25.6	28.07

Appendix 3.1 Calculation of density of coal particle

Weight of (coal particle + platinum wire in air) = 0.5057 g

Weight of (coal particle + platinum wire in water) = 0.4468 g

Weight loss due to buoyancy for coal particle and platinum wire (length of the portion immersed in water = 3 cm, and its diameter = 0.03 cm) = 0.0589 g

Density of water at 295.4 K = 0.998 g/cm^3

Weight loss of the portion of platinum wire immersed

$$= \pi \times (0.03/2)^2 \times 3 \times 0.998 = 2.1163 \times 10^{-3} \text{ g}$$

Weight loss of the coal particle = $0.0589 - 2.1163 \times 10^{-3} = 0.0568$ g

Volume of coal particle = $\left(\frac{0.0568}{0.998} \right) = 0.0569 \text{ cm}^3$

Radius of coal particle = $\left(\frac{0.0569 \times 3}{4\pi} \right)^{1/3} = 0.239 \text{ cm} = 2.39 \text{ mm}$

Appendix 3.2 Calculation of error

Sample: Baragolai A coal particle of 4.9 mm diameter devolatilized in oxygen-enriched air

Time (s)	Actual mass of coal particle (g)	Calculated Mass (g)
0.0	0.068	0.068
0.9	0.066	0.064
1.8	0.062	0.059
2.7	0.060	0.056
3.6	0.057	0.052
4.5	0.055	0.050
5.4	0.052	0.047
6.3	0.050	0.045
7.2	0.048	0.044
8.1	0.046	0.043
9.0	0.044	0.042
9.9	0.042	0.041

Calculated mass at any time (t), $V = V_0 + (V_\infty - V_0)\left[1 - \exp\left(-ct^m\right)\right]$

where,

$V_0 =$ initial mass of coal particle = 0.068 g

$V_0 - V_\infty =$ total amount of volatile matter evolved

= $V_0 \times$ volatile matter content (in fraction) $\times p$ (ratio of yield to proximate volatile matter content)

$$p = 66.315 \times (\text{Volatile matter content, } \%)^{-1.104} = 1.293$$

$$c = 7.38 d_v^{-2.38}$$

$$d_v = 4.9 \text{ mm}$$

$$m = 1.1$$

$$V = 0.068 - 0.068 \times 0.354 \times 1.293 \times \left[1 - \exp\left(-0.168 t^{1.1}\right)\right]$$

From Eq. (3.2),

$$\text{Error} = \left[\left(V_{\text{Expt}} - V_{\text{Calc}}\right)^2 / N\right]^{1/2}$$

$N =$ number of experimental data = 12

$$\text{Error} = 3.57 \times 10^{-3}$$

Appendix 3.3 Calculation of the moisture content of coal sample on air-dried basis.

The weight percentage of moisture was calculated from the following equation [29].

$$\text{Moisture (\% by weight)} = \frac{100 \times (M_2 - M_3)}{M_2 - M_1} \qquad \text{(A3.3.1)}$$

where M_1 is the mass of the dish, M_2 is the mass of dish and sample before heating, and M_3 is the mass of the dish and sample after drying.

Example:

Sample: Baragolai Coal

M_1=22.8926 g

M_2=23.9171 g

M_3=23.8812 g

Moisture (% by weight) = 3.5 %

Appendix 3.4 Calculation of the volatile matter of the coal sample on air-dried basis

The volatile content of the coal was calculated from the following equation [29].

$$V_m = \frac{100\times\left(M_2' - M_3'\right)}{M_2' - M_1'} - M_0 \qquad \text{(A3.4.1)}$$

where V_m is the volatile matter (in wt. %), M_0 is the percentage (wt.) of moisture in the sample on air-dried basis, M_1' is the mass of the empty crucible and lid, M_2' is the mass of the crucible with lid and the sample before heating, and M_3' is the mass of the crucible with lid and the residue after heating.

Example:

Sample: Baragolai coal

M_1' = 10.8092 g

M_2' = 11.8102 g

M_3' = 11.4629 g

Given: M_0 = 3.5%

$\therefore \quad V_m$ = 31.2%

Appendix 3.5 Calculation of the ash of the coal sample on air-dried basis

The ash content of the coal was calculated from the following equation [29].

$$\text{Ash (\% by mass)} = \frac{100 \times \left(M_3'' - M_1'' \right)}{M_2'' - M_1''} \qquad \text{(A3.5.1)}$$

where M_1'' is the mass of the dish, M_2'' is the mass of the dish and sample before heating, and M_3'' is the mass of the dish and ash.

Example:

Sample: Baragolai coal

M_1'' =15.6988 g

M_2'' =16.6998 g

M_3'' =15.9871 g

Ash (% by mass) = 28.8 %

Appendix 3.6 Determination of the percentages of carbon and hydrogen

The weight percentage of carbon in coal is given by [30],

$$\text{Carbon (\% by weight)} = 27.29 \times \left(\frac{X_2 - X_1}{W} \right) \qquad \text{(A3.6.1)}$$

where X_2 is the weight of the carbon dioxide absorption unit after combustion, X_1 is the weight of the carbon dioxide absorption unit before combustion, and W is the weight of the material taken for the test.

The weight percentage of hydrogen in coal is given by [30],

$$\text{Hydrogen (\% by weight)} = 11.2 \times \left(\frac{Y_2 - Y_1}{W} \right) \qquad \text{(A3.6.2)}$$

where Y_2 is the weight of the water absorption unit after combustion, Y_1 is the weight of the water absorption unit before combustion, and W is the weight of the material taken for the test.

Example:

Sample: Baragolai coal

X_2 = 66.9761 g

X_1 = 65.5965 g

W = 0.4648 g

Carbon = 81.0 % (by weight)

Y_2 = 61.6715 g

Y_1 = 61.4350 g

W = 0.4648 g

Hydrogen = 5.7 % (by weight)

Appendix 3.7 Determination of nitrogen in coal

The nitrogen in coal was calculated by the following equation [31].

$$\text{Nitrogen (\% by weight)} = \frac{28.57 \times (B - V_N) N_N}{W} \qquad \text{(A3.7.1)}$$

where B is the volume of standard sulfuric acid used in the test, V_N is the volume of sulfuric acid used in the blank, N_N is the concentration of the standard sulfuric acid, and W is the weight of the material taken for the test.

Example

Sample: Baragolai coal

B = 16.74 cm^3

V_N = 0.02 cm^3

N_N = 13 mol/m^3

W = 0.4057 g

Nitrogen = 1.5 % (by weight)

Appendix 3.8 Determination of sulfur in coal

The weight percentage of sulfur in coal was calculated by the following equation [32].

$$\text{Sulfur (\% by weight)} = 13.74 \times \frac{(A_s - B_s + 0.008)}{W} \qquad \text{(A3.8.1)}$$

where A_s is the weight of barium sulfate found in the determination, B_s is the weight of barium sulfate found in the blank determination, and W is the weight of the coal taken for the test.

Example:

Sample: Baragolai coal

$A_s = 0.1685$ g

$B_s = 0.0309$ g

$W = 0.5$ g

Sulfur = 4.0% (by weight)

Appendix 3.9 Calculation of gross calorific value [33]

The following method was used for the calculation of the gross calorific value. Let us define the following quantities. Let W_1 be the weight of the crucible and thread, W_2 be the weight of crucible, thread and the coal sample, H_1 be the effective heat capacity of the calorimeter at T_1, T_2 be the room temperature, T_n be the final temperature (to which the calorimeter temperature has risen because of combustion of coal sample), and T be the thermometer correction. Therefore,

$$\text{Weight of air-dried coal} = W_2 - W_1 \tag{A3.9.1}$$

$$\text{Uncorrected temperature rise} = T_n - T_2 \tag{A3.9.2}$$

$$\text{Corrected temperature rise} = T_n - T_2 + T \tag{A3.9.3}$$

$$\text{Heat liberated} = H_1\left(T_n - T_2 + T\right) \tag{A3.9.4}$$

Let H_2 be the correction for heat of ignition of thread. Therefore,

$$\text{Heat liberated} = H_1\left(T_n - T_2 + T\right) - H_2 \tag{A3.9.5}$$

$$\text{Calorific value of coal} = \frac{H_1\left(T_n - T_2 + T\right) - H_2}{W_2 - W_1} \tag{A3.9.6}$$

Example:

Sample: Baragolai coal

$W_2 - W_1 = 0.6770$ g

$T_n - T_2 = 1.12$ K

$T_n - T_2 + T = 1.12 + 0.014 = 1.134$ K

H_1 = 12828 J/K

H_2 = 65.2 J

Calorific value of coal = 21.39 MJ/kg

Notations

A	ash content of coal, %
A_s	mass of the barium sulfate found in the determination of sulfur in coal, kg
B	volume of standard sulfuric acid solution used in the blank determination of nitrogen in coal, cm^3
B_s	mass of the barium sulfate found in the determination of sulfur in the blank Eschka's mixture, kg
c	constant in mass loss correlation, s^{-m}
d_v	mass-equivalent volumetric diameter, m
F	fixed carbon content of coal, %
H_1	effective heat capacity of Bomb calorimeter, J/K
H_2	correction for heat evolution from combustion of thread, J
M	mass of coal particle, kg
M_0	moisture content of coal, %
M_1	mass of dish used for moisture content determination with lid, kg
M_2	mass of dish used for moisture content determination with lid and coal sample before heating, kg
M_3	mass of dish used for moisture content determination with lid and coal sample after moisture removal, kg
M_1'	mass of crucible used for volatile matter determination with lid, kg
M_2'	mass of crucible used for volatile matter determination with lid and coal sample before heating, kg
M_3'	mass of crucible used for volatile matter determination with lid and residue after removal of volatile from coal sample, kg

M_1'' mass of dish used for ash content determination, kg

M_2'' mass of dish used for ash content determination and coal sample before combustion, kg

M_3'' mass of dish used for ash content determination and residue after combustion, kg

M constant in mass loss correlation

N number of experimental data

N_N normality of standard sulfuric acid, mol/m^3

p ratio of yield of volatile matter to proximate volatile content of coal

R correlation coefficient

T_1 reference temperature for effective heat capacity of bomb calorimeter, 298 K

T_2 room temperature, K

T_n final temperature of the bomb calorimeter after combustion, K

T correction for thermometer reading of bomb calorimeter, K

t time, s

V mass of coal particle at any time t, kg

V_0 mass of coal particle at the beginning, kg

V_∞ mass of coal particle after devolatilization, kg

V_{Expt} experimental data on mass of coal particle at any time t , kg

V_{Calc} calculated value of mass of coal particle at any time t, kg

V_m volatile matter content of coal, %

V_N volume of standard sulfuric acid used in blank of nitrogen determination of coal, cm^3

W mass of coal sample, kg

W_1 mass of crucible and thread in the bomb calorimeter, kg

W_2 mass of crucible, thread and coal sample in the bomb calorimeter, kg

X_1 mass of carbon dioxide absorption unit before combustion, kg

X_2 mass of carbon dioxide absorption unit after combustion, kg

Y_1 mass of water absorption unit before combustion, kg

Y_2 mass of water absorption unit after combustion, kg

Reference

1. J.F. Stubington, K.W.K. Ng, B. Moss, P.K. Peeler, Comparison of experimental methods for determining coal particle devolatilization times under fluidized bed combustor conditions, Fuel 76 (1997) 233–240.
2. M.K. Urkan, M. Arikol, Burning times of volatiles from Turkish coals during fluidized bed combustion, Fuel 73 (1994) 768–772.
3. J.F. Stubington, T.Y. Chui, S. Saisithidej, Experimental factors affecting coal devolatilization time in fluidized bed combustion. Fuel Science and Technology International 10 (1992) 397–419.
4. G. Van der Honing, Volatile and Char Combustion in Large Scale Fluidized Bed Coal Combustor, Ph. D. Thesis, University of Twente, The Netherlands, 1991.
5. R.D. LaNauze, Coal devolatilization in fluidized bed combustors, Fuel 61 (1982) 771–774.
6. R.H. Essenhigh, Influence of coal rank on the burning times of single captive particles, Journal of Engineering for Power 85 (1963) 183–190.
7. J.F. Stubington, S.W. Chan, S.J. Clough, A model for volatiles release into a bubbling fluidized-bed combustor, AIChE Journal 36 (1990) 75–85.
8. J.F. Stubington, T. M. Linjewile, The effects of fragmentation on devolatilization of large coal particles, Fuel 68 (1989) 155–160.
9. J.P. Morris, D.L. Keairns, Coal devolatilization studies in support of the Westinghouse fluidized-bed coal gasification process, Fuel 58 (1979) 465–471.
10. J.F. Stubington, G. Huang, A.W. Scaroni, Devolatilization times of mm-size coal particles, Fuel 70 (1991) 1105–1108.
11. L. Jia, H.A. Becker, R.K. Code, Devolatilization and char burning of coal particles in a fluidized bed combustor, The Canadian Journal of Chemical Engineering 71 (1993) 11–19.
12. K.K. Pillai, Influence of coal type on devolatilization and combustion in fluidized beds, Journal of the Institute of Energy 54 (1981) 142–150.
13. E. Ekinci, G. Yalkin, H. Atakul, A. Erdem-Senatalar, The combustion of volatiles from some Turkish coals in a fluidized bed, Journal of the Institute of Energy 61 (1988) 189–191.
14. C.N. Eatough, L.D. Smoot, Devolatilization of large coal particles at high pressure, Fuel 75 (1996) 1601–1605.

15. S. Halder, R.K. Saha, Studies of mechanism of evolution and combustion of volatiles in fluidized bed combustor, Indian Chemical Engineer 35 (1993) 145–153.
16. J.Q. Zhang, H.A. Becker, R.K. Code, Devolatilization and combustion of large coal particles in a fluidized bed, The Canadian Journal of Chemical Engineering 68 (1990) 1010–1017.
17. K.K. Pillai, Devolatilization and combustion of large coal particles in a fluidized bed, Journal of the Institute of Energy 58 (1985) 3–7.
18. J.F. Stubington, Sumaryono, Release of volatiles from large coal particles in a hot fluidized bed, Fuel 63 (1984) 1013–1019.
19. D.P. Ross, C.A. Heidenreich, D.K. Zhang, Devolatilization times of coal particles in a fluidised-bed, Fuel 79 (2000) 873–883.
20. R.C. Borah, B. Mazumder, M.M. Bora, Atmospheric fluidized bed combustion of high sulphur high volatile N.E. region coals of India, Research and Industry 40 (1995) 315–321.
21. F. Winter, M.E. Prah, H. Hofbauer, Temperature in a fuel particle burning in a fluidized bed: the effect of drying, devolatilization, and char combustion, Combustion and Flame 108 (1997) 302–314.
22. J.P.K. Peeler, H.J. Poynton, Devolatilization of large coal particles under fluidized bed conditions, Fuel 71 (1992) 425–430.
23. S.S. Zabrodsky, Heat transfer between solid particles and a gas in a nonuniformly aggregated fluidized bed, International Journal of Heat and Mass Transfer 6 (1963) 23–31.
24. J.F. Davidson, R. Clift, D. Harrison, Fluidization, Academic Press, Orlando (Florida), 1985.
25. American Society for Testing and Materials, Standard Test Method for Density of Glass by Buoyancy, C693-93(2008), West Conshohocken (Pennsylvania), 2008 (DOI**:** 10.1520/C0693-93R08).
26. S.N. Oka, Fluidized Bed Combustion, Marcel Dekker, New York, 2004.
27. J.G. Speight, Handbook of Coal Analysis, John Wiley, Hoboken (New Jersey), 2005.
28. Bureau of Indian Standards, Indian Standard Method of Sampling of Coal, Manual Sampling (IS: 436, Part I/Section 1), New Delhi, 1964 (Reaffirmed 2007).

29. Bureau of Indian Standards, Indian Standard Method of Test for Proximate Analysis of Coal, IS: 1350 (Part I), New Delhi, 1984 (Reaffirmed 2007).
30. Bureau of Indian Standards, Indian Standard Method of Test for Ultimate Analysis of Coal, Determination of Carbon and Hydrogen, IS: 1350 (Part IV/Section 1), New Delhi, 1974 (Reaffirmed 2005).
31. Bureau of Indian Standards, Indian Standard Method of Test for Ultimate Analysis of Coal, Determination of Nitrogen, IS: 1350 (Part IV/Section 2), New Delhi, 1975 (Reaffirmed 2005).
32. Bureau of Indian Standards, Indian Standard Method of Test for Ultimate Analysis of Coal, Determination of Sulfur, IS: 1350 (Part III), New Delhi, 1969 (Reaffirmed 2005).
33. Bureau of Indian Standards, Indian Standard Method of Test for Determination of Calorific Value of Coal, IS: 1350 (Part II), New Delhi, 1970 (Reaffirmed 2005).

CHAPTER 4

DEVOLATILIZATION OF COAL SAMPLES IN ARGON ATMOSPHERE UNDER FLUIDIZED BED CONDITIONS

4.1 Introduction

Reactions in coal particles are very important aspects in all coal conversion processes. Often these reactions are the rate-limiting steps which control the nature and magnitude of coal conversion processes. In addition, these reactions have a direct effect on the formation of fine particulates, nitrogen and sulfur-containing species, and other pollutants. Coal reactions are generally divided into two distinct components: (i) devolatilization of raw coal, and (ii) oxidation of the residual char [1].

The devolatilization reactions take place as the raw coal is heated in an inert (or an oxidizing) environment. The particle can soften (i.e., become plastic) and sustain internal transformation. Moisture present in the coal evolves early as the temperature rises. As the temperature continues to increase, gases and heavy tarry substances are emanated. The degree of pyrolysis can vary from a few percent up to 70–80% of the total weight of the particle. It can take place in a few milliseconds or over several minutes, depending upon the size and type of coal, and on the environment surrounding the coal particle. The residual mass rich in carbon and depleted in oxygen, hydrogen, nitrogen and sulfur is referred to as ‘char’. The char particle often retains the shape of the original coal particle. It has many cracks or holes in it, which are made by the escaping gases. It may swell to a size which is larger than that of the particle, and become porous internally. The nature of the char

depends upon the type of the coal, and also on the conditions of pyrolysis. The residual char particles can be oxidized or burned-out by direct contact with oxygen at a sufficiently high temperature.

The volatile material released during devolatilization can account for up to half of the coal's heating value [2]. The yield of volatile matter can be determined by pyrolysis, which gives the proportion of coal volatilized during the devolatilization step. The release of volatiles and their subsequent mixing with oxygen for combustion is important for the design of fluidized bed combustion and gasification units. The rate of devolatilization of coal in a fluidized bed combustor depends on several variables such as particle size, atmosphere, fluidization velocity, bed temperature, coal type, and the amount of volatile matter. The small particles are likely to release the volatile matter fast. However, the large particles can release volatile matter above the bed because they are heated at a slower rate than the smaller particles [3]. This causes non-uniformities in the composition in the gas. For a particular design of the bed, this non-uniformity can retard the conversion of the gaseous components and shift the conversion to the downstream region of the furnace, which can influence burn-up and cause undesirable emissions. In some cases, extra air has to be introduced in the freeboard to reduce the emission levels [4]. Hence, it is important to determine the amount of volatile matter released by a single coal particle over time after its injection into the bed.

In this chapter, devolatilization studies of coal samples collected from five collieries of northeastern India in argon atmosphere are reported. The data on mass-loss of coal particles with time are recorded. The effect of particle size on devolatilization time is investigated and a correlation is developed based on these data. A correlation for 95% devolatilization time is also developed. The parameters of

these correlations are found to vary with the superficial gas velocity. These variations are expressed by exponential and polynomial equations. Correlations for the variation of fractional loss of volatile matter with time are developed. The performance of these correlations for single coal particles, and for a batch of coal particles is investigated.

4.2 Analysis of the data on devolatilization in argon atmosphere

4.2.1 Correlation between devolatilization time and particle diameter

The total devolatilization time (i.e. the total time required for a single coal particle to remove all the volatile matter under the given conditions such as temperature, superficial velocity and inert atmosphere) $\left(t_v\right)$ was correlated with the particle diameter $\left(d_v\right)$ as, $t_v = Ad_v^{\,n}$, where A and n are constants. Regressing the data from all coal samples, it was found that $A = 0.74$ s mm^{-n} and $n = 2.01$ $(R^2 = 0.87)$. The 95% confidence intervals of A and n are $(0.40, 1.35)$ and $(1.69, 2.33)$, respectively. Figure 4.1 depicts the variation of total devolatilization time with the particle diameter. This value of n is in agreement with results reported in the literature [5,6]. The exponent n in the correlation, $t_v = Ad_v^n$ usually varies in the range 0.5–2 [7–9,10]. From the results reported in the literature [10], it appears that an exponent value of 1.3 corresponds to the case when the control process is heat transfer from the fluidized bed to the coal particle. In the range of $n = 1.3 - 2$, both external and internal heat transfer processes can be important.

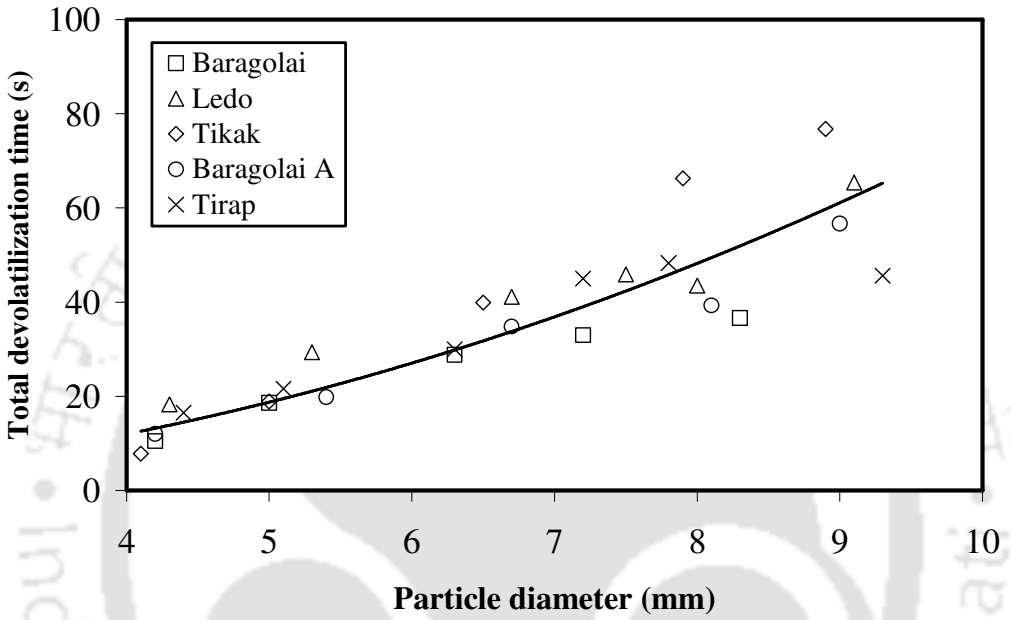

Figure 4.1 Correlation between total devolatilization time (t_v) and particle diameter (d_v): $t_v = 0.74 d_v^{2.01}$.

Therefore the dominant processes are heat transfer between particle and bed, and heat conduction through the particle[10]. It can be observed from Figure 4.1 that the accuracy of the correlation is decreased for the large coal particles. This may be due to the fact that the heterogeneity in the composition of the coals from different collieries caused the variations in the devolatilization times, and this effect was significant for the large particles.

The 95% devolatilization time $\left(t_v^{0.95}\right)$ was correlated with the particle diameter as, $t_v^{0.95} = A_1 d_v^{n_1}$, where A_1 and n_1 are constants. Regressing the data for all coal samples, we obtained, $A_1 = 0.81\ \mathrm{s\,mm^{-n_1}}$ and $n_1 = 1.81$ ($R^2 = 0.91$). The 95% confidence intervals of A_1 and n_1 are $(0.53, 1.25)$ and $(1.58, 2.04)$, respectively. Figure 4.2 shows the variation of 95% devolatilization time with particle diameter. It can be observed from this figure that the accuracy of the correlation decreased with the increase in size of the particles.

There is no report in the literature on the devolatilization time of a coal particle in a fluidized bed in an inert atmosphere at a fluidizing velocity of 1 m/s. However, there are reports on devolatilization time at lower gas velocities [3,11,12]. The correlations reported in the literature vary considerably. The probable reason for this variation lies in the type of coal studied and the superficial velocity employed. A best-fit correlation was obtained from the data reported by Stubington and Sumaryono [11] for three bituminous coals covering a wide range of volatile matter, viz. 19–43%. They had studied coals from the Bulli, Great Northern and Greta collieries of Australia.

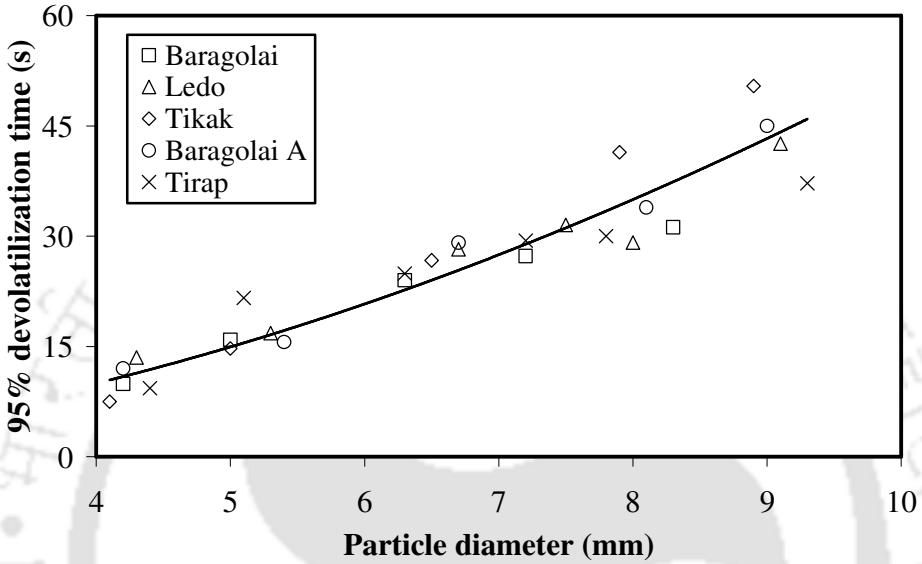

Figure 4.2 Correlation between 95% devolatilization time $\left(t_v^{0.95}\right)$ and particle diameter $\left(d_v\right)$: $t_v^{0.95} = 0.81 d_v^{1.81}$.

For nitrogen gas flowing at a velocity of 0.217 m/s, it was found that, $A_1 = 7.46\,\mathrm{s\ mm^{-n_1}}$ and $n_1 = 1.2$ $\left(R^2 = 0.87\right)$. The 95% confidence intervals of A_1 and n_1 are $(4.34, 12.83)$ and $(0.89, 1.5)$, respectively. The fit of this correlation to the data of Stubington and Sumaryono [11] is shown in Figure 4.3. The values of A_1 and n_1 obtained in the present work agree well with the values reported in the literature [3,11,12]. It has been found from these values that A_1 diminishes exponentially with the superficial velocity (v) as per the following equation.

$$A_1 = 15.08\exp(-3.92v), \qquad R^2 = 0.99 \tag{4.1}$$

The 95% confidence interval for 15.08 is (8.006, 22.15) and the same for –3.92 is (–6.281, –1.565). In addition, it has been found that n_1 increases with the superficial velocity, which can be described by the following polynomial equation.

$$n_1 = 1.085v^2 - 0.315v + 1.037, \qquad R^2 = 0.94 \tag{4.2}$$

The 95% confidence intervals for 1.085, –0.315 and 1.037 are (–3.576, 5.747), (–25.45, 24.82) and (–19.92, 22.00), respectively.

The variations of A_1 and n_1 with the superficial velocity of argon are depicted in Figure 4.4. The coals used in the other studies are different in composition from the coals used in the present study. Also, the superficial gas velocities employed in these studies are quite different in magnitude. Therefore, these correlations can be considered as approximate. However, based on the available data, they depict definite trends in the variation of the correlation parameters A_1 and n_1.

It is clear from Eqs. (4.1), (4.2) and Figure 4.4 that the velocity of the fluidizing gas has an important influence on the devolatilization time. Devolatilization rates

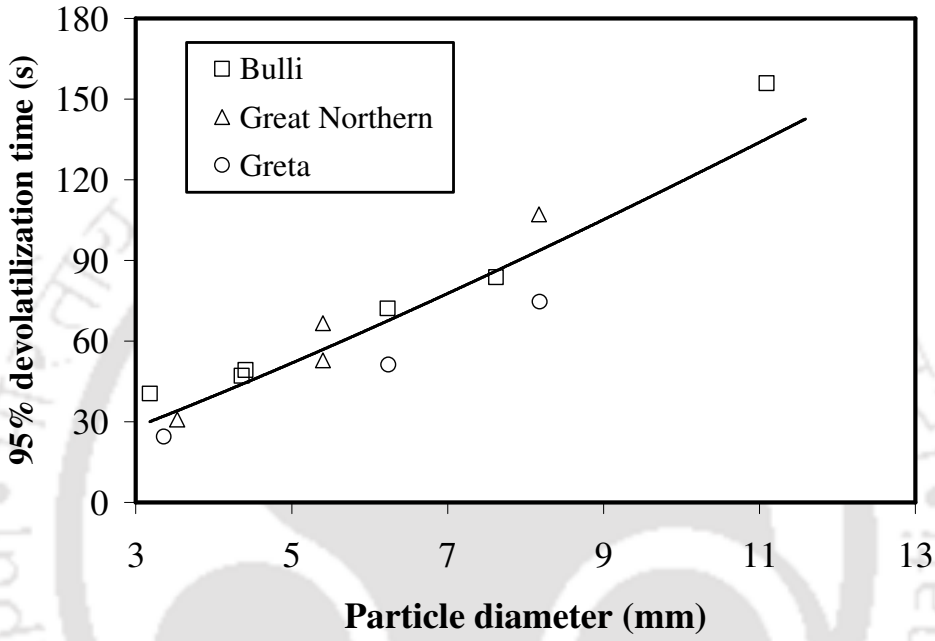

Figure 4.3 Correlation between 95% devolatilization time $\left(t_v^{0.95}\right)$ and particle diameter $\left(d_v\right)$ at 0.217 m/s superficial velocity (based on the data reported by Stubington and Sumaryono [10]): $t_v^{0.95} = 7.46 d_v^{1.2}$.

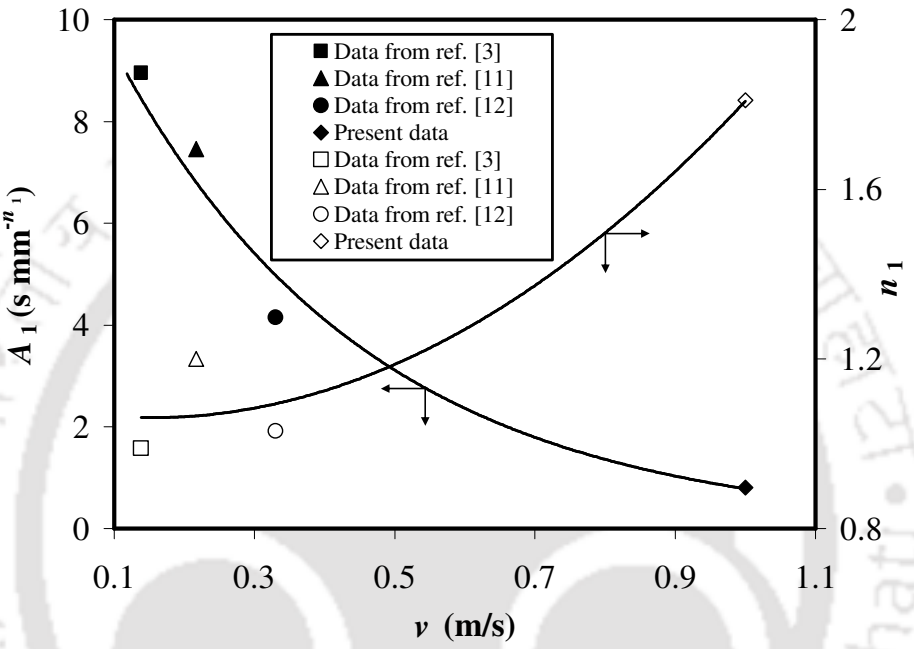

Figure 4.4 Variations of the parameters A_1 and n_1 with superficial gas velocity.

have been reported to be higher at the higher superficial velocities [13]. This is very likely due to the greater convective heat transfer as a consequence of the turbulence created by the higher superficial gas velocity.

4.2.2 Correlation for mass-loss with time

The change of the mass of particles with time for five coals of different size during devolatilization is shown in Figures 4.5–4.9. From these profiles, it can be observed that devolatilization was sluggish in the beginning and then accelerated. The rate decreased towards the end of devolatilization. The initial slow rate is anticipated because a large amount of heat is necessary for the depolymerization reactions. The initial rate of mass-loss was slower for the bigger particles than that for the smaller particles because the rate of heating of the bigger particles was slower than the same of the smaller particles [3]. The middle portion of the curve depicts the major part of devolatilization. The devolatilization rate during this period is dependent on particle size and volatile matter content of the particle. The rate is smaller for the low volatile coal.

The devolatilization rate is high for high volatile coals during this period. Also, the rate is high for larger particles than the smaller particles with the same volatile content. The devolatilization rate was slow towards the end because the volatile content became small. Fragmentation of particles was not observed in any of the experiments. For all other high volatile coals the rate of mass loss is not constant. For large particles it is most pronounced.

The fractional loss of mass (i.e., the fractional release of volatile matter at time t), $v(t)$, was represented by a simple profile,

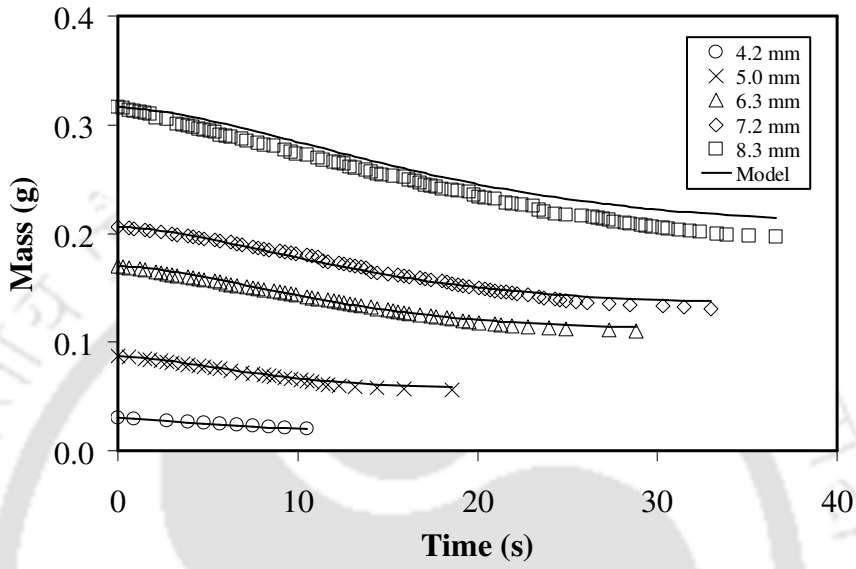

Figure 4.5 Mass versus time profiles for Baragolai coal particles of different size in argon atmosphere. The lines indicate fit according to the equation,

$$V = V_0 - 1.107 V_0 V_m \left[1 - \exp\left(-3.07 d_v^{-2.84} t^{1.6}\right)\right] .$$

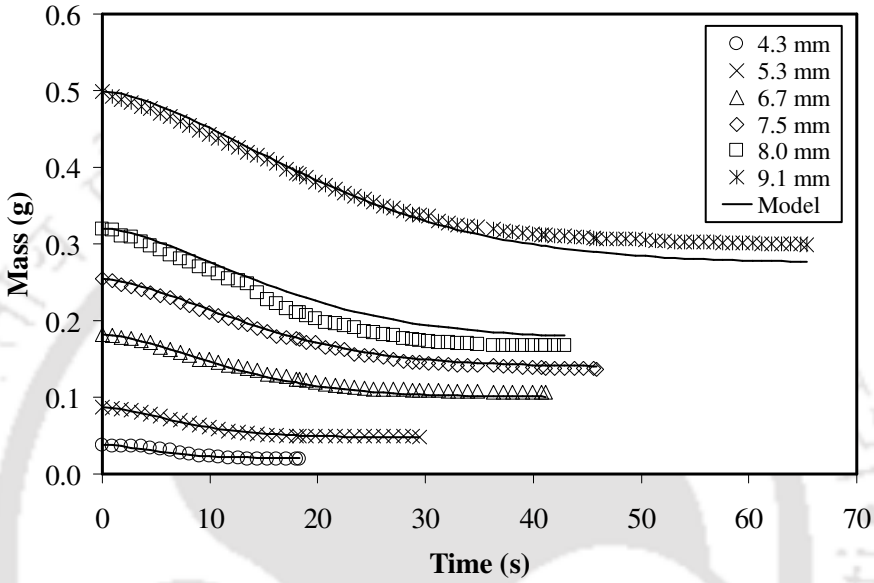

Figure 4.6 Mass versus time profiles for Ledo coal particles of different size in argon atmosphere. The lines indicate fit according to the equation,

$$V = V_0 - 1.107 V_0 V_m \left[1 - \exp\left(-3.07 d_v^{-2.84} t^{1.6}\right)\right].$$

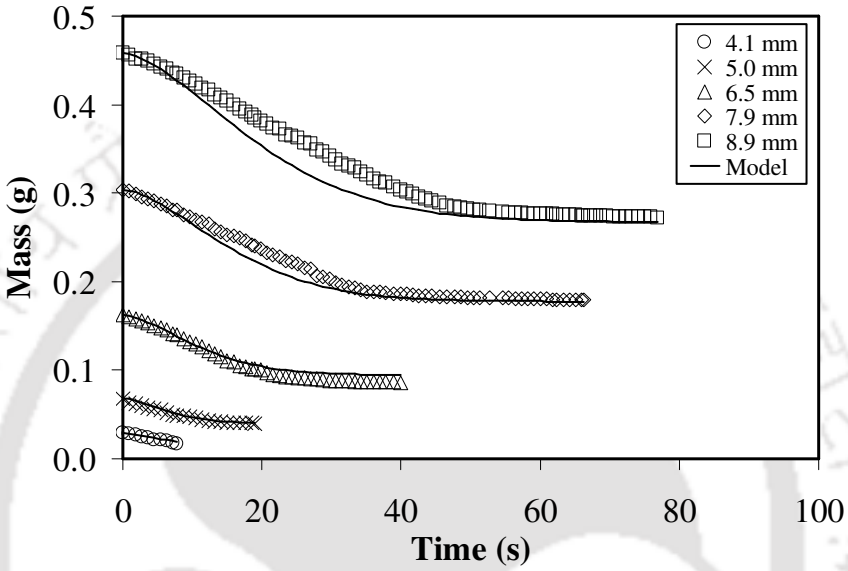

Figure 4.7 Mass versus time profiles for Tikak coal particles of different size in argon atmosphere. The lines indicate fit according to the equation,

$$V = V_0 - 1.107 V_0 V_m \left[1 - \exp\left(-3.07 d_v^{-2.84} t^{1.6}\right)\right].$$

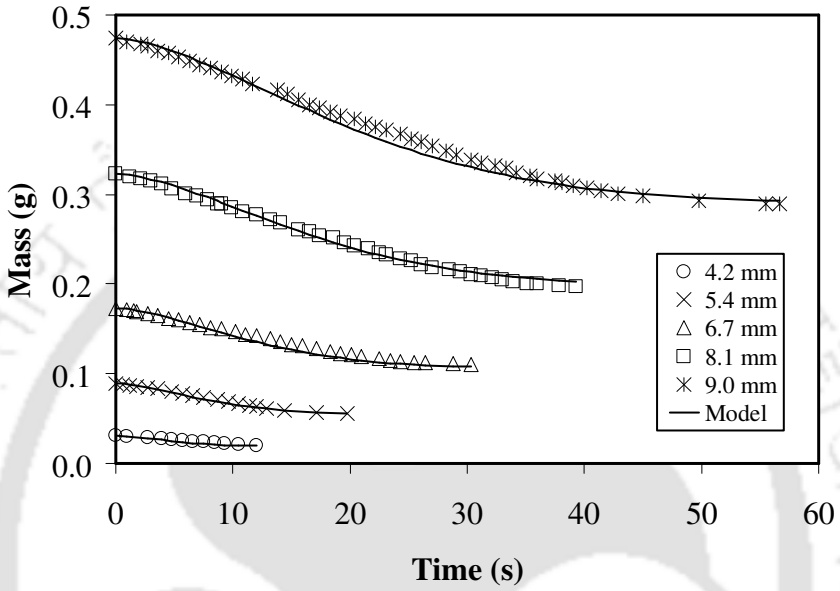

Figure 4.8 Mass versus time profiles for Baragolai A coal particles of different size in argon atmosphere. The lines indicate fit according to the equation,

$$V = V_0 - 1.107 V_0 V_m \left[1 - \exp\left(-3.07 d_v^{-2.84} t^{1.6}\right)\right].$$

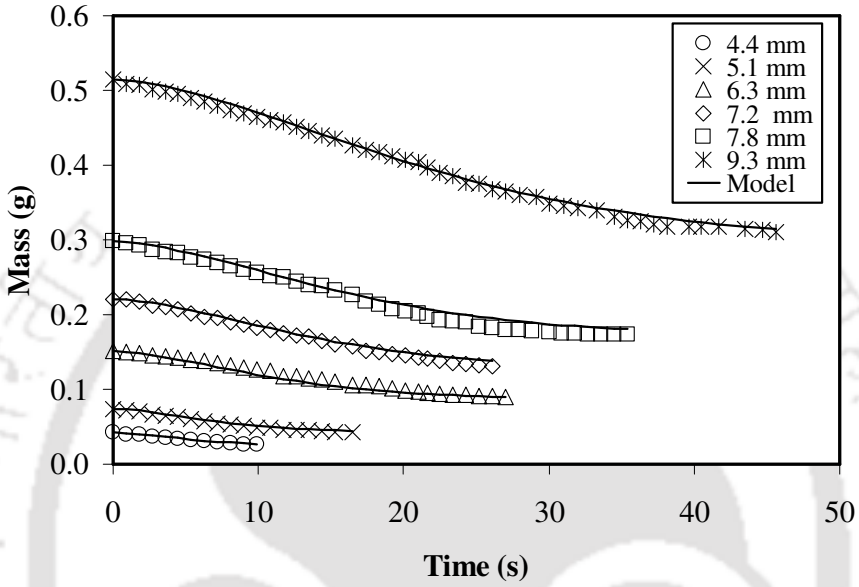

Figure 4.9 Mass versus time profiles for Tirap coal particles of different size in argon atmosphere. The lines indicate fit according to the equation,

$$V = V_0 - 1.107 V_0 V_m \left[1 - \exp\left(-3.07 d_v^{-2.84} t^{1.6}\right)\right].$$

$$v(t) = \frac{V - V_0}{V_\infty - V_0} = 1 - \exp\left(-ct^m\right), \qquad 0 \le t \le t_v \tag{4.3}$$

where c and m are constants, $v(t)$ is the fraction devolatilized, V is the mass at any time, and V_0 and V_∞ represent the total mass before and after devolatilization, respectively. The constants c and m were obtained by fitting the experimental data for coals from the five collieries having a broad range of particle size by minimizing the root mean square error (RMSE) defined by Eq. (3.2) as,

$$\Delta = \left[\Sigma \left[v(t)_{\text{Expt}} - v(t)_{\text{Model}} \right]^2 \Big/ N \right]^{1/2} \tag{4.4}$$

where $v(t)_{\text{Expt}}$ represents the experimental value of the devolatilized fraction, $v(t)_{\text{Model}}$ represents the value calculated from Eq. (4.3) and N represents the number of data points. The value of m was found to be constant and equal to 1.6 for the coals used in this study. The 95% confidence interval for m is (1.58, 1.62). The parameter c was correlated with d_v as, $c = A_2 d_v^{n_2}$, where $A_2 = 3.07\ \text{s}^{-m}\ \text{mm}^{-n_2}$ and $n_2 = -2.84$ $\left(R^2 = 0.96\right)$. The 95% confidence interval for A_2 is (2.03, 4.64) and the same for n_2 is (–3.06, –2.62). The variation of c with the particle diameter is depicted in Figure 4.10. The best fit values of c are given in Table 4.1. The 95% confidence intervals and values of R^2 are given in Table 4.2.

The ratio of the volatile yield to the air-dried proximate volatile content varied from 0.98 to 1.24. This is presented in Table 4.1. The mean ratio for 27 coal samples was 1.1, which is similar to the values reported in the literature [11,14]. Equation

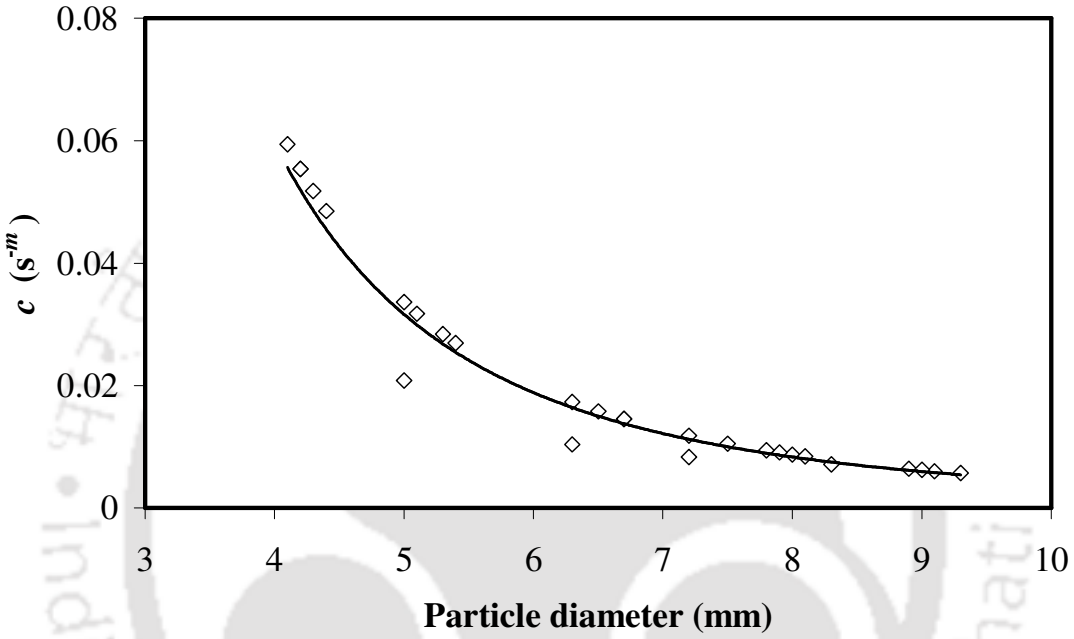

Figure 4.10 Variation of c with particle diameter d_v.

Table 4.1 Summary of experimental results on devolatilization in Argon

Colliery	Size (mm)	Total Devolatilization Time (s)	Yield of Devolatilization (%)	Proximate Volatile Matter (%)	Ratio of Volatile Matter Yield to Proximate Volatile Matter	95% Devolatilization Time (s)	$c\left(\mathrm{s}^{-m}\right)$	Δ
Baragolai	4.2	10.5	33.3	31.2	1.07	9.9	0.0554	0.0008
	5.0	18.6	35.6		1.14	15.9	0.0208	0.0017
	6.3	28.8	35.3		1.13	24.0	0.0104	0.0019
	7.2	33.0	36.4		1.17	27.3	0.0083	0.0027
	8.3	36.6	37.6		1.21	31.2	0.0071	0.0117
Ledo	4.3	18.3	50.0	40.8	1.23	13.5	0.0518	0.0018
	5.3	29.4	44.8		1.10	16.8	0.0284	0.0009
	6.7	41.1	41.8		1.02	28.2	0.0145	0.0039
	7.5	45.9	46.1		1.13	31.5	0.0105	0.0046
	8.0	43.5	48.1		1.18	29.1	0.0087	0.0186
	9.1	65.4	40.1		0.98	42.6	0.0060	0.0134
Tikak	4.1	7.8	41.4	37.8	1.09	7.5	0.0594	0.0012
	5.0	18.9	41.2		1.09	14.7	0.0336	0.0019
	6.5	39.9	46.9		1.24	26.7	0.0158	0.0056
	7.9	66.3	41.1		1.09	41.4	0.0091	0.0089
	8.9	76.8	40.6		1.07	50.4	0.0064	0.0180
Baragolai A	4.2	12.0	35.5	35.4	1.00	12.0	0.0554	0.0014
	5.4	19.8	37.1		1.05	15.6	0.0269	0.0010
	6.7	34.8	37.3		1.05	29.1	0.0145	0.0033
	8.1	39.3	39.0		1.10	33.9	0.0084	0.0036
	9.0	56.7	39.0		1.10	45.0	0.0062	0.0054
Tirap	4.4	16.5	40.5	38.1	1.06	9.3	0.0485	0.0011
	5.1	21.6	44.6		1.17	21.6	0.0317	0.0023
	6.3	30.0	41.7		1.10	24.9	0.0173	0.0035
	7.2	45.0	44.3		1.16	29.4	0.0118	0.0056
	7.8	48.3	43.0		1.13	30.0	0.0094	0.0085
	9.3	45.6	39.8		1.04	37.2	0.0057	0.0073

Table 4.2 Summary of 95% confidence interval for the parameter c and R^2

Colliery	Size (mm)	R^2	$c\left(s^{-m}\right)$	95% confidence interval
Baragolai	4.2	1.00	0.0554	–
	5.0	0.98	0.0208	0.0198–0.0218
	6.3	0.98	0.0104	0.0100–0.0107
	7.2	0.98	0.0083	0.0081–0.0085
	8.3	0.99	0.0071	0.0069–0.0072
Ledo	4.3	1.00	0.0518	–
	5.3	1.00	0.0284	–
	6.7	1.00	0.0145	–
	7.5	1.00	0.0105	–
	8.0	1.00	0.0087	–
	9.1	1.00	0.0060	–
Tikak	4.1	1.00	0.0594	–
	5.0	1.00	0.0336	–
	6.5	1.00	0.0158	–
	7.9	1.00	0.0091	–
	8.9	1.00	0.0064	–
Baragolai A	4.2	1.00	0.0554	–
	5.4	1.00	0.0269	–
	6.7	1.00	0.0145	–
	8.1	1.00	0.0084	–
	9.0	1.00	0.0062	–
Tirap	4.4	1.00	0.0485	–
	5.1	1.00	0.0317	–
	6.3	1.00	0.0173	–
	7.2	1.00	0.0118	–
	7.8	1.00	0.0094	–
	9.3	1.00	0.0057	–

(4.3) can be used to compute the mass of a single coal particle at any until devolatilization is complete.

The total yield of volatile matter $\left(V_0 - V_\infty\right)$ can be taken as 1.107 times the proximate volatile content of the coal. The mass of coal samples was computed by using Eq. (4.3) putting $m = 1.6$. The value of c was computed from the correlation: $c = 3.07 d_v^{-2.84}$. The variation of mass predicted by Eq. (4.3) is indicated by the lines in Figures 4.5–4.9. The root mean square error (Δ) for each particle is given in Table 4.1. A sample calculation is given in the Appendix 4.1.

4.2.3 Variation of the yield of volatile matter with the volatile content of coals

The ratio of the yield of volatile matter to the proximate volatile content (shown in Table 4.1, column 7) was found to decrease with the increasing volatile content, and an increasing trend was observed with the increasing ash content (however, Baragolai A coal was an exception). Similar observations can be made from the results reported in the literature [8,15,16]. This is probably because of the variation in the specific heat of the coals with the variation in their volatile content. The specific heat of a coal of low volatile content is smaller than that of a high-volatile coal [17].

The rate of increase in temperature for a low-volatile coal is higher than that for a high-volatile coal. It has been reported in the literature [18] that the rapid increase in temperature at the high heating rates reduces the residence time of volatile material. It reduces the effect of cracking of tarry matters inside the particle and hence more tarry liquid is produced. However, the yield of the light hydrocarbon gases remains nearly constant. It has also been reported in the literature [18] that the gain in

tar yield with increasing heating rate is higher for the low-volatile coals than that for the high-volatile coals. This also supports the fact that the low-volatile coals are heated more quickly than the high-volatile coals. Therefore, the residence time of volatile matter is less for the low-volatile coals than that for the high-volatile coals. Therefore, the ratio of the volatile yield to the proximate volatile content diminished with the increasing volatile content of the coals.

4.2.4 Devolatilization in multi-particle system

To study the validity of the correlations developed in this chapter for the single coal particles in multi-particle systems, the variation of mass with time for a batch of four particles of Ledo coal was studied. The agreement between the experimental data and Eq. (4.3) was good, as depicted in Figure 4.11. Therefore, it is confirmed that the correlations developed in this study can be used to predict devolatilization of a group of coal particles. The values of c and error (Δ) are reported in Table 4.3.

4.2.5 Visual observation of the coal particles at different times of pyrolysis

The cross-sections of the particles of Baragolai A coal were examined under a microscope after the particles were pyrolyzed at 1123 K for a certain amount of time in the fluidized bed at a fluidizing velocity of 1 m/s. The photographs are shown in Figure 4.12. Two types of particles were observed, viz. partially pyrolyzed and completely pyrolyzed. For the partially pyrolyzed particles, the core was very dull gray, but the outer layer was shiny, porous and black.

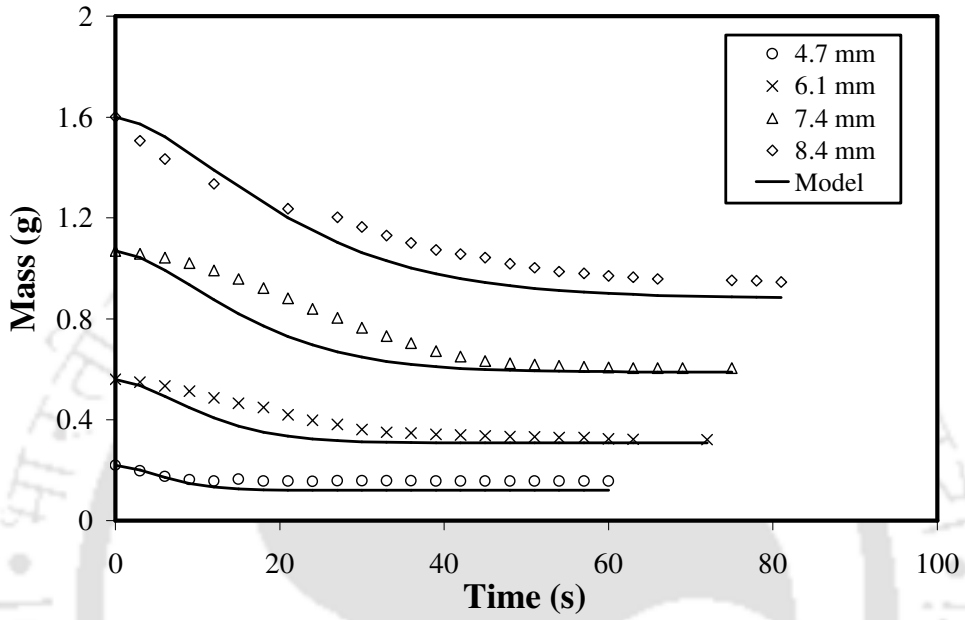

Figure 4.11 Mass versus time profiles for a batch of four particles of Ledo coal in argon atmosphere, and comparison with the model. The average diameters of the particles are shown in the figure.

Table 4.3 Values of c and errors in multi-particle experiments

Particle size (mm)	$c\left(\mathrm{s}^{-m}\right)$	Δ
4.64	0.0391	0.0120
4.71	0.0374	
4.56	0.0410	
4.77	0.0362	
6.43	0.0155	0.0331
6.28	0.0166	
5.99	0.0189	
5.81	0.0207	
8.30	0.0075	0.0702
7.51	0.0099	
7.73	0.0092	
6.15	0.0175	
8.47	0.0071	0.0774
8.34	0.0074	
10.28	0.0041	
6.66	0.0139	

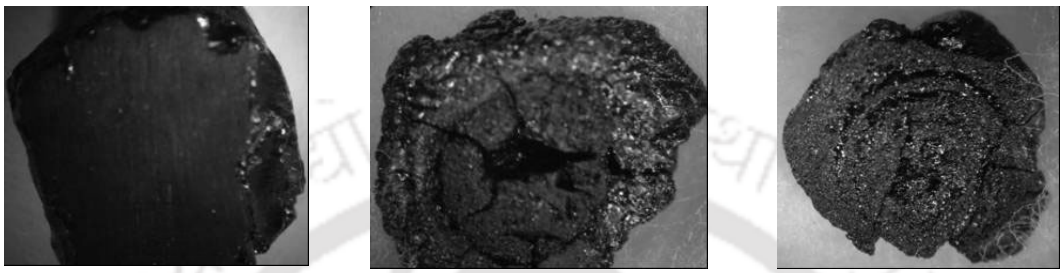

(a) (b) (c)

Figure 4.12 Cross-sectional views of Baragolai A coal particles at different stages of devolatilization: (a) before pyrolysis, (b) after being pyrolyzed for 50 s in argon atmosphere, and (c) after being pyrolyzed for 60 s in argon atmosphere. Magnification = 15×.

The central regions of the partially pyrolyzed coal particles had obviously not reacted, and looked like the original coal. The boundary between these two areas was sharp and distinct. The shrinking-core pattern of devolatilization was clearly discernible.

4.2.6 Mechanism of devolatilization

It has been proposed in the literature [3] that coal devolatilization is controlled by three main factors: (i) heat transfer to and within the particle, (ii) chemical kinetics of pyrolysis, and (iii) mass transfer of volatile products within the particle. A number of models have been developed based on the hypothesis that either internal mass transfer or heat transfer (both to and through the particle) is the rate controlling mechanism. The work of Agarwal et al. [19] reveals that chemical reaction kinetics controls the devolatilization time for particles having diameter less than 0.1 mm. As the particle size increases, the rate-limiting step shifts to a mixed regime between chemical reaction and heat transfer control. For particles larger than 1 mm, it has been found that the rate is controlled by heat transfer, and the devolatilization time varies with the square of the particle diameter. Juntgen and van Heek [20] have reported that chemical kinetics controls the devolatilization rate for particles having diameter below 0.6 mm. Measurements of the center temperature of coal particles of size ranging between 6.4 and 20 mm in fluidized beds have shown that a time lag is exhibited (which is proportional to the size of the particles) before the center of the particles attains the bed temperature [21,22]. This also supports the fact that devolatilization time for large particles is controlled by heat transfer.

It has been shown in the literature [23] that devolatilization of coal can be interpreted by the shrinking-core model with no change in the size of the particle. To analyze the experimental data, a shrinking-core model was used. In this model, it was

assumed that devolatilization was driven by the enthalpy provided by heat transfer through the surface by convection and inside the particles by conduction. The thermal decomposition takes place endothermally at the temperature of the moving (and possibly molten) reaction zone. The char offers no resistance to the gases and vapors leaving the thin reaction zone (where coal undergoes thermal decomposition) due to its relatively high porosity. The following equation has been given by Chern and Hayhurst [23] for the devolatilization time, t_v.

$$\frac{t}{t_v} = 1 - \frac{\frac{3}{2}\left(\frac{r_c}{a}\right)^2 - \left(1 - \frac{k}{ah}\right)\left(\frac{r_c}{a}\right)^3}{\left(\frac{k}{ah} + \frac{1}{2}\right)} \tag{4.5}$$

where a is the radius of the particle, r_c is the radius of the reaction front (i.e., the coal kernel), h is the convective heat transfer coefficient and k is the thermal conductivity of the coal material. From the shrinking-core model, we know that at any instant t, the volumetric ratio of unconverted core to the original coal is given by [23],

$$\left(\frac{r_c}{a}\right)^3 = \frac{V - V_\infty}{V_0 - V_\infty} \tag{4.6}$$

The ratio, r_c/a at any time can be calculated using Eq. (4.6) using the experimental data. The values of $k/(ah)$ for different particle size were calculated from Eq. (4.5) by the regression of the experimental data. The RMSE (Δ) was calculated by the following equation.

$$\Delta = \sqrt{\frac{\Sigma\left[(t/t_v)_{\text{Expt}} - (t/t_v)_{\text{Model}}\right]^2}{N}} \tag{4.7}$$

The values of the Biot number $\left[\text{Bi} = ha/(3k)\right]$ for the coal particles have been presented in Table 4.4.

Table 4.4 Biot numbers for devolatilization in argon atmosphere

Colliery and proximate volatile matter (%)	Diameter (mm)	Bi	Δ
Baragolai (31.2)	4.2	0.055	0.055
	5.0	0.368	0.038
	6.3	0.340	0.022
	7.2	0.254	0.034
	8.3	0.254	0.016
Ledo (40.8)	4.3	0.017	0.055
	5.3	0.203	0.047
	6.7	0.296	0.024
	7.5	0.308	0.020
	8.0	0.193	0.028
	9.1	0.398	0.021
Tikak (37.8)	4.1	0.055	0.052
	5.0	0.393	0.026
	6.5	0.485	0.056
	7.9	0.286	0.047
	8.9	0.110	0.023
Baragolai A (35.4)	4.2	0.055	0.055
	5.4	0.111	0.054
	6.7	0.314	0.026

	8.1	0.031	0.034
	9.0	0.101	0.014
Tirap (38.1)	4.4	0.094	0.015
	5.1	0.312	0.021
	6.3	0.094	0.033
	7.2	0.246	0.024
	7.8	0.128	0.008
	9.3	0.042	0.018

Chern and Hayhurst [23] have reported the Biot numbers corresponding to their data in the range of $0.067 < \mathrm{Bi} < 3.33$. In this region, (r_c/a) varies with (t/t_v) linearly. They have also shown that at $\mathrm{Bi} = 0.66$, Eq. (4.5) shows a prolonged linearity. It can be observed from Table 4.4 that the Biot numbers for devolatilization in argon atmosphere lie between 0.017 and 0.485. A sample calculation has been given in the Appendix 4.2 of this chapter. Biot numbers smaller than 0.1 suggest that the heat conduction resistance inside the particle is much lower than the heat transfer resistance at the surface. It also suggests that the temperature is constant inside the particles. The lumped-capacitance model of transient heat transfer is applicable for Biot numbers less than 0.1 [24]. From Table 4.4, it can be observed that for coal particles having diameter of ~4 mm, this condition is satisfied. Hence, it can be concluded that the internal resistance to conduction is significantly smaller than the external resistance to convection for particles of ~4 mm diameter. For $0.1 < \mathrm{Bi} < 1$, the temperature inside the particle cannot be assumed to be constant. For Biot numbers greater than unity, the internal heat transfer resistance is higher than external heat transfer resistance. The coal samples studied in this work belong to the second category. The Biot numbers of the particles ($\geq 5\,\mathrm{mm}$) used in our study fall in the same range as that reported by Chern and Hayhurst [23]. For coal particles of size > 4 mm, it can be observed from the results presented in Table 4.4 that the Biot number decreases with the increase in particle size. The apparent decrease in Biot number is a consequence of the reduction in the heat transfer co-efficient with the increase in particle size. The large amount of volatile matter released from the large coal particles forms a thick film around the particles. This increases the resistance to heat transfer. Consequently, the external heat transfer by convection decreases.

Appendix 4.1 Calculation of root mean square error (RMSE)

Sample: Baragolai A coal particle of 8.1 mm diameter

Time	Actual mass of coal particle (g)	Calculated mass (g)
0.0	0.323	0.323
1.2	0.320	0.322
2.1	0.317	0.320
3.0	0.315	0.317
3.9	0.312	0.314
4.8	0.306	0.311
6.0	0.301	0.306
6.9	0.298	0.302
7.8	0.294	0.298
8.7	0.290	0.294
9.0	0.289	0.292
9.9	0.285	0.288
10.8	0.281	0.284
12.0	0.277	0.278
13.2	0.272	0.272
14.1	0.268	0.268
15.6	0.261	0.261
16.5	0.258	0.257
17.4	0.254	0.254
18.6	0.252	0.249
19.5	0.246	0.245
20.4	0.243	0.242
21.6	0.239	0.238
22.5	0.235	0.235
23.1	0.233	0.233
24.3	0.228	0.229

25.2	0.226	0.227
26.1	0.222	0.224
27.0	0.218	0.222
29.4	0.214	0.219
30.3	0.211	0.217
31.2	0.209	0.215
32.1	0.207	0.213
33.0	0.205	0.212
33.9	0.203	0.211
35.1	0.201	0.209
36.0	0.200	0.208
37.8	0.198	0.207
39.3	0.197	0.205

Calculated mass at any time $= V = V_0 + (V_\infty - V_0)\left[1 - \exp\left(-ct^m\right)\right]$

where,

$V_0 =$ initial mass of coal particle = 0.323 g

$V_0 - V_\infty =$ total amount of volatile matter evolved

$= V_0 \times$ volatile matter content $\times$ average ratio of the yield of volatile matter

$c = 3.07 d_v^{-2.84}$

$d_v = 8.1$ mm

$m = 1.6$

$V = 0.323 - 0.323 \times 0.354 \times 1.107 \times \left[1 - \exp\left(-0.0075 t^{1.6}\right)\right]$

From Eq. (4.4),

$$\text{Error} = \left[\left(V_{\text{Expt}} - V_{\text{Model}}\right)^2 \Big/ N\right]^{1/2}$$

where, N = Number of experimental data = 40

Therefore, Error = 3.584×10^{-3}

Appendix 4.2 Sample calculation for the determination of Biot number

Sample: 5.1 mm diameter Tirap coal

Time	Mass	r_c/a	Experimental value of t/t_v	Calculated value of t/t_v
0.0	0.074	1.000	0.000	0.000
0.9	0.072	0.978	0.059	0.044
1.8	0.070	0.955	0.118	0.090
2.7	0.066	0.905	0.176	0.184
3.6	0.064	0.878	0.235	0.232
4.5	0.063	0.864	0.294	0.258
5.4	0.06	0.819	0.353	0.335
6.3	0.057	0.767	0.412	0.417
7.2	0.055	0.729	0.471	0.475
8.1	0.053	0.686	0.529	0.536
9.0	0.051	0.637	0.588	0.601
9.9	0.049	0.578	0.647	0.671
10.8	0.048	0.544	0.706	0.710
11.7	0.046	0.459	0.765	0.794
12.6	0.045	0.401	0.824	0.843
13.5	0.045	0.401	0.882	0.843
14.4	0.044	0.318	0.941	0.902
15.3	0.043	0.000	1.000	1.000

Let us calculate t/t_v from Eq. (4.7),

$$\frac{t}{t_v} = 1 - \frac{1.5\left(\frac{r_c}{a}\right)^2 - \left(1 - \frac{k}{ah}\right)\left(\frac{r_c}{a}\right)^3}{\left(\frac{k}{ah} + 0.5\right)}$$

$$\frac{r_c}{a} = \left(\frac{V - V_\infty}{V_0 - V_\infty}\right)^{1/3}$$

t_v = devolatilization time = 15.3 s

r_c = radius of unreacted core, mm

a = radius of the coal particle = 5.1 mm

k = thermal conductivity of coal, W K^{-1} m^{-1}

h = convective heat transfer coefficient, W K^{-1} m^{-2}

The value of $\left(\frac{k}{ah}\right)$ is determined by minimizing the error, as described by Chern and Hayhurst [22].

V = total mass at any time t, kg

V_0 = value of V at $t \to 0 = 0.074$ g

V_∞ = value of V at $t \to \infty = 0.043$ g

$$\text{Bi} = \frac{ha}{3k} = \frac{1}{3 \times 1.0676} = 0.312$$

From Eq. (4.7),

$$\text{Error} = \sqrt{\frac{\left[(t/t_v)_{\text{Expt}} - (t/t_v)_{\text{Calc}}\right]^2}{N}} = 0.021$$

where N = Number of experimental data = 18

Notations

a	radius of the coal particle, m
A	constant in the power law correlation for total devolatilization time, s mm^{-n}
A_1	constant in the power law correlation for 95% devolatilization time, s mm^{-n_1}
A_2	constant in the power law correlation for parameter c, $\text{s}^{-m}\ \text{mm}^{-n_2}$
c	constant in mass-loss correlation, s^{-m}
d_v	mass-equivalent volumetric diameter, m
h	convective heat transfer coefficient, $\text{W K}^{-1}\ \text{m}^{-2}$
k	thermal conductivity, $\text{W K}^{-1}\ \text{m}^{-1}$
m	constant in mass-loss correlation
n	constant in power law correlation for total devolatilization time
n_1	constant in power law correlation for 95% devolatilization time
n_2	constant in power law correlation for parameter c
N	number of experimental data points
r_c	radius of the central core, m
R^2	coefficient of determination
t	time, s
t_v	total devolatilization time, s
$v(t)$	fraction devolatilized
$v(t)_{\text{Expt}}$	experimental value of the fraction devolatilized
$v(t)_{\text{Model}}$	value of the fraction devolatilized predicted by the correlation

V total mass at any time t, kg

V_0 value of V at $t \to 0$

V_∞ value of V at $t \to \infty$

Greek letters

Δ root mean square error (RMSE)

Reference

1. L.D. Smoot, P.J. Smith, Coal Combustion and Gasification, Plenum Press, New York, 1985.
2. K.L. Smith, L.D. Smoot, T.H. Fletcher, R.J. Pugmire, The Structure and Reaction Processes of Coal, Plenum, New York, 1994.
3. D.P. Ross, C.A. Heidenreich, D.K. Zhang, Devolatilization times of coal particles in a fluidized-bed, Fuel 79 (2000) 873–883.
4. R.C. Borah, B. Mazumder, M.M. Bora, Atmospheric fluidized bed combustion of high sulphur high volatile N.E. region coals of India, Research and Industry 40 (1995) 315–321.
5. R.H. Essenhigh, M.W. Thring, Measurement of burning times of single coal particles, Proceedings of the Conference on Scientific use of Coal, Sheffield, 1958, pp. D21−D27.
6. R.H. Essenhigh, Influence of coal rank on the burning times of single captive particles, Journal of Engineering for Power, 85 (1963) 183–190.
7. P.K. Agarwal, W.E. Genetti, Y.Y. Lee, S.N. Prasad, Model for drying during fluidized-bed combustion of wet low-rank coals, Fuel 63 (1984) 1020–1027.
8. D.B. Anthony, J.B. Howard, Coal devolatilization and hydrogasification, AIChE Journal 22 (1976) 625–656.
9. R.D. LaNauze, Coal devolatilization in fluidized bed combustors, Fuel 61 (1982) 771–774.
10. S.N. Oka, E.J. Anthony, Fluidized Bed Combustion, Marcel Dekker, New York, 2004.
11. J.F. Stubington, Sumaryono, Release of volatiles from large coal particles in a hot fluidized bed, Fuel 63 (1984) 1013–1019.
12. J.P. Morris, D.L. Keairns, Coal devolatilization studies in support of the Westinghouse fluidized-bed coal gasification process, Fuel 58 (1979) 465 – 471.
13. F. Winter, M.E. Prah, H. Hofbauer, Temperature in a fuel particle burning in a fluidized bed: the effect of drying, devolatilization, and char combustion, Combustion and Flame 108 (1997) 302–314.
14. J.Q. Zhang, H.A. Becker, R.K. Code, Experimental study on devolatilization of large coal particles in a fluidized bed, Proceedings of 9th International Conference on Fluidized Bed Combustion, vol. 2, ASME, New York, 1987, pp. 1203−1210.

15. J.P.K. Peeler, H.J. Poynton, Devolatilization of large coal particles under fluidized bed conditions, Fuel 71 (1992) 425–430.
16. A.S. Jamaluddin, J.S. Truelove, T.F. Wall, Devolatilization of bituminous coals at medium to high heating rates, Combustion and Flame 63 (1986) 329–337.
17. J. Tomeczek, H. Palugniok, Specific heat capacity and enthalpy of coal pyrolysis at elevated temperatures, Fuel 75 (1996) 1089–1093.
18. P. Arendt, K.-H. van Heek, Comparative investigations of coal pyrolysis under inert gas and H_2 at low and high heating rates and pressures up to 10 MPa, Fuel 60 (1981) 779–787.
19. P.K. Agarwal, W.E. Genetti, Y.Y. Lee, Model for devolatilization of coal particles in fluidized beds, Fuel 63 (1984) 1157–1165.
20. H. Jüntgen, K.-H. van Heek, An update of German non-isothermal coal pyrolysis work, Fuel Processing Technology 2 (1979) 261–293.
21. C.N. Eatough, L.D. Smoot, Devolatilization of large coal particles at high pressure, Fuel 75 (1996) 1601–1605.
22. J.Q. Zhang, H.A. Becker, R.K. Code, Devolatilization and combustion of large coal particles in a fluidized bed, The Canadian Journal of Chemical Engineering 68 (1990) 1010–1017.
23. J.S. Chern, A.N. Hayhurst, Does a large coal particle in a hot fluidised bed lose its volatile content according to the shrinking core model? Combustion and Flame 139 (2004) 208–221.
24. F.P. Incropera, D.P. DeWitt, T.L. Bergman, A.S. Lavine, Fundamentals of Heat and Mass Transfer, John Wiley, New York, 2007.

CHAPTER 5

DEVOLATILIZATION OF COAL SAMPLES IN AIR UNDER FLUIDIZED BED CONDITIONS

5.1 Introduction

Combustion of coal in fluidized beds is a complex process. Numerous parallel reactions take place from the time the coal particle enters a fluidized bed until it is burnt out completely. It is difficult to infer on the various processes that occur during combustion, from a single experiment or a set of experiments. Parameters have to be selected and investigated independently to acquire knowledge on the effect of different environments.

It has been mentioned in Section 4.1 that the coal reactions can be divided into two distinct components, viz. devolatilization of raw coal, and oxidation of the residual char [1]. Devolatilization is the first step in any coal conversion process in which the volatile matter is released. Devolatilization can be accomplished in a few milliseconds or it can occur over a period of several minutes, depending upon the size and type of coal. It also depends on the environment surrounding the coal particle. The remaining solid matrix is called char. The nature of the char depends on the type of the coal, and also on the conditions of pyrolysis. In fact, coal combustion in fluidized bed can be regarded as combustion of two fuels, viz. combustion of volatile matter (homogeneous), and combustion of char (heterogeneous). In reality, mutual influences exist between these two processes, and they take place simultaneously.

From the discussion in Section 4.1, it is evident that knowledge on the extent of devolatilization of coal particles of different size with respect to time in a fluidized bed is essential to optimize the particle size and the height of the bed. There are several reports in the literature [2,3–5] on the devolatilization times of coal particles in presence of air. However, these works have not reported the mass-loss of single particles with time. Thunman and Lackner [6] have studied the devolatilization of a batch of coal particles in air, and developed an empirical correlation for the change of mass with time. For practical purposes, it would be better to examine a batch of coal particles, but it has been reported in the literature [7] that the coal particles having caking properties fuse together during pyrolysis, and grow into a single large particle. Therefore, care has to be taken for studying devolatilization of a batch of coal particles. Moreover, there is no report in the literature on the devolatilization time of coals in a fluidized bed in the presence of air at high fluidizing velocities (e.g., 1 m/s).

In this chapter, devolatilization studies of coal samples from five collieries of northeastern India in air are reported. The data on mass-loss of coal particles with time are analyzed as discussed in Section 4.1.

5.2 Analysis of the data on devolatilization in air

5.2.1 Correlation between devolatilization time and particle diameter

The devolatilization time (t_v) was correlated with the particle diameter (d_v) as, $t_v = Ad_v^n$, where A and n are constants. Regressing the data for all coal samples, it was found that $A = 0.60\,\mathrm{s\,mm^{-n}}$ and $n = 1.92$. The 95% confidence intervals for A and n are $(0.38, 0.94)$ and $(1.67, 2.16)$, respectively $(R^2 = 0.92)$. Figure 5.1 shows the

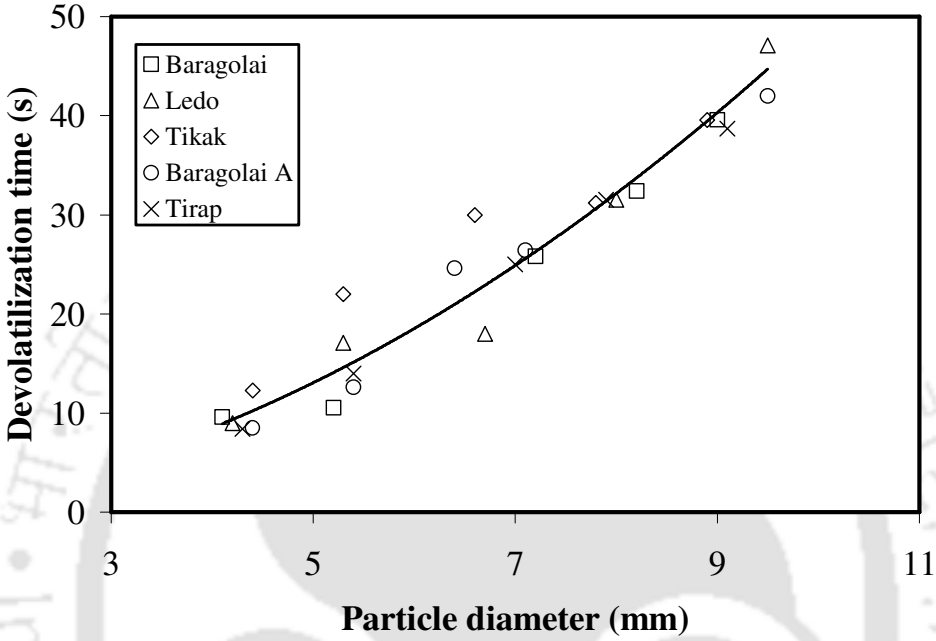

Figure 5.1 Correlation between devolatilization time (t_v) and particle diameter (d_v): $t_v = 0.60 d_v^{1.92}$.

variation of devolatilization time with the particle diameter. These results are in agreement with the results reported in the literature [3,5,6]. If we compare the devolatilization time (reported in terms of the flame extinction time) correlations given in the literature [3,5,6] with our correlation, it is found that our experimental data follow the trend of the results reported in the literature (Figure 5.2). It has also been reported in the literature that the devolatilization time decreases as the superficial velocity increases [10]. This is depicted in Figure 5.2.

5.2.2 Correlation of parameters of devolatilization time with superficial velocity

There is no report in the literature on the devolatilization time of a coal particle in a fluidized bed in air at a fluidizing velocity of 1 m/s. However, there are reports on devolatilization time at lower velocities [2,3,4]. The effect of superficial air velocity on devolatilization time has been shown in Figure 5.2. It is observed from this figure that the devolatilization time decreased as the superficial velocity was increased. The correlation parameters A and n varied with the superficial gas velocity in a manner similar to that observed for the devolatilization in the argon atmosphere (Chapter 4). It was observed that A exponentially decreased with the increase in the superficial velocity (v), which can be described by the correlation,

$$A = 2.02\exp(-1.24v),\ R^2 = 0.99 \tag{5.1}$$

The 95% confidence interval for 2.02 is $(1.77, 2.27)$ and the same for 1.24 is $(-1.70, -0.78)$. The parameter n increased with the increase in superficial velocity following the correlation,

$$n = -0.0762v^2 + 0.5506v + 1.446,\ R^2 = 1 \tag{5.2}$$

The 95% confidence intervals of –0.0762, 0.5506 and 1.446 are (–0.0946, –0.0578),

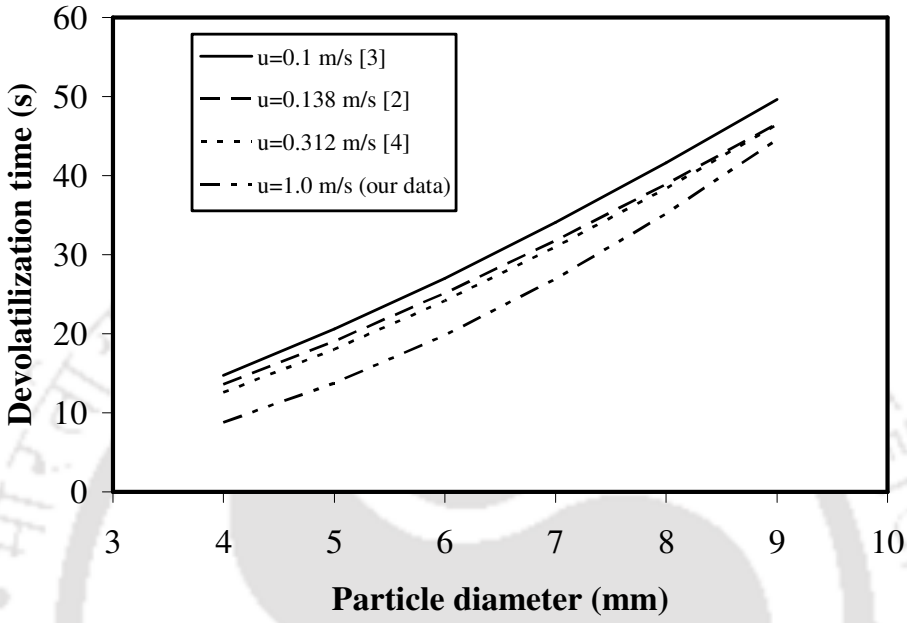

Figure 5.2 Comparison of correlations for the variation of devolatilization time with particle diameter.

$(0.5295, 0.5717)$ and $(1.442, 1.449)$, respectively. The variations of A and n with the superficial velocity of air are depicted in Figure 5.3. It is evident from Eqs. (5.1) and (5.2) that the velocity of the fluidizing gas has a significant effect on the devolatilization time. It has been reported in the literature that the devolatilization rate increases with the increase in the superficial velocity [8]. This is probably due to the greater convective heat transfer as a consequence of the turbulence created by the higher gas velocity.

5.2.3 Correlation for mass-loss with time

The variation of the mass of the particles with time for five coals of different size during devolatilization is presented in Figures 5.4–5.8. From these profiles, it can be observed that the curves consist of two distinct linear segments. The first segment represents devolatilization and the second segment represents the combustion of char. In this work, only the devolatilization segments were examined. It can be seen from these figures that the point of intersection of the two linear segments is not sharp. This reflects that in this region, both devolatilization and char combustion processes are prevalent. To mark the end of devolatilization, two straight lines are drawn for both the segments, and the point of intersection of these two lines is taken as the devolatilization time. This has been illustrated in Figure 3.4. Fragmentation of the particles was not observed in any of the experiments. It can be observed from Figures 5.4–5.8 that the devolatilization time increased with the increase in the particle diameter. The slope of the devolatilization line increased as the particle diameter increased, which indicates that the devolatilization rate increased with the increase in particle diameter. The amount of volatile matter evolved increased as the particle diameter increased. Since all the particles were exposed to the same atmosphere, it is

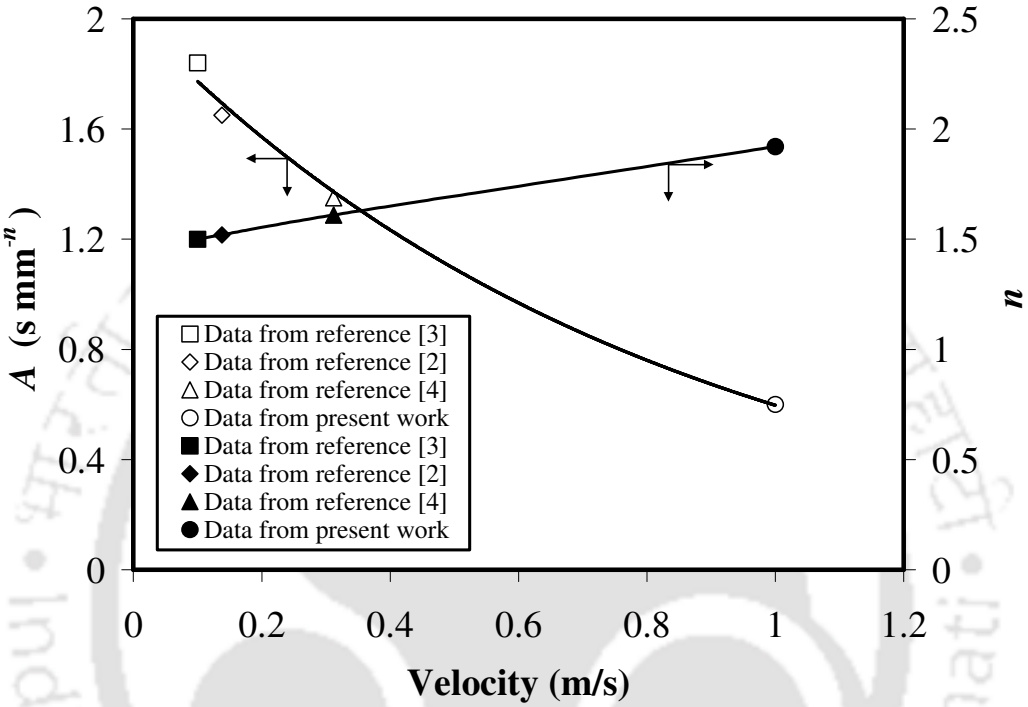

Figure 5.3 Variations of *A* and *n* with the superficial gas velocity.

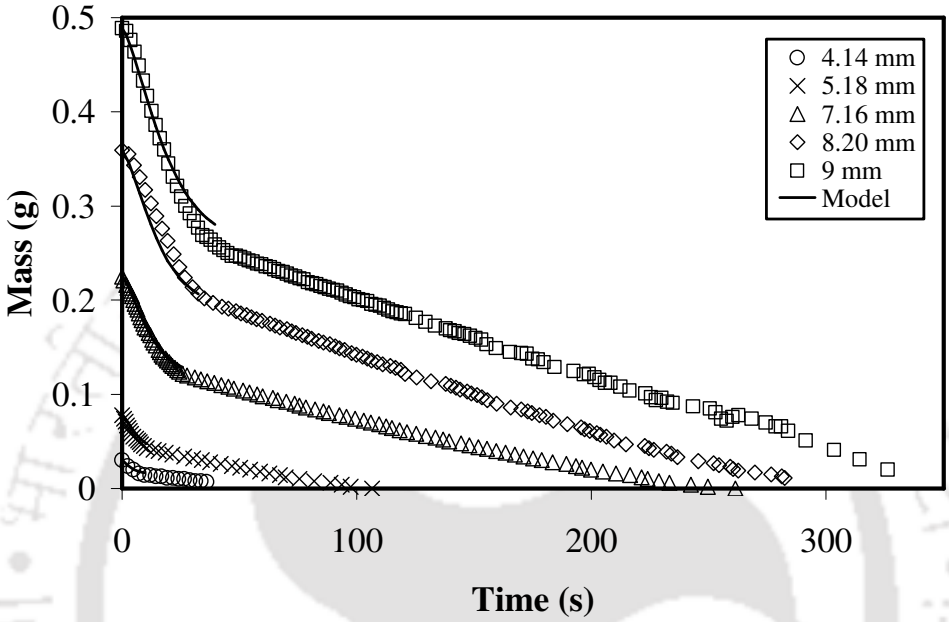

Figure 5.4 Mass versus time profiles for Baragolai coal particles of different size in air. The lines indicate fit according to the equation,

$$V = V_0 - 1.48 V_0 V_m \left[1 - \exp\left(-6.64 d_v^{-2.78} t^{1.4}\right)\right] .$$

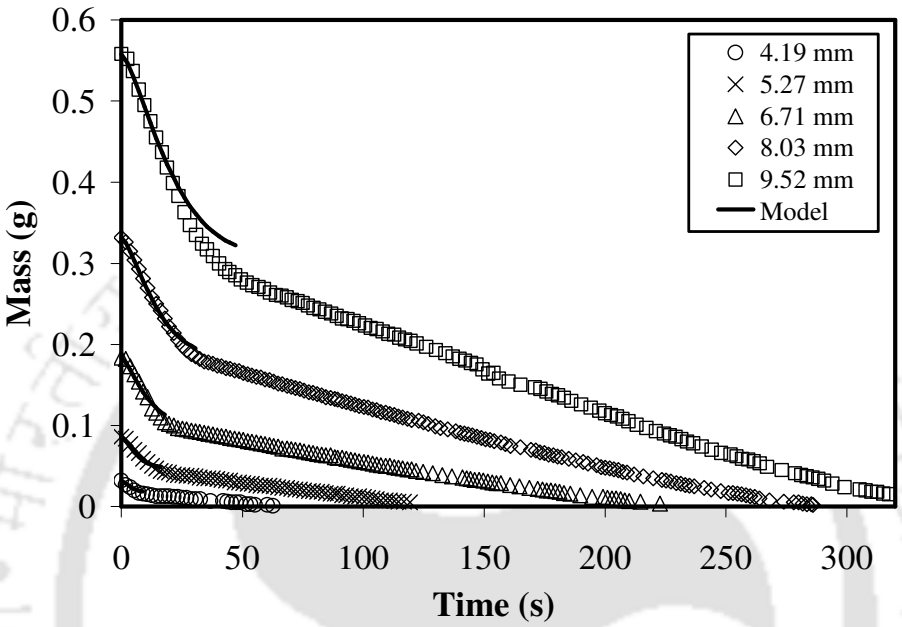

Figure 5.5 Mass versus time profiles for Ledo coal particles of different size in air.

The lines indicate fit according to the equation,

$$V = V_0 - 1.103 V_0 V_m \left[1 - \exp\left(-6.64 d_v^{-2.78} t^{1.4}\right)\right].$$

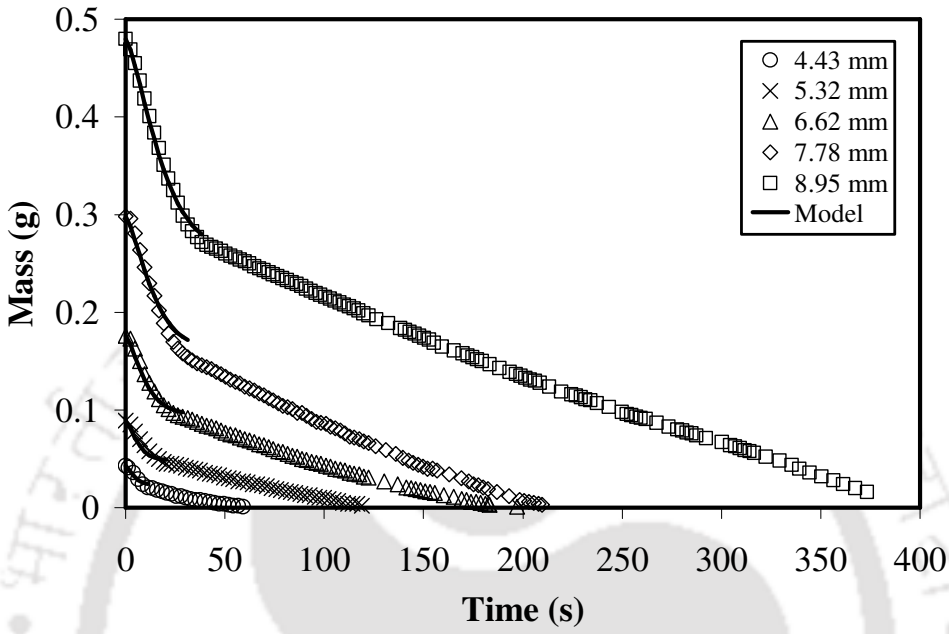

Figure 5.6 Mass versus time profiles for Tikak coal particles of different size in air.

The lines indicate fit according to the equation,

$$V = V_0 - 1.199 V_0 V_m \left[1 - \exp\left(-6.64 d_v^{-2.78} t^{1.4}\right)\right] .$$

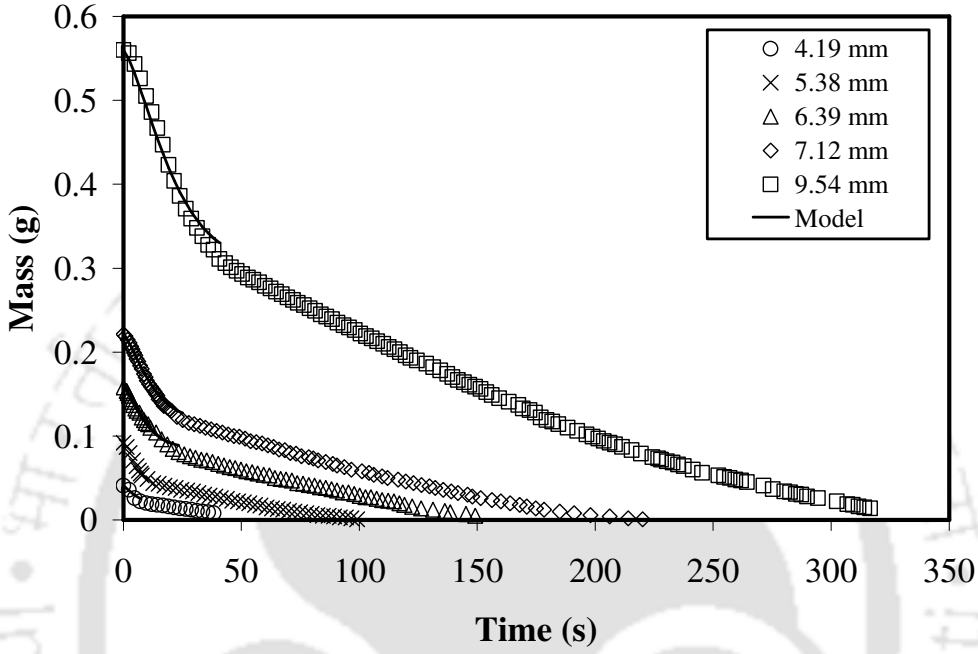

Figure 5.7 Mass versus time profiles for Baragolai A coal particles of different size in air. The lines indicate fit according to the equation,

$$V = V_0 - 1.29 V_0 V_m \left[1 - \exp\left(-6.64 d_v^{-2.78} t^{1.4}\right)\right] .$$

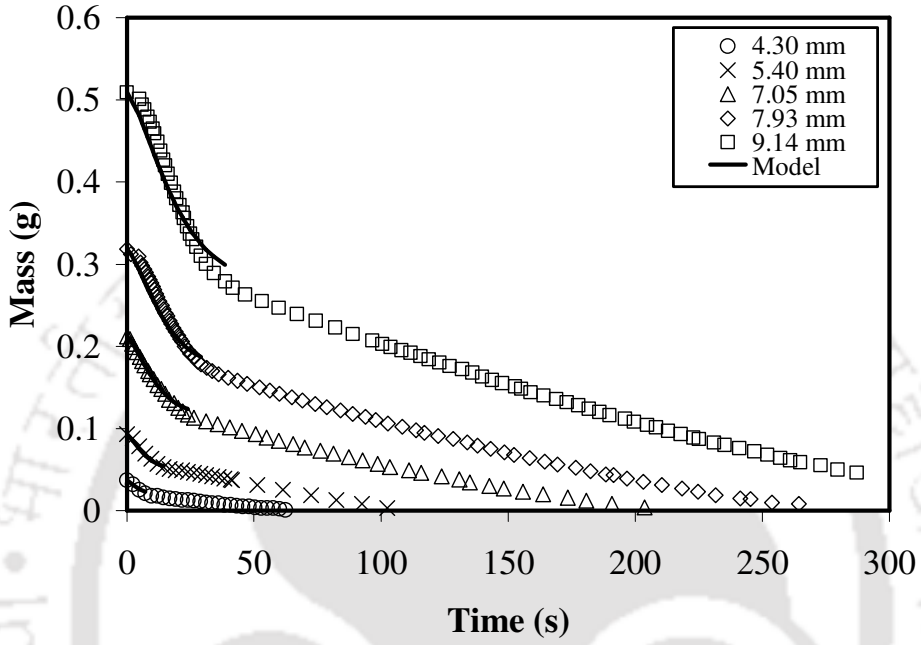

Figure 5.8 Mass versus time profiles for Tirap coal particles of different size in air.

The lines indicate fit according to the equation,

$$V = V_0 - 1.19 V_0 V_m \left[1 - \exp\left(-6.64 d_v^{-2.78} t^{1.4}\right)\right].$$

obvious that the loss of volatile matter with respect to time increased as the amount of devolatilization increased with the increase in volatile content. This apparently is the reason for the decrease in overall rate of heating as the particle diameter increased.

The fractional loss of mass (i.e., the fractional release of volatile matter) at time *t*, *v*(*t*), was represented by a simple profile as given by Eq. (4.3). However the values of c and m have been found to be different from that in the inert atmosphere. The value of m was found to be 1.4 for the coals used in this study. The 95% confidence interval for m is $(1.35, 1.45)$. The values of c are given in Table 5.1. The parameter c was correlated with d_v as, $c = A_2 d_v^{n_2}$, where $A_2 = 6.64$ $s^{-m}mm^{-n_2}$ and $n_2 = -2.78$ $\left(R^2 = 0.93\right)$. The 95% confidence interval for A_2 is (3.536, 12.491) and the same for n_2 is (–3.120, –2.450). The variation of c with the particle diameter is depicted in Figure 5.9. The values of 95% confidence intervals of *c* and coefficient of determination $\left(R^2\right)$ are given in Table 5.2.

The ratio of the yield of volatile matter to that of the proximate volatile matter varied between 1.03 and 1.60 (see Table 5.1). The average ratio for 25 coal samples was 1.25. These results agree well with the data reported by Peeler and Poynton [9]. The ratio of the total yield of volatile matter to the proximate volatile matter decreased with the increase in particle diameter (see Table 5.1). This agrees with the results reported in the literature [1,10]. The reason for this variation is that the heating rate is greater for the smaller particles and the release of volatile matter is faster, which reduces the possibility of cracking of the volatiles inside the particles. This increases the total yield of volatile matter, and the opposite phenomenon occurs for the larger particles. Equation (4.3) can be used to compute the mass of a single coal particle at any time until the devolatilization is complete.

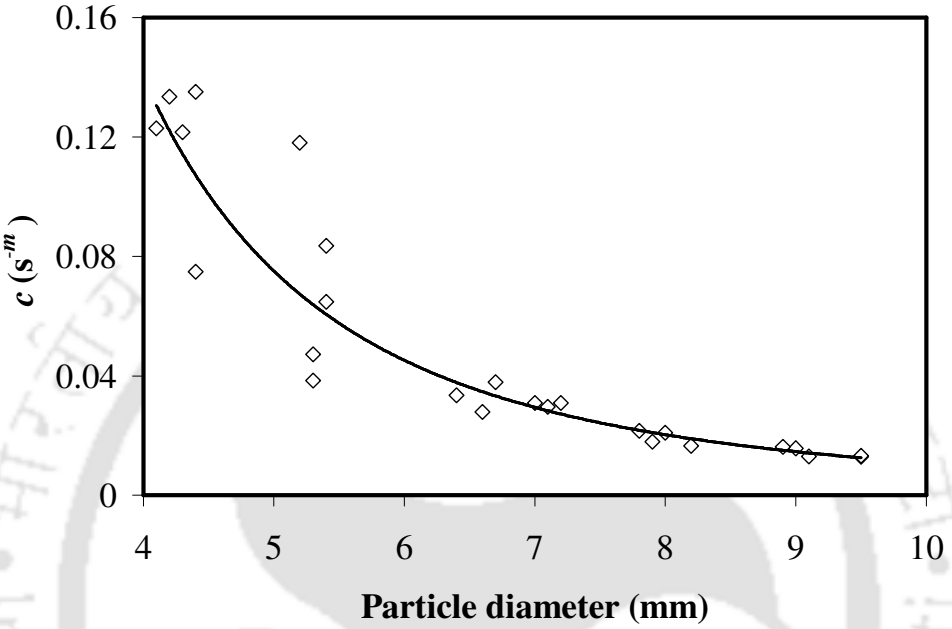

Figure 5.9 Variation of *c* with particle diameter.

Table 5.1 Summary of experimental results on devolatilization in air

Colliery	Size (mm)	Devolatilization Time (s)	Yield of Devolatilization (%)	Proximate Volatile Matter (%)	Ratio of Yield of Volatile Matter to Proximate Volatile Matter	c (s^{-m})	Δ
Baragolai	4.1	9.6	50.0	31.2	1.60	0.1229	0.0014
	5.2	10.5	46.0		1.47	0.1181	0.0049
	7.2	25.8	47.0		1.51	0.0309	0.0034
	8.2	32.4	45.0		1.44	0.0166	0.0145
	9.0	39.6	45.0		1.44	0.0158	0.0119
Ledo	4.2	9.0	49.0	40.8	1.20	0.1335	0.0016
	5.3	17.1	47.0		1.15	0.0472	0.0033
	6.7	18.0	44.0		1.08	0.0378	0.0047
	8.0	31.5	42.0		1.03	0.0209	0.0050
	9.5	47.1	45.0		1.10	0.0129	0.0208
Tikak	4.4	12.3	51.0	37.8	1.35	0.0748	0.0023

	5.3	22.0	44.0		1.16	0.0384	0.0044
	6.6	30.0	41.0		1.08	0.0280	0.0051
	7.8	31.2	46.0		1.27	0.0216	0.0097
	8.9	39.6	42.0		1.11	0.0162	0.0051
Baragolai A	4.4	8.5	49.0	35.4	1.38	0.1351	0.0026
	5.4	12.6	45.0		1.27	0.0835	0.0078
	6.4	24.6	44.0		1.24	0.0335	0.0030
	7.1	26.4	44.0		1.24	0.0296	0.0036
	9.5	42.0	44.0		1.24	0.0133	0.0109
Tirap	4.3	8.4	48.0	38.1	1.26	0.1216	0.0014
	5.4	14.0	41.0		1.08	0.0647	0.0022
	7.0	25.0	46.0		1.21	0.0309	0.0025
	7.9	31.5	45.0		1.18	0.0180	0.0110
	9.1	38.7	47.0		1.23	0.0130	0.0180

Table 5.2 Summary of 95% confidence interval for the parameter c and R^2

Colliery	Size (mm)	R^2	c (s^{-m})	95% confidence interval
Baragolai	4.1	0.99	0.1229	0.1102–0.1357
	5.2	0.99	0.1181	0.1123–0.1239
	7.2	0.99	0.0309	0.0303–0.0314
	8.2	0.97	0.0166	0.0152–0.0180
	9.0	0.99	0.0158	0.0151–0.0164
Ledo	4.2	0.98	0.1335	0.1184–0.1486
	5.3	0.97	0.0472	0.0433–0.0511
	6.7	0.96	0.0378	0.0339–0.0417
	8.0	0.99	0.0209	0.0201–0.0218
	9.5	0.99	0.0129	0.0123–0.0134
Tikak	4.4	0.97	0.0748	0.0640–0.0855
	5.3	0.99	0.0384	0.0361–0.0407
	6.6	0.99	0.0280	0.0262–0.0297
	7.8	0.98	0.0216	0.0202–0.0231
	8.9	0.99	0.0162	0.0155–0.0169
Baragolai A	4.4	0.95	0.1351	0.1003–0.1699
	5.4	0.97	0.0835	0.0790–0.0880
	6.4	0.99	0.0335	0.0323–0.0346
	7.1	0.99	0.0296	0.0291–0.0301

	9.5	0.98	0.0133	0.0126–0.0141
Tirap	4.3	0.98	0.1216	0.1004–0.1428
	5.4	0.97	0.0647	0.0562–0.0733
	7.0	0.99	0.0309	0.0299–0.0319
	7.9	0.96	0.0180	0.0172–0.0189
	9.1	0.94	0.0130	0.0121–0.0139

To determine total yield of volatile matter in air, $(V_0 - V_\infty)$, let us denote the ratio of the total yield of volatile matter to that of the proximate volatile content of coal as p. The total yield of volatile matter, $(V_0 - V_\infty)$, can therefore be represented as p times the proximate volatile matter in the particle. As the amount of heat required for volatile content of the coal. The mass of coal samples was calculated by using Eq. (4.3) with $m = 1.4$ and c calculated from the correlation: $c = 6.64 d_v^{-2.78}$. The mass versus time profiles have been shown by the lines in Figures 5.4–5.8. The RMSE (Δ) for each sample is given in Table 5.1.

5.2.4 Variation of the yield of volatile matter with the volatile content of the coals

The ratio of the yield of volatile matter to the proximate volatile content (Table 5.1, column 6) was found to decrease with the increase in volatile content, and an increasing trend was observed with the increase in ash content (however, the Baragolai A coal was an exception). Similar observations can be made from the results reported in the literature [9–11]. This is probably due to the variation of the specific heat of the coals with the variation in their volatile content. The specific heat of a coal of low volatile content is lower than that of a high-volatile coal [12]. The rate of increase in temperature for a low-volatile coal is higher than that for a high-volatile coal. It has been reported in the literature [13] that the rapid increase in temperature at the high heating rates decreases the residence time of the volatile material. It reduces the influence of cracking and more tarry liquid is produced. However, the yield of the light hydrocarbon gases remains nearly constant. It has also been reported in the literature [13] that the increase in tar yield with increase in heating rate is greater for the low-volatile coals than that for the high-volatile coals,

which also supports the fact that the low-volatile coals are heated more rapidly than the high-volatile coals. Therefore, the residence time of volatile matter is lower for the low-volatile coals than that for the high-volatile coals, which is reflected in the higher volatile yield for the former. Therefore, the ratio decreased with increasing volatile-content of the coals, which is depicted in Figure 5.10. The ratio (p) has a power law correlation with the proximate volatile matter content (V_m) of coal as,

$$p = 64.58 V_m^{-1.1}, \quad R^2 = 0.99 \tag{5.7}$$

The 95% confidence interval for 64.58 is $(37.15, 112.28)$ and the same for 1.1 is $(0.94, 1.25)$.

5.2.5 Devolatilization in multi-particle system

To study the validity of the correlations developed for the single coal particles in multi-particle systems, the variation of mass with time for a batch of four particles of Baragolai A coal was studied. The agreement between the experimental data and Eq. (4.3) was good, as shown in Figure 5.11. Thus, it was confirmed that the correlations developed in this study can be used to predict the devolatilization time of a batch of coal particles as well. The values of c and error (Δ) are reported in Table 5.3.

5.2.6 Visual observation of the coal particles at different times of pyrolysis

The cross-sections of the Baragolai A coal particles were analyzed under a microscope after the particles were pyrolyzed at 1123 K for 40 s and 60 s in the fluidized bed at a fluidizing velocity of 1 m/s. The photographs are shown in Figure 5.12. Two types of particles were observed, viz. partially pyrolyzed and completely

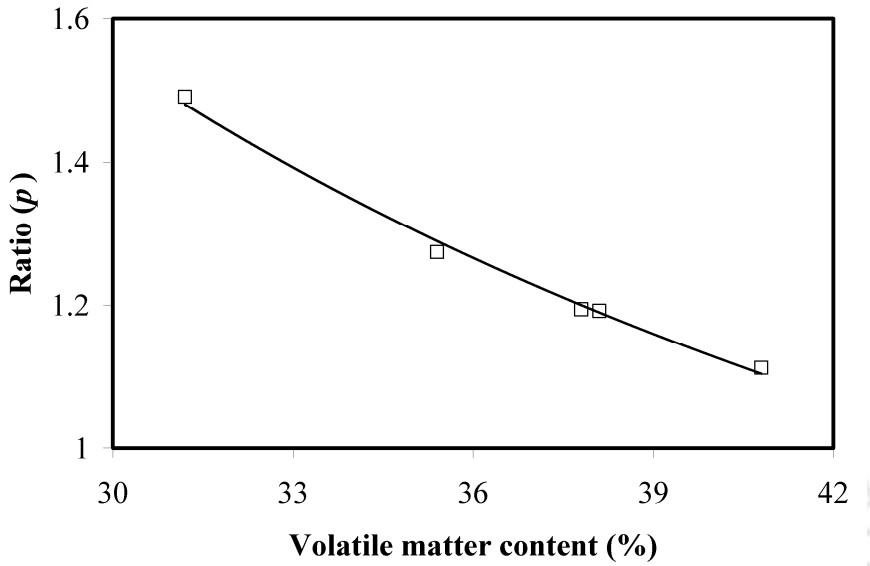

Figure 5.10 Correlation of ratio of volatile yield in air to proximate volatile matter (p) with the proximate volatile content of coal.

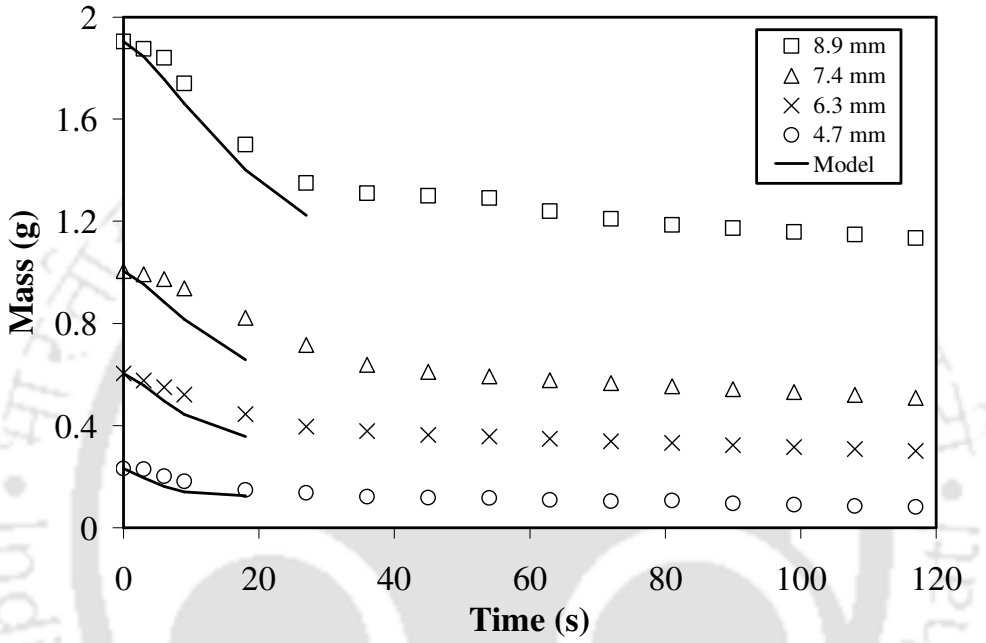

Figure 5.11 Mass versus time profiles for a batch of four particles of Baragolai A coal in air, and comparison with the correlation. The average diameters of the particles are shown in the figure.

Table 4.3 Values of c and error in multi-particle experiments

Particle size (mm)	$c\left(\mathrm{s}^{-m}\right)$	Δ
4.68	0.0909	0.0313
4.73	0.0882	
4.82	0.0835	
4.70	0.0899	
6.14	0.0428	0.0587
6.20	0.0417	
6.41	0.0379	
6.41	0.0379	
7.53	0.0242	0.1014
7.35	0.0258	
7.53	0.0242	
7.53	0.0242	
8.85	0.0154	0.0818
8.97	0.0149	
9.03	0.0146	
8.82	0.0156	

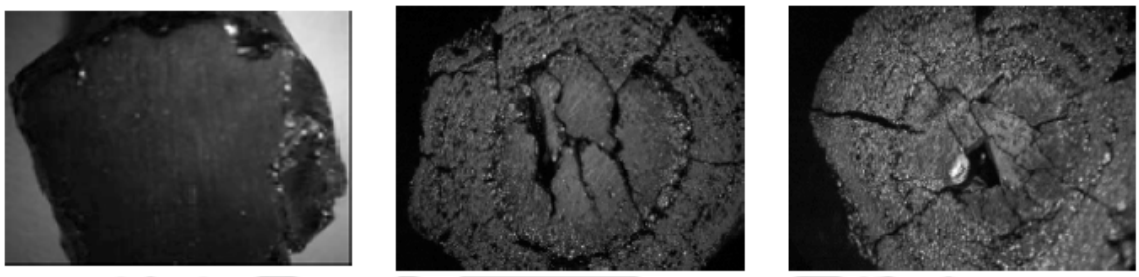

(a) (b) (c)

Figure 5.12 Cross-sectional views of Baragolai A coal particles at different stages of devolatilization: (a) before pyrolysis, (b) after being pyrolyzed for 40 s in air, and (c) after being pyrolyzed for 60 s in air. Magnification = 15×.

pyrolyzed. For the partially pyrolyzed particles, the core was very dull gray, but the outer layer was shiny, porous and black. The central regions of the partially pyrolyzed coal particles had clearly not reacted, and resembled the original coal. The boundary between these two regions was sharp and distinguishable. The shrinking-core pattern was clearly discernible. For the completely pyrolyzed particles, the entire cross-section of the coal particle was shiny, porous and black.

It can be observed from this figure that pyrolysis in air was more intense than the pyrolysis in argon atmosphere (described in Chapter 4), and there were several cracks in the particles [see Figures 5.12(b) and (c)]. In presence of air, oxidation of volatile matter occurs at the surface of the coal particles, which intensifies the rate of heating of the particles. Consequently the release of volatile matter is faster. The possible reason for the higher release of volatile matter is the increase of the thermal stress and the increase in the pressure inside the particles due to the enhanced rate of release of volatile matter.

5.2.6 Mechanism of devolatilization

In Chapter 4, the mechanism of devolatilization in inert atmosphere has been elaborated in detail. The same model is expected to be applicable for devolatilization in air. The values of the Biot number $\left[\mathrm{Bi} = ha/(3k)\right]$ obtained by the procedure described in Chapter 4 have been presented in Table 5.4.

It can be observed from Table 5.4 that the Biot numbers obtained from our experimental data on devolatilization in air are in the range of 0.033 to 0.536. Hence, all coal particles studied in the present work fall in the category in which the resistance to external heat transfer is higher than the resistance for internal heat transfer.

The values of Bi for devolatilization in argon and air are comparable, except for the particles having ~4 mm diameter. The results for these particles would suggest that the external heat transfer coefficient *h* increased in air due to the combustion of volatiles at the surface of the coal particles. However, for many other coal particles, the values of Bi were lower than those in argon, which would suggest a decrease in *h* in air. Therefore, it seems that the shrinking-core model of Chern and Hayhurst [14] does not explain the devolatilization in air accurately. This model was developed for devolatilization in inert atmosphere. Several assumptions were made in its development, which were discussed in Section 4.2.6. It is likely that some of these assumptions (e.g., no change in the size of the particles, and no resistance offered by the char to the gases and vapors leaving the thin reaction zone) are not valid when oxidation of the volatile film surrounding the coal particles takes place.

Table 5.4 Biot numbers for devolatilization in air

Colliery and proximate volatile matter (%)	Diameter (mm)	Bi	Δ
Baragolai (31.2)	4.1	0.220	0.015
	5.2	0.536	0.023
	7.2	0.485	0.012
	8.2	0.254	0.034
	9.0	0.090	0.030
Ledo (40.8)	4.2	0.467	0.048
	5.3	0.028	0.038
	6.7	0.043	0.033
	8.0	0.254	0.023
	9.5	0.111	0.015
Tikak (37.8)	4.4	0.101	0.046
	5.3	0.046	0.023
	6.6	0.044	0.047
	7.8	0.087	0.035
	9.0	0.091	0.016
Baragolai A (35.4)	4.4	0.243	0.052
	5.4	0.094	0.032
	6.4	0.260	0.017
	7.1	0.233	0.022
	9.5	0.112	0.040
Tirap (38.1)	4.3	0.075	0.027
	5.4	0.093	0.025
	7.1	0.203	0.014
	7.9	0.040	0.042
	9.1	0.033	0.067

Notations

a	radius of the coal particle, m
A_1	constant in the power law correlation for devolatilization time, $\mathrm{s\,mm^{-n_1}}$
A_2	constant in the power law correlation for the parameter c, $\mathrm{s^{-m}mm^{-n_2}}$
c	constant in mass loss correlation, $\mathrm{s^{-m}}$
d_v	mass-equivalent volumetric diameter, m
h	convective heat transfer coefficient, $\mathrm{W\,K^{-1}\,m^{-2}}$
k	thermal conductivity, $\mathrm{W\,K^{-1}\ m^{-1}}$
m	constant in mass loss correlation
n_1	constant in power law correlation for devolatilization time
n_2	constant in power law correlation for the parameter c
N	number of experimental data points
p	ratio of yield of volatile matter to the proximate volatile content of coal
R^2	coefficient of determination
r_c	radius of the central core, m
t	time, s
t_v	devolatilization time, s
v	velocity, m/s
$v(t)$	fraction devolatilized
$v(t)_{\mathrm{Expt}}$	experimental value of the fraction devolatilized
$v(t)_{\mathrm{Model}}$	value of the fraction devolatilized predicted by the correlation
V	total mass at any time t, kg

V_0 value of V at $t \to 0$

V_∞ value of V at $t \to \infty$

V_m volatile matter content of coal

Greek letters

Δ root mean square error (RMSE)

Reference

1. L.D. Smoot, P.J. Smith, Coal Combustion and Gasification, Plenum Press, New York, 1985.
2. D.P. Ross, C.A. Heidenreich, D.K. Zhang, Devolatilization times of coal particles in a fluidised-bed, Fuel 79 (2000) 873–883.
3. J.F. Stubington, K.W.K. Ng, B. Moss, P.K. Peeler, Comparison of experimental methods for determining coal particle devolatilization times under fluidized bed combustor conditions, Fuel 76 (1997) 233−240.
4. J.Q. Zhang, H.A. Becker, R.K. Code, Devolatilization and combustion of large coal particles in a fluidized bed. The Canadian Journal of Chemical Engineering, 68 (1990) 1010–1017.
5. J.F. Stubington, T.Y.S. Chui, S. Saisithidej, Experimental factors affecting coal devolatilization time in fluidized bed combustion, Fuel Science Technology International 10 (1992) 397–419.
6. H. Thunman, B. Lackner, Principles and Models of Solid Fuel Combustion: Fuel Loading of a Fluidized Bed Combustor (Report of the Department of Energy Conversion), Chalmers University of Technology, Göteborg, 2001.
7. C.N. Eatough, L.D. Smoot, Devolatilization of large coal particles at high pressure, Fuel 75 (1996) 1601–1605.
8. F. Winter, M.E. Prah, H. Hofbauer, Temperature in a fuel particle burning in a fluidized bed: the effect of drying, devolatilization, and char combustion, Combustion and Flame 108 (1997) 302–314.
9. J.P.K. Peeler, H.J. Poynton, Devolatilization of large coal particles under fluidized bed conditions, Fuel 71 (1992) 425–430.
10. D.B. Anthony, J.B. Howard, Coal devolatilization and hydrogasification, AIChE Journal 22 (1976) 625–656.
11. A.S. Jamaluddin, J.S. Truelove, T.F. Wall, Devolatilization of bituminous coals at medium to high heating rates, Combustion and Flame 63 (1986) 329–337.
12. J. Tomeczek, H. Palugniok, Specific heat capacity and enthalpy of coal pyrolysis at elevated temperatures, Fuel 75 (1996) 1089–1093.
13. P. Arendt, K.-H. van Heek, Comparative investigations of coal pyrolysis under inert gas and H_2 at low and high heating rates and pressures up to 10 MPa, Fuel 60 (1981) 779–787.

14. J.S. Chern, A.N. Hayhurst, Does a large coal particle in a hot fluidised bed lose its volatile content according to the shrinking core model? Combustion and Flame 139 (2004) 208–221.

CHAPTER 6

DEVOLATILIZATION OF COAL SAMPLES IN OXYGEN-ENRICHED AIR UNDER FLUIDIZED BED CONDITIONS

6.1 Introduction

Among the fluidized bed technologies, atmospheric fluidized bed combustion (AFBC) is an uncomplicated and low-cost process because it can use particles of large size. Expensive preparation of fuel such as crushing of coal is not mandatory. It offers high fuel flexibility in the size, rank, and type of coal used. It involves a high heat transfer coefficient, low combustion temperature, and utilization of low-grade fuels (e.g., fuels with moisture content up to 60%, or ash up to 70 %) is possible. Atmospheric fluidized bed combustion boilers are capable of using biomass and waste fuels as well. Even though the other types of fluidized bed, viz. pressurized and circulating fluidized beds are more efficient in combustion as well as sulfur-capture on account of lower particle size, higher recirculation rate, and presence of the higher amount of air, still the costs of production are comparatively higher than that of the AFBC.

Every technology or engineering design is, however, associated with some shortcomings. This is also true for the atmospheric fluidized bed combustion boilers. The disadvantages of AFBC are: (i) relatively small quantity of heat generated per unit area of the furnace cross-section when high-volatile fuels are burnt, (ii) difficulties associated with the design of high-capacity units because of the requirement of a large number of fuel feeding points, (iii) small turn down ratio, (iv)

relatively high SO_2 and NO_x emission levels, (v) relatively inadequate fuel flexibility, (vi) relatively low combustion efficiency, and (vii) erosion of the immersed heat transfer surfaces.

By the introduction of oxygen-enriched air in AFBC, the deficiencies in combustion and thermal efficiency can be reduced, and the performance can be made at par with the pressurized and circulating fluidized bed combustors. In oxygen-enriched environment, both devolatilization and combustion of coal particles are distinctly quicker than that with air. Also, the combustion of volatile matter occurs because of the presence of the extra oxygen in the combustion system, which increases the combustion efficiency [1,2]. The thermal efficiency of the system also increases due to the lowering of the total volume of the flue gas leaving the combustion chamber [3]. Oxygen-enriched combustion method is an effective method for producing a flue gas rich in carbon dioxide, which can be separated easily [4,5], and sequestered [6]. It is also recognized that the use of oxygen-enriched air and recycle of char help a gasifier to increase the heating value of the product gas and cold gas efficiency. The ratio of conversion of carbon to CO_2 and CO boosts with the increase of oxygen concentration in the combustion chamber [7]. Air enriched with oxygen can curtail the emission of carbon monoxide in the flue gas of a fluidized bed combustor. In some plants, secondary air is injected for combustion of volatiles in the free-board to bring the emission of carbon monoxide below the pollution limits [8]. The quantity of unburned carbon in the flue gas is considerably reduced in the presence of extra oxygen. However, the cost for oxygen enrichment is higher, owing to the cost involved in the liquefaction of air [9].

Research on combustion of pulverized coal with oxygen-enriched air has shown that there is an increase in the flux of oxygen molecules from the bulk towards

the particles. As a result, the temperature of the surface of the particles becomes higher. This enhances the pyrolysis rate, Stefan flow and oxidation in the boundary layer [10]. There is no work reported in the literature on devolatilization of large coal particles under fluidized bed conditions in presence of oxygen-enriched air. There is a difference between the higher oxygen concentration in the fluidizing gas and introduction of excess air. The latter process leads to a higher fluidization velocity. At higher fluidization velocities, the rate of release of volatile matter is slightly higher because of the better convective heat transfer to the particle [11]. As the inert gas does not participate in combustion, the volume of nitrogen is quite high at the higher fluidization velocities, and the sensible heat is lost, which is carried away by the excess nitrogen.

During the heating of the coal particles in fluidized bed, the average heating rate of the individual coal particles depends on their size. From the data reported in the literature [12], it is observed that the average heating rate of large particles is lower than the average heating rate of small particles. It is also reported that the differences in temperature history of the center of the coal particles are mostly influenced by the type of coal and the particle size [13].

Heat transferred from the fluidized bed medium to the coal particle is utilized in the drying of the coal particle as well as in the endothermic reactions leading to the formation of the volatile matter. Exothermic reactions on the surface of the char increase the temperature of the coal particle. Increase in particle temperature increases the rate of drying and devolatilization of coal. In the presence of excess oxygen, exothermic reactions release sensible heat from the combustion of volatile matter and char. This can accelerate drying and formation of volatiles. Hence it is important to study devolatilization of coals of different particle size in oxygen-enriched air.

The characteristics of devolatilization significantly differ in inert atmosphere, air, and air enriched with oxygen. In this chapter, we describe devolatilization in oxygen-enriched air. We have studied coals having a wide range of volatile content collected from five collieries located in the northeastern India. Particles having diameter between 4 mm and 9 mm were studied. The uninterrupted variation of mass with time was measured in a gas medium constituted of 30% oxygen (the rest is nitrogen) under fluidized bed conditions. A correlation of devolatilization time with particle size was developed. The total yields of volatile matter in these three atmospheres were compared.

6.2 Analysis of data on devolatilization in oxygen-enriched air

6.2.1 Correlation between devolatilization time and particle diameter

The devolatilization time t_v was correlated with the particle diameter d_v as, $t_v = Ad_v^n$, where A and n are constants. Regressing the data from all coal samples, it was found that $A = 0.34\,\text{s mm}^{-n}$ and $n = 2.16$ $\left(R^2 = 0.90\right)$. The 95% confidence interval for A is $(0.18, 0.63)$ and the same for n is $(1.84, 2.48)$. Figure 6.1 shows the variation of devolatilization time with particle diameter.

6.2.2 Correlation for variation of mass with time

The variation of the mass of the particles with time for the five coals of different size during devolatilization is shown in Figures 6.2–6.6. From these profiles, it can be observed that the curves consist of two distinct linear segments, as discussed in Chapters 3 and 5. The first segment pertains to devolatilization and the second

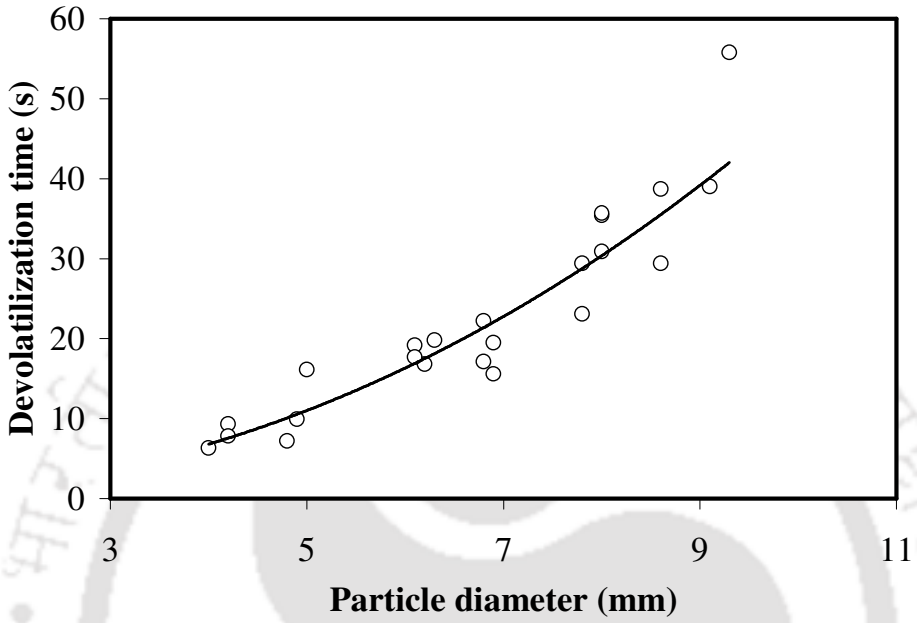

Figure 6.1 Correlation between the devolatilization time (t_v) and particle diameter (d_v) in oxygen-enriched air: $t_v = 0.34 d_v^{2.16}$.

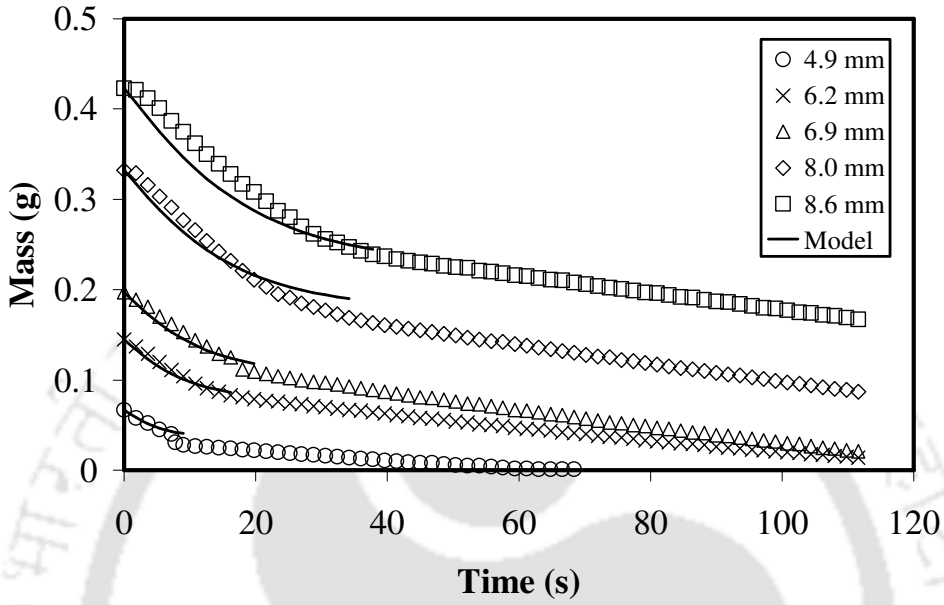

Figure 6.2 Mass versus time profiles for Baragolai coal particles of different size in oxygen-enriched air. The lines indicate fit according to the equation,

$$V = V_0 - 1.49 V_0 V_m \left[1 - \exp\left(-7.38 d_v^{-2.38} t^{1.1}\right)\right].$$

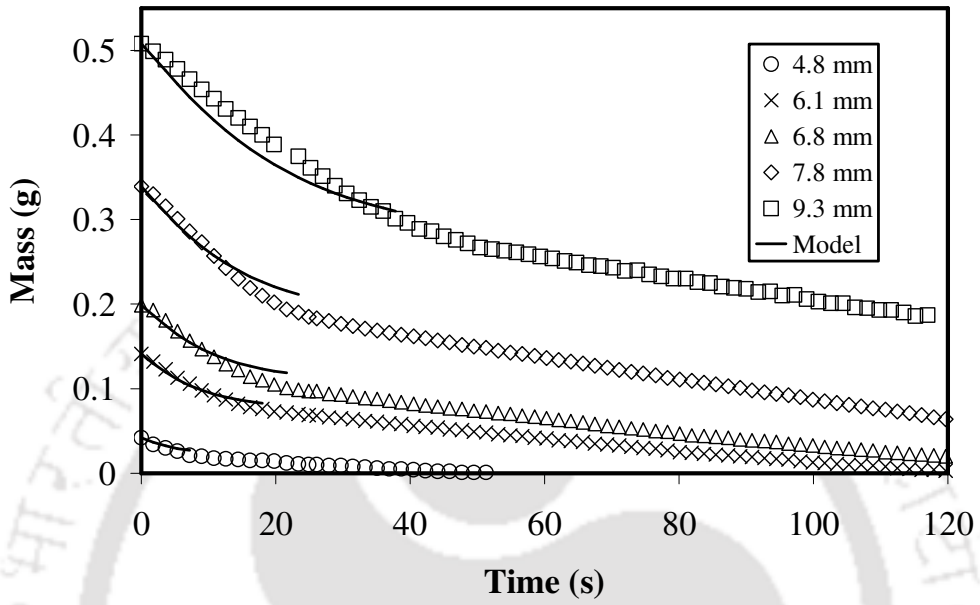

Figure 6.3 Mass versus time profiles for Ledo coal particles of different size in oxygen-enriched air. The lines indicate fit according to the equation,

$$V = V_0 - 1.105 V_0 V_m \left[1 - \exp\left(-7.38 d_v^{-2.38} t^{1.1}\right)\right].$$

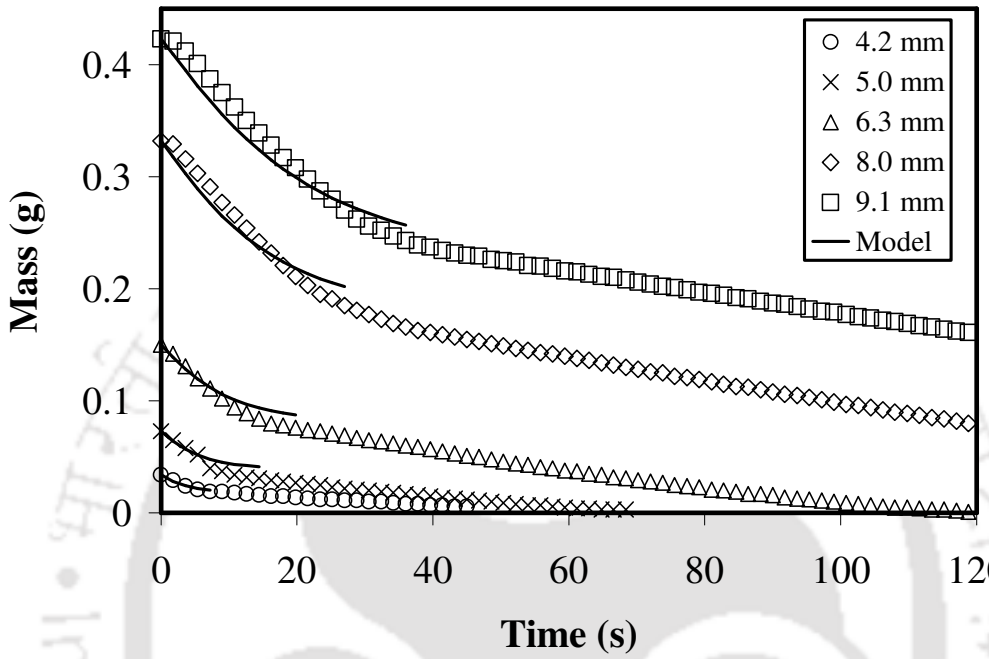

Figure 6.4 Mass versus time profiles for Tikak coal particles of different size in oxygen-enriched air. The lines indicate fit according to the equation,

$$V = V_0 - 1.202 V_0 V_m \left[1 - \exp\left(-7.38 d_v^{-2.38} t^{1.1}\right)\right].$$

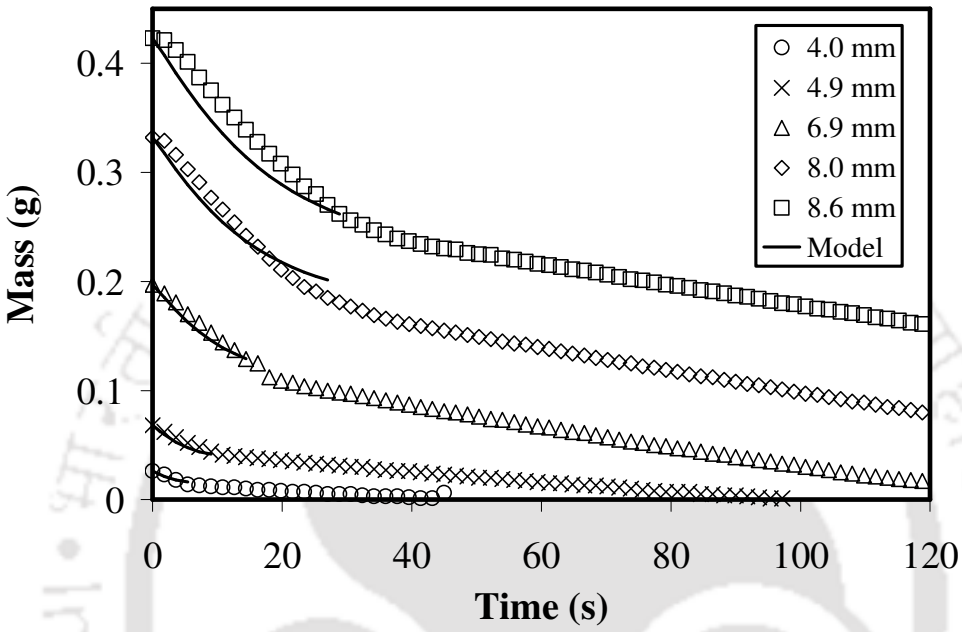

Figure 6.5 Mass versus time profiles for Baragolai A coal particles of different size in oxygen-enriched air. The lines indicate fit according to the equation,

$$V = V_0 - 1.293 V_0 V_m \left[1 - \exp\left(-7.38 d_v^{-2.38} t^{1.1}\right)\right].$$

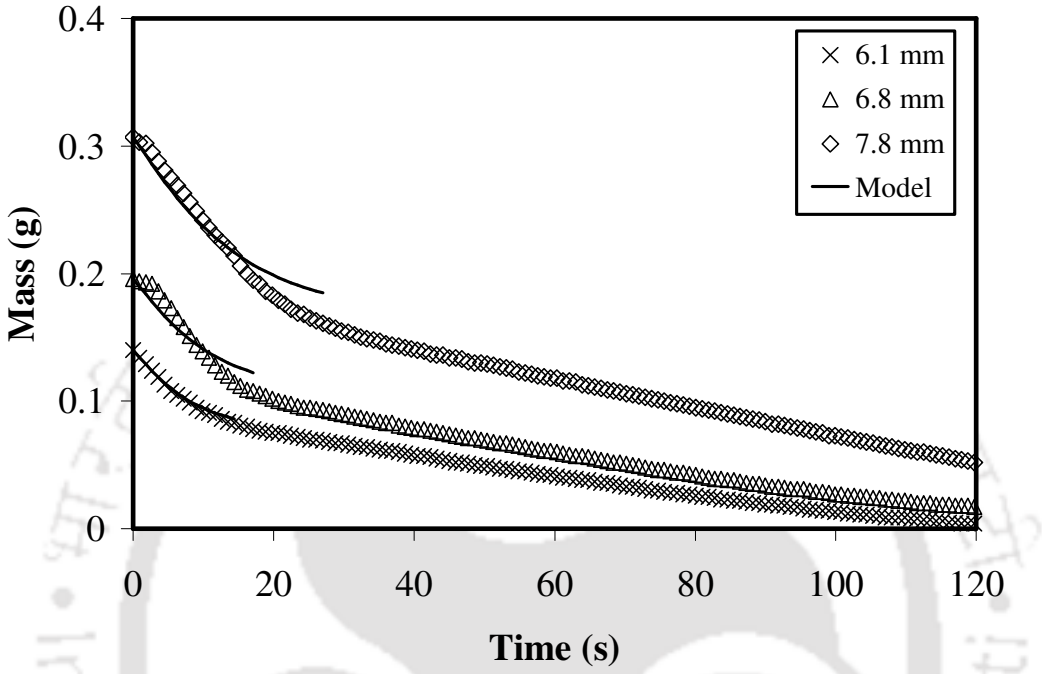

Figure 6.6 Mass versus time profiles for Tirap coal particles of different size in oxygen-enriched air. The lines indicate fit according to the equation,

$$V = V_0 - 1.192 V_0 V_m \left[1 - \exp\left(-7.38 d_v^{-2.38} t^{1.1}\right)\right].$$

segment pertains to the combustion of char. In this work, only the devolatilization segments of these curves were analyzed. It can be observed from these figures that the point of intersection is not sharp. This means that both devolatilization and char combustion occur simultaneously in these systems.

To mark the end of devolatilization, two straight lines are drawn for each part, and the point of intersection of these two lines is taken as the devolatilization time (as described in the Chapter 3). It is evident that the devolatilization time increases as the particle diameter increases. Furthermore, the slope of the devolatilization line increases as the particle diameter increases, which signifies that the devolatilization rate increases with the increase in particle diameter. As the particle diameter increases, the amount of volatile matter increases. Since all the particles are subjected to identical experimental conditions, therefore, the loss of volatile matter with respect to time increases as the amount of volatile matter increases. Because the heat requirement for devolatilization also increases with the increase in volatile content, a decrease in overall rate of heating is observed as the particle diameter increases. Fragmentation of the particles was not observed in any of the experiments.

The fractional loss of mass (i.e., the fractional release of volatile matter at time t), $v(t)$, was represented by a simple profile as given by Eq. (4.3). However the values of constants c and m have been found to be different from that in the inert atmosphere. The value of m was found to be 1.1 for the coals used in this study. The 95% confidence interval for m is $(1.05, 1.15)$. The parameter c was correlated with particle diameter, d_v, as, $c = A_1 d_v^{n_1}$, where $A_1 = 7.38\ \mathrm{s}^{-m}\mathrm{mm}^{-n_1}$ and $n_1 = -2.38\ \left(R^2 = 0.94\right)$. The values of c are given in Table 6.1. The 95% confidence interval for A_1 is $(4.393, 12.404)$ and the same for n_1 is $(-2.660, -2.111)$. The

Table 6.1 Summary of experimental results on devolatilization in oxygen-enriched air

Colliery	Size (mm)	Total Devolatilization Time (s)	Yield of Devolatilization (%)	Proximate Volatile Matter (%)	Ratio of Yield of Volatile Matter to Proximate Volatile Matter	$c\left(\mathrm{s}^{-m}\right)$	Δ
Baragolai	4.2	9.3	58.2	31.2	1.86	0.1545	0.0068
	6.2	16.8	43.5		1.39	0.0998	0.0037
	6.9	19.5	44.2		1.42	0.0723	0.0061
	8.0	35.4	49.7		1.59	0.0469	0.0202
	8.6	38.7	43.7		1.40	0.0391	0.0182
Ledo	4.8	7.2	50.0	40.8	1.23	0.2393	0.0033
	6.1	19.2	34.0		0.83	0.0961	0.0041
	6.8	22.2	49.8		1.22	0.0757	0.0096
	7.8	23.1	37.2		0.91	0.0660	0.0121
	9.3	55.8	49.3		1.21	0.0291	0.0196
Tikak	4.2	7.8	44.1	37.8	1.19	0.2692	0.0009
	5.0	16.1	60.3		1.59	0.1379	0.0076
	6.3	19.8	49.3		1.31	0.0958	0.0074
	8.0	35.7	50.0		1.32	0.0466	0.0143
	9.1	39.0	44.0		1.16	0.0391	0.0131
Baragolai A	4.0	6.3	46.2	35.4	1.30	0.2721	0.0012
	4.9	9.9	38.2		1.08	0.1590	0.0035
	6.9	15.6	35.5		1.00	0.0952	0.0054
	8.0	30.9	47.0		1.33	0.0508	0.0119
	8.6	29.4	38.3		1.08	0.0446	0.0195
Tirap	6.1	17.7	45.0	38.1	1.18	0.1130	0.0026
	6.8	17.1	44.9		1.18	0.0829	0.0099
	7.8	29.4	49.2		1.29	0.0551	0.0147

variation of c with the particle diameter is depicted in Figure 6.7. The 95% confidence interval for c and the values of R^2 are given in Table 6.2.

The ratio of the yield of volatile matter to the proximate volatile matter has been found to vary between 0.83 and 1.86. These are presented in Table 6.1. The average ratio for 23 coal samples is 1.264. Using Eq. (4.3) and the correlation, $c = 7.38 d_v^{-2.38}$, the mass of a single coal particle at any instant was computed until the completion of devolatilization.

The total yield of volatile matter, $\left(V_0 - V_\infty\right)$, can be expressed as p (viz. the ratio of total yield of volatiles to that of the proximate volatile content of the coal) times the proximate volatile content of the coal. The mass of coal particle, calculated by Eq. (4.3), is shown by the lines in Figures 6.2–6.6. The root mean square error (RMSE) for each particle is presented in Table 6.1.

6.2.3 Variation of the yield of volatile matter with the volatile content of the coals

The ratio of the yield of volatile matter to proximate volatile matter (Table 6.1, column 6) decreased with the increase in the volatile content of the coals. The average values of the ratio for the coal samples of one colliery have been plotted against the volatile content of the coals in Figure 6.8. It can be observed from this figure that the ratio showed a decreasing trend with the increase in volatile content. Similar observations can be made from the results reported in the literature [15–17]. This is likely due to the difference in specific heat of the coals having different volatile matter. The specific heat of the low-volatile coals is lower than the specific heat of the high-volatile coals [18]. The rate of increase of temperature of the low-volatile coals

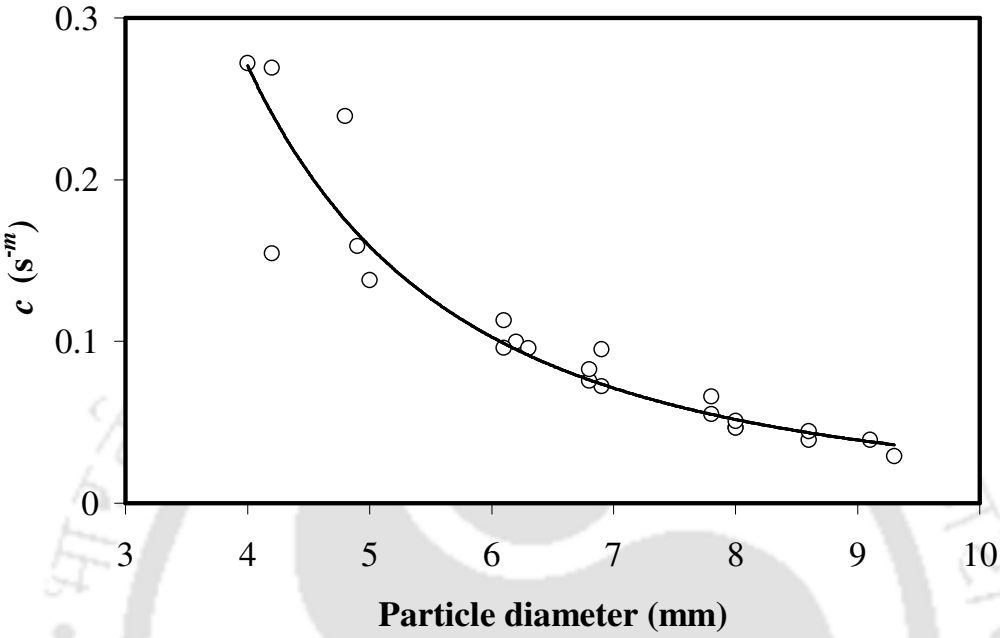

Figure 6.7 Variation of the parameter *c* with particle diameter.

Table 6.2 Summary of 95% confidence interval for the parameter c and R^2

Colliery	Size (mm)	R^2	$c\left(\mathrm{s}^{-m}\right)$	95% confidence interval
Baragolai	4.2	0.91	0.1545	0.1252–0.1839
	6.2	0.96	0.0998	0.0892–0.1103
	6.9	0.95	0.0723	0.0650–0.0796
	8.0	0.96	0.0469	0.0436–0.0501
	8.6	0.95	0.0391	0.0361–0.0422
Ledo	4.8	0.97	0.2393	0.2030–0.2757
	6.1	0.98	0.0961	0.0890–0.1032
	6.8	0.96	0.0757	0.0690–0.0824
	7.8	0.95	0.0660	0.0593–0.0727
	9.3	0.97	0.0291	0.0276–0.0305
Tikak	4.2	0.97	0.2692	0.2208–0.3176
	5.0	0.97	0.1379	0.1251–0.1507
	6.3	0.97	0.0958	0.0884–0.1033
	8.0	0.96	0.0466	0.0434–0.0498
	9.1	0.95	0.0391	0.0361–0.0422
Baragolai A	4.0	0.92	0.2721	0.1825–0.3618
	4.9	0.96	0.1590	0.1367–0.1812
	6.9	0.94	0.0952	0.0827–0.1077
	8.0	0.95	0.0508	0.0464–0.0552
	8.6	0.93	0.0446	0.0401–0.0491
Tirap	6.1	0.99	0.1130	0.1076–0.1185
	6.8	0.90	0.0829	0.0680–0.0978
	7.8	0.96	0.0551	0.0506–0.0596

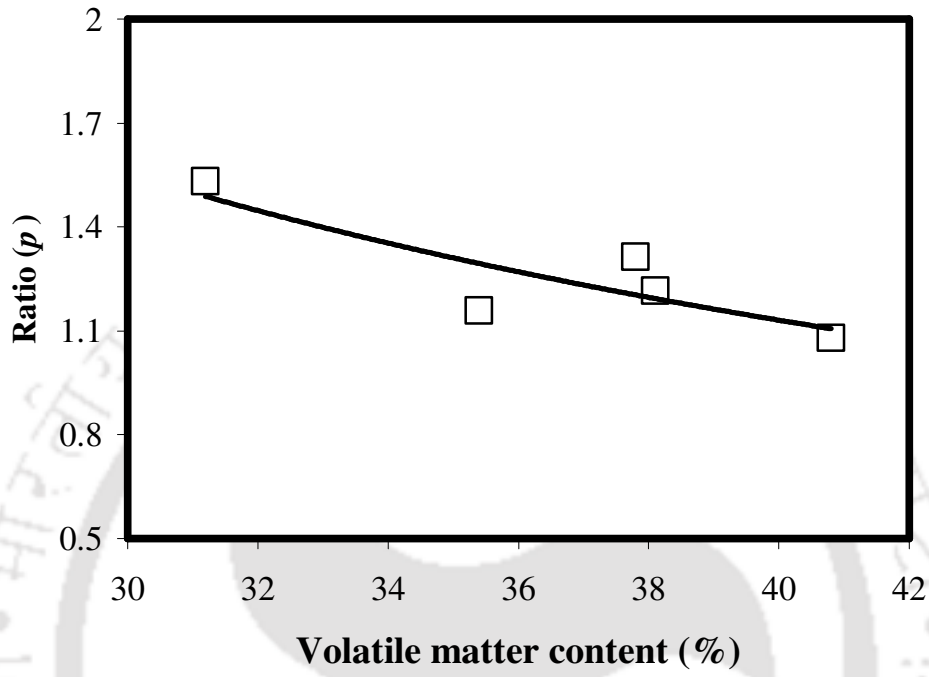

Figure 6.8 Variation of the ratio of volatile yield (in oxygen-enriched air) to proximate volatile matter (p) with the proximate volatile content of coal.

is higher than that of the high-volatile coals. In our experiments, the effective rate of heating was quite high due to the presence of oxygen. It has been reported in the literature [19] that the rapid increase of temperature during the high heating rate decreases the residence time of volatile matter, diminishes the influence of cracking, and more tarry liquid is produced. The yield of light hydrocarbon gases, however, remains nearly constant. It has also been reported in literature [19] that the increase in the yield of tar with the increase in heating rate is higher for the low-volatile coals than that for the high-volatile coals, which also supports the fact that the low-volatile coals are heated more rapidly than the high-volatile coals. Therefore, the residence time of volatile matter of the low-volatile coals is lower than that of the high-volatile coals, which is reflected in the higher yield of volatile matter for the low-volatile coals. Therefore, the ratio decreased with the increase in volatile-content of the coals.

The ratio, p, has a power law correlation with the volatile matter of coal (V_m) as shown below.

$$p = 66.315 V_m^{-1.104},\ R^2 = 0.70 \tag{6.1}$$

The 95% confidence interval for 66.315 is $(0.532, 8266.777)$ and the same for 1.104 is $(-2.445, 0.237)$. The variation of p with V_m has been shown in Figure 6.8.

6.2.4 Devolatilization in multi-particle system

The variation of mass with time for a batch of four particles of Baragolai A coal was studied. The agreement between the experimental data and Eq. (4.3) was good, as shown in Figure 6.9. Thus, it was confirmed that the correlations developed in this study can be used to predict the devolatilization of a batch of coal particles. The errors of the model in the multi-particle system are given in Table 6.3.

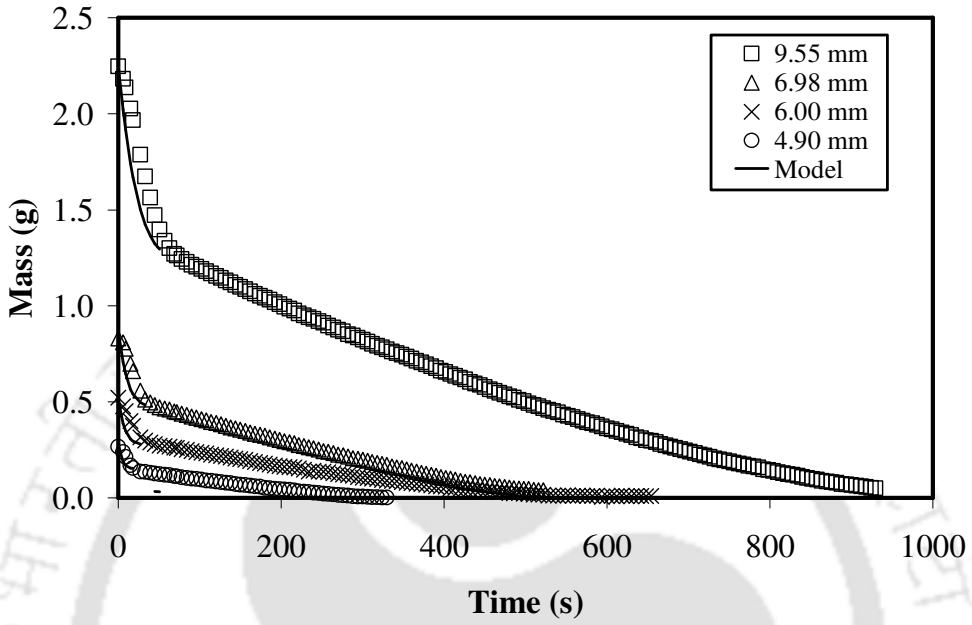

Figure 6.9 Mass versus time profiles of a batch of four particles of Baragolai A coal in oxygen-enriched air, and comparison with the model. The average diameters of the particles are shown in the figure.

Table 6.3 Values of c and errors in multi-particle experiments

Particle size (mm)	$c\left(\mathrm{s}^{-m}\right)$	Δ
4.96	0.1627	0.0281
4.93	0.1656	
4.50	0.2052	
5.22	0.1443	
5.95	0.1056	0.0754
6.01	0.1029	
6.02	0.1026	
6.01	0.1029	
7.08	0.0699	0.0944
6.99	0.0719	
6.95	0.0730	
6.91	0.0741	
9.56	0.0341	0.2201
9.49	0.0348	
9.55	0.0342	
9.61	0.0337	

6.2.5 Mechanism of devolatilization

In Chapter 4, the mechanism of devolatilization in inert atmosphere has been discussed in detail. The same model is expected to be valid for devolatilization in oxygen-enriched air. Chern and Hayhurst [20] have found Biot numbers in the range of 0.067 to 3.33 corresponding to their data. In this region, (r_c/a) varies with (t/t_v) almost linearly. The Biot numbers calculated from our experimental data lie between 0.029 and 0.828 (see Table 6.4). The values of Bi for devolatilization in argon, air, and oxygen-enriched air are comparable, except for the particles having ~4 mm diameter. The results for these small particles would suggest that the external heat transfer coefficient h increased in oxygen-enriched air due to the combustion of volatiles at the surface of the coal particles. However, for many other coal particles, the values of Bi were lower than those in argon, which would suggest a decrease in h in oxygen-enriched air. Therefore, it seems that the shrinking-core model of Chern and Hayhurst [20] does not explain the devolatilization in oxygen-enriched air accurately. The reason for these anomalies has been discussed in Section 5.2.6 and the same is applicable for oxygen-enriched air atmosphere also.

6.3 Comparison of devolatilization in argon, air, and oxygen-enriched air

6.3.1 Comparison of devolatilization time

The devolatilization time decreased with the increase in the concentration of oxygen in the fluidizing gas. This is depicted in Figure 6.10. The intensity of surface-oxidation increased with the increase in oxygen concentration in the gas. This increased the rate of heat transfer and hence, increased the rate of release of volatile matter. The parameters A and n of the correlation, $t_v = Ad_v^n$, vary with the concentration of oxygen in the fluidizing gas. Comparing the devolatilization times

Table 6.4 Biot numbers for devolatilization in oxygen-enriched air

Colliery and proximate volatile matter (%)	Devolatilization in oxygen-enriched air		
	Size (mm)	Bi	Δ
Baragolai (31.2)	4.2	0.033	0.048
	6.2	0.261	0.014
	6.9	0.076	0.016
	8.0	0.282	0.026
	8.6	0.111	0.054
Baragolai (40.8)	4.8	0.146	0.038
	6.1	0.348	0.017
	6.8	0.301	0.017
	7.8	0.185	0.019
	9.3	0.244	0.018
	4.8	0.146	0.038
Tikak (37.8)	4.2	0.310	0.024
	5.0	0.828	0.038
	6.3	0.507	0.017
	8.0	0.358	0.022
	9.1	0.230	0.024
Baragolai A (35.4)	4.0	0.066	0.047
	4.9	0.090	0.015
	6.9	0.107	0.014
	8.0	0.251	0.022

	8.6	0.029	0.028
Tirap (38.1)	6.1	0.511	0.024
	6.8	0.092	0.055
	7.8	0.269	0.021

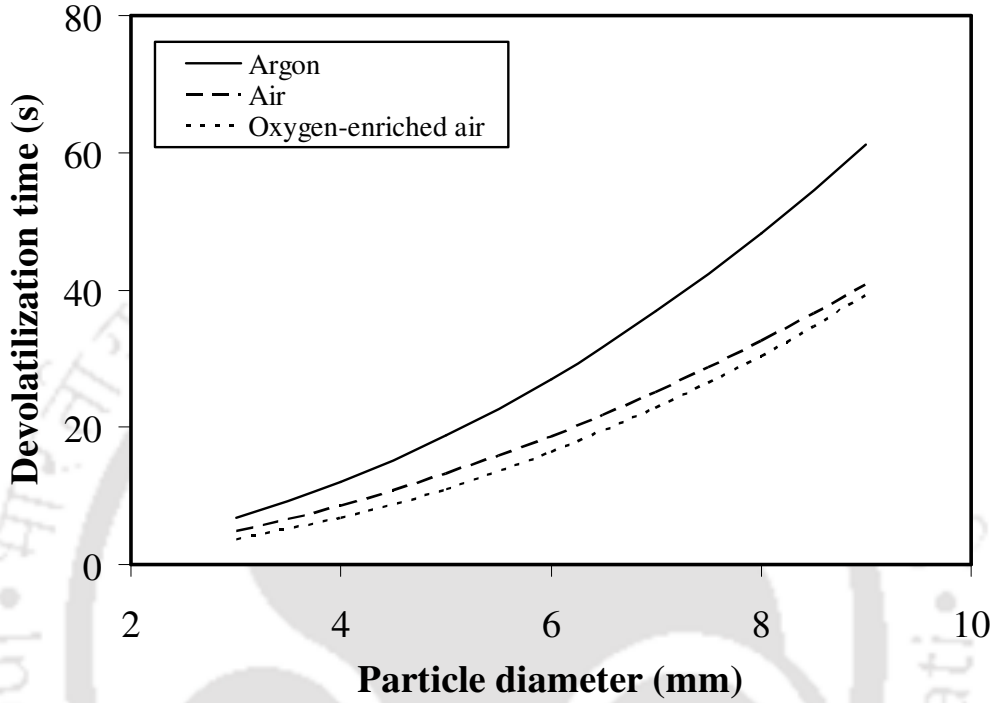

Figure 6.10 Comparison of the devolatilization times in inert atmosphere, air and oxygen-enriched air as predicted by the correlations.

in argon, air and oxygen-enriched air, it can be observed that the value of n increased, but the parameter A decreased with the increase in oxygen concentration in the fluidizing gas (see Figure 6.11 and Table 6.5). The devolatilization time in oxygen-enriched air is lower than that in air, which is lower than the devolatilization time in argon atmosphere. The constant A varies with the oxygen concentration following a second-order polynomial as shown below.

$$A = -0.0006\left(c_{O_2}\right)^2 + 0.0032c_{O_2} + 0.81, \qquad R^2 = 1 \tag{6.2}$$

The correlation parameter n varies with the oxygen concentration following the equation given below.

$$n = 1.801 + 0.009\exp\left(0.1227c_{O_2}\right), \quad R^2 = 1 \tag{6.3}$$

6.3.2 Variation of c and m in the equation, $v(t) = 1 - \exp\left(-ct^m\right)$, with oxygen concentration

The constant c increased, whereas, the constant m decreased with the increase in the oxygen concentration. These variations are depicted in Figures 6.12 and 6.13, respectively. The overall effect was such that the fractional loss of volatile matter increased with the increase in oxygen content of the fluidizing gas. The parameters A_1 and n_1 of the correlation, $c = A_1 d_v^{n_1}$, also varied with the concentration of oxygen in the fluidizing gas. Both the parameters increased with the increase in oxygen concentration in the gas, as shown in Figure 6.14. The overall value of c increased with the increase in oxygen concentration in the fluidizing gas. The parameter A_1 varies with the oxygen concentration of the fluidizing gas as described by the polynomial,

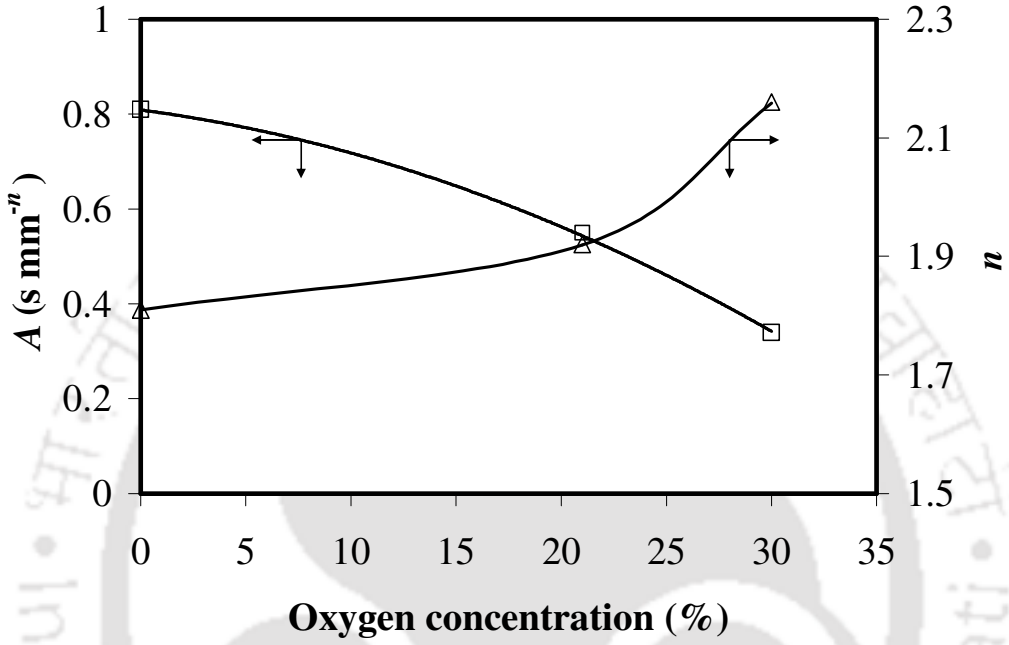

Figure 6.11 Variation of parameters *A* and *n* with the oxygen concentration in the fluidizing gas.

Table 6.5 Comparison of devolatilization in argon, air, and oxygen-enriched air

Correlation and/or parameter		Devolatilization in argon	Devolatilization in air	Devolatilization in oxygen-enriched air
$t_v = Ad_v^n$	A	0.81	0.60	0.34
	n	1.81	1.92	2.16
$c = A_1 d_v^{n_1}$	A_1	3.39	6.64	7.38
	n_1	–2.87	–2.78	–2.38
m		1.6	1.4	1.1
Yield of volatile matter/proximate volatile matter		1.11	1.25	1.26

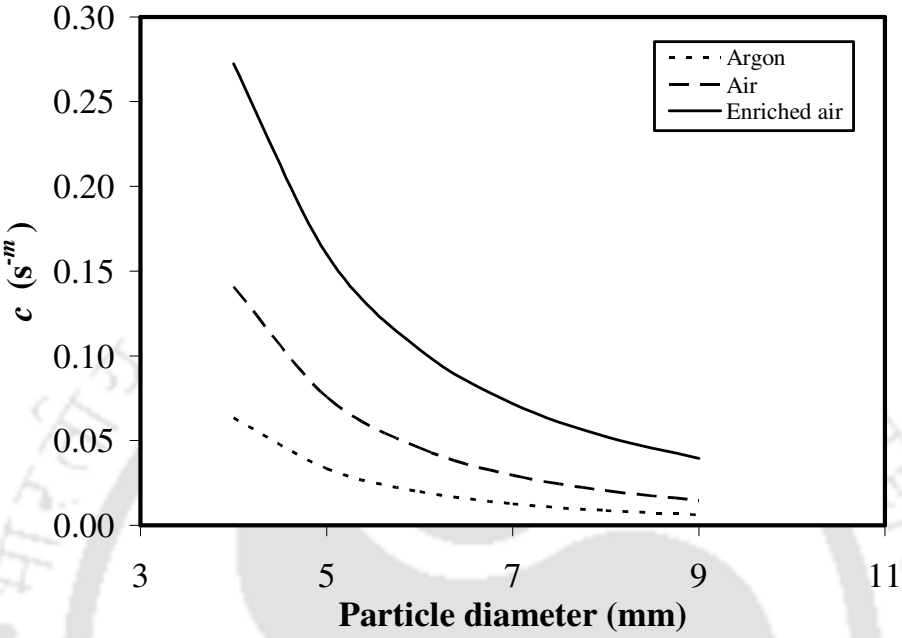

Figure 6.12 Variation of c with oxygen concentration in the fluidizing gas.

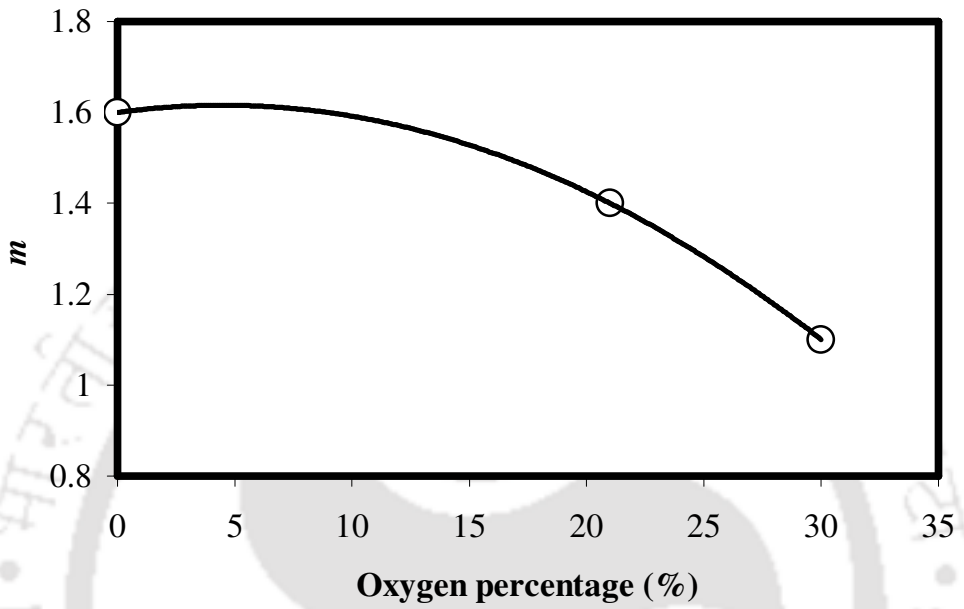

Figure 6.13 Variation of m with oxygen concentration in the fluidizing gas.

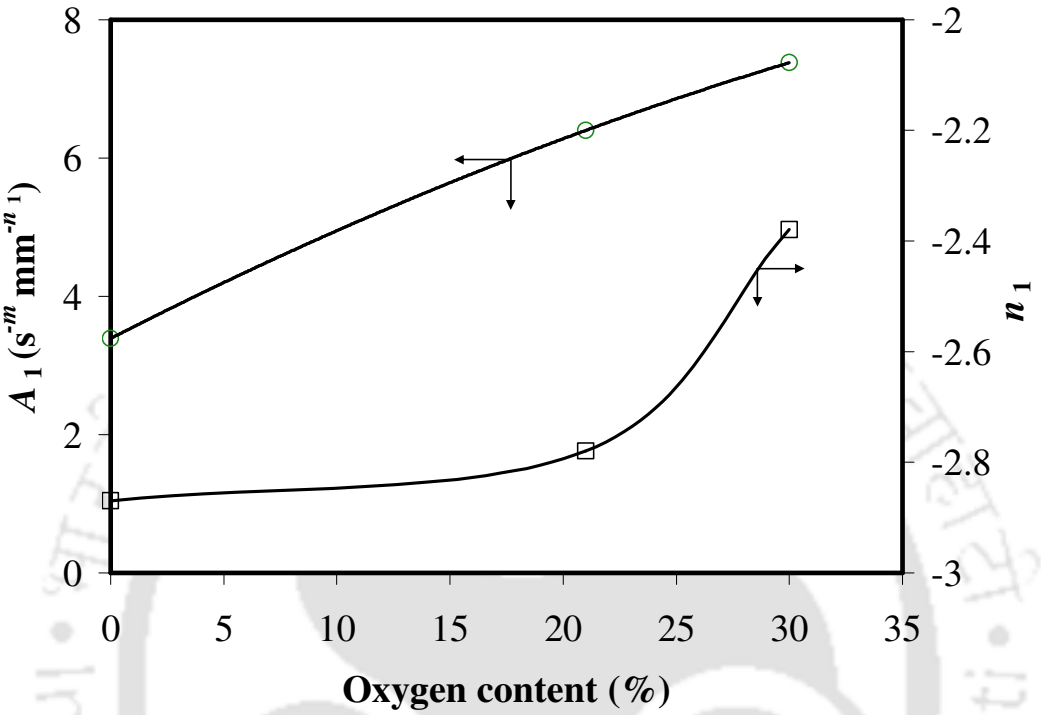

Figure 6.14 Variation of parameters A_1 and n_1 with oxygen concentration in the fluidizing gas.

$$A_1 = -0.0011\left(c_{O_2}\right)^2 + 0.1674 c_{O_2} + 3.39, \quad R^2 = 1 \tag{6.4}$$

The parameter n_1 varies with the oxygen concentration in the fluidizing gas as described by the following equation,

$$n_1 = \frac{-2.871}{1+\exp\left[\left(c_{O_2} - 37.72\right)/4.896\right]}, \quad R^2 = 1 \tag{6.5}$$

The constant m varies with oxygen concentration as shown below.

$$m = -0.0008\left(c_{O_2}\right)^2 + 0.0071 c_{O_2} + 1.6, \quad R^2 = 1 \tag{6.6}$$

6.3.3 Mechanism of devolatilization

It has been discussed in Section 4.2.6 that the values of Biot number for devolatilization in argon follow the model of Chern and Hayhurst [20]. For ~4 mm coal particles in argon atmosphere, the average value of Biot number of all five coals is less than 0.1, and therefore, it can be concluded that the internal resistance to conduction is significantly smaller than the external resistance to convective heat transfer.

It seems that the shrinking-core model of Chern and Hayhurst [20] does not explain accurately the devolatilization in air and oxygen-enriched air. This model was developed for devolatilization in inert atmosphere. Several assumptions were made in its development. It is likely that some of these assumptions (e.g., no change in the size of the particles, and no resistance offered by the char to the gases and vapors leaving the thin reaction zone) are not valid when oxidation of the volatile film surrounding the coal particles takes place.

Notations

a	radius of the coal particle, m
A	constant in power law correlation for devolatilization time, s mm^{-n}
A_1	constant in power law correlation for constant c, s^{-m} mm^{-n_1}
Bi	Biot number
c	constant in mass loss correlation, s^{-m}
d_v	mass-equivalent volumetric diameter, m
h	convective heat transfer coefficient, W K^{-1} m^{-2}
k	thermal conductivity, W K^{-1} m^{-1}
m	constant in mass-loss correlation
n	constant in power law correlation for devolatilization time
n_1	constant in power law correlation for constant c
N	number of experimental data points
p	ratio of yield of volatile matter to the proximate volatile content of coal
r_c	radius of the central core in the shrinking-core model, m
R^2	coefficient of determination
t	time, s
t_v	devolatilization time, s
$v(t)$	fraction devolatilized
$v(t)_{\text{Expt}}$	experimental value of the fraction devolatilized
$v(t)_{\text{Model}}$	value of the fraction devolatilized predicted by the correlation
V	total mass at any time t, kg
V_0	value of V at $t \to 0$, kg
V_∞	value of V at $t \to \infty$, kg

V_m volatile matter content of coal, kg

Greek letters

Δ root mean square error (RMSE)

Reference

1. Y.Q. Hu, H. Nikzat, M. Nawata, N. Kobayashi, M. Hasatani, The characteristics of coal-char oxidation under high partial pressure of oxygen, Fuel 80 (2001) 2111–2116.
2. N. Kimura, K. Omata, T. Kiga, S. Takano, S. Shikisima, The characteristics of pulverized coal combustion in O_2/CO_2 mixtures for CO_2 recovery, Energy Conversion and Management 36 (1995) 805–808.
3. Y. Tan, M.A. Douglas, K.V. Thambimuthu, CO_2 capture using oxygen enhanced combustion strategies for natural gas power plants, Fuel 81 (2002) 1007–1016.
4. Y.Q. Hu, N. Kobayashi, M. Hasatani, The reduction of recycled-NO_x in coal combustion with O_2/recycled flue gas under low recycling ratio, Fuel 80 (2001) 1851–1855.
5. Y. Hu, S. Naito, N. Kobayashi, M. Hasatani, CO_2, NO_x and SO_2 emissions from the combustion of coal with high oxygen concentration gases, Fuel 79 (2000) 1925–1932.
6. Y. Tan, E. Croiset, M.A. Douglas, K.V. Thambimuthu, Combustion characteristics of coal in a mixture of oxygen and recycled flue gas, Fuel 85 (2006) 507–512.
7. T. Czakiert, Z. Bis, W. Muskala, W. Nowak, Fuel conversion from oxy-fuel combustion in a circulating fluidized bed, Fuel Processing Technology 87 (2006) 531–538.
8. R.C. Borah, B. Mazumder, M.M. Bora, Atmospheric fluidized bed combustion of high sulphur high volatile N. E. region coals of India, Research and Industry 40 (1995) 315–321.
9. Alstom Power Inc., Greenhouse Gas Emissions Control by Oxygen Firing in Circulating Fluidized Bed Boilers (PPL Report No. PPL-03-CT-09), US Department of Energy, Pennsylvania, 2003, p. 340.
10. C.A. Gurgel Veras, J. Saastamoinen, J.A. Carvalho Jr., M. Aho, Overlapping of the devolatilization and char combustion stages in the burning of coal particles, Combustion and Flame 116 (1999) 567–579.
11. F. Winter, M.E. Prah, H. Hofbauer, Temperature in a fuel particle burning in a fluidized bed: the effect of drying, devolatilization, and char combustion, Combustion and Flame 108 (1997) 302–314.

12. D.P. Ross, C.A. Heidenreich, D.K. Zhang, Devolatilization times of coal particles in a fluidised-bed, Fuel 79 (2000) 873–883.
13. M. Komatina, V. Manovic, D. Dakic, An experimental study of temperature of burning coal particle in fluidized bed, Energy and Fuels 20 (2006) 114–119.
14. P.K. Agarwal, R.D. La Nauze, Transfer processes local to the coal particle: a review of drying, devolatilization and mass transfer in fluidized bed combustion, Chemical Engineering Research and Design 67 (1989) 457–480.
15. J.P.K. Peeler, H.J. Poynton, Devolatilization of large coal particles under fluidized bed conditions, Fuel 71 (1992) 425–430.
16. D.B. Anthony, J.B. Howard, Coal devolatilization and hydrogasification, AIChE Journal 22 (1976) 625–656.
17. A.S. Jamaluddin, J.S. Truelove, T.F. Wall, Devolatilization of bituminous coals at medium to high heating rates, Combustion and Flame 63 (1986) 329–337.
18. J. Tomeczek, H. Palugniok, Specific heat capacity and enthalpy of coal pyrolysis at elevated temperatures, Fuel 75 (1996) 1089–1093.
19. P. Arendt, K.-H. van Heek, Comparative investigations of coal pyrolysis under inert gas and H_2 at low and high heating rates and pressures up to 10 MPa, Fuel 60 (1981) 779–787.
20. J.S. Chern, A.N. Hayhurst, Does a large coal particle in a hot fluidised bed lose its volatile content according to the shrinking core model? Combustion and Flame 139 (2004) 208–221.

CHAPTER 7

CONCLUSIONS AND SCOPE FOR FUTURE RESEARCH

7.1 Conclusions

This section presents the major conclusions drawn from the research work reported in this thesis. Devolatilization of five coals of northeastern India in argon, air and oxygen-enriched air was studied in this work under fluidized bed conditions. These coals have a wide range of volatile matter, which varies between 31 and 41%. The diameter of the coal particles varies between 4 mm and 9.5 mm. The major conclusions are as follows.

1. A prototype fluidized bed combustor was designed, fabricated and installed. All necessary calibrations for temperature using thermocouples, pressure corrections, and buoyancy corrections were made. A personal computer with data- logging software was installed to continuously record the mass of coal particle during devolatilization.
2. Thermogravimetric data for single coal particles (4–9 mm diameter) were generated in argon atmosphere at 1123 K at 1 m/s superficial velocity at 101.325 kPa. Mass versus time profiles were obtained for the coal sample. A correlation was developed to describe these profiles. The calculated profiles have been found to fit reasonably well with the experimental data. The correlation developed for a single particle was found to predict the profiles for a batch of four particles. Therefore, this correlation can be used to predict the evolution of volatile matter of single and multiple coal particles with respect to time in inert atmosphere under similar experimental conditions. A similar procedure can be adopted for other conditions.

3. Thermogravimetric data for single coal particles (4–9 mm particle diameter) were obtained in air at 1123K and 1 m/s superficial velocity at 101.325 kPa under the fluidized bed conditions. A mass versus time correlation was developed similar to the same in argon atmosphere. The calculated profile has been found to fit reasonably well with the experimental data. The correlation developed for a single particle has been found to predict the devolatilization profile reasonably well for multiple particles. Therefore, this correlation can be used to predict the evolution of volatile matter of single and multiple coal particles with respect to time in air under identical experimental conditions.
4. Thermogravimetric data for single coal particles (4–9 mm particle diameter) were generated in oxygen-enriched air containing 30% oxygen at 1123 K and 1 m/s superficial velocity at 101.325 kPa. A correlation for the variation of mass with time was developed. The calculated profile based on this correlation has been found to fit reasonably well with experimental data. Furthermore, the correlation developed for a single particle has been found to predict devolatilization reasonably well for multiple particles. Therefore, the correlation can be used to predict devolatilization in oxygen-enriched air under similar experimental conditions.
5. The parameters of the correlations for the three systems mentioned above have been found to vary with the oxygen content of the fluidizing gas. Correlations have been developed to depict these variations.
6. Correlations between devolatilization time and particle diameter have been developed. In argon atmosphere, correlations for total and 95% devolatilization time have been developed. The correlation for 95% devolatilization time with particle diameter was compared with the data reported in the literature at 1123 K,

but at different superficial velocities. It has been found that the superficial velocity has a significant role in devolatilization. The correlation parameters have been correlated with the superficial velocity of the fluidizing gas.

7. Correlation for the variation of devolatilization time with particle diameter has been developed for devolatilization in air. The correlation predicts reasonable values, which compare well with the data reported in the literature. It has been observed that the superficial velocity has a significant role in devolatilization time. The correlation parameters have been correlated with the superficial velocity of the fluidizing gas.
8. Correlation for devolatilization time with particle diameter has been developed for devolatilization in oxygen-enriched air. There is no data available in the literature on devolatilization of large coal particles in the oxygen-enriched air under fluidized bed conditions. The correlation and the experimental data will be useful for predicting devolatilization of coal in oxygen-enriched air.
9. The parameters of these correlations have been found to vary with the oxygen content of the fluidizing gas. Correlations were developed for these variations. In presence of oxygen, oxidation of volatile matter at the surface of the coal particle occurs, which facilitates the heat transfer at the surface of the particle. This augments devolatilization rate.
10. The ratio of the total yield of volatile matter to the proximate volatile matter in air and oxygen-enriched air decreases with the increase in proximate volatile content of the coals. The probable reason for this variation is that the specific heat of low-volatile coal is less than the specific heat of high-volatile coal. So, coals having low volatile matter are heated more rapidly than the high-volatile coals. Some volatile matter of the low-volatile coal may escape without getting

cracked inside the particle. This is the likely reason for the increase in the total yield of volatile matter. Therefore, the values of the ratio for the low-volatile coals are higher.

11. Devolatilization in argon is found to follow the shrinking-core model. For these coal particles, the value of the Biot number is less than 0.1. Therefore, it has been concluded that the internal resistance to conduction is significantly smaller than the external resistance to convective heat transfer. It seems that the shrinking-core model does not explain the devolatilization in the air and oxygen-enriched air accurately. This model was developed for devolatilization in the inert atmosphere. Several assumptions were made in its development. It is likely that some of these assumptions (such as, no change in the size of the particles, and no resistance offered by the char to the gases and vapors leaving the thin reaction zone) are not valid when oxidation of the volatile film surrounding the coal particles takes place.

7.2 Scope for future work

- Oxygen concentration in the fluidizing gas needs to be optimized for best possible results in terms of cost and efficiency.
- Mass-loss characteristics at higher superficial velocities should to be studied as per the requirements of the industrial fluidized bed combustors.
- The combustion efficiency need to be investigated in pilot-plant scale to ascertain the effect of increase of oxygen concentration in fluidizing gas.
- Cost analysis should be performed to analyze the commercial viability of the increase in efficiency of combustion and sulfur absorption keeping into consideration the cost of liquefaction of air.

- Effect on the flue gas emission needs to be explored in oxygen-enriched condition.
- The shrinking-core model should be extended with the inclusion of the enhancement in heat transfer in the presence of oxygen in the fluidizing gas.